Functional protein display on the surface of biobeads produced by recombinant *Escherichia coli*

A thesis presented in partial fulfilment of the

requirements for the degree of

Master of Science

In

Biochemistry

at Massey University, Palmerston North,

New Zealand

Shuxiong Chen

2013

Appendix D

MASSEY UNIVERSITY
Application for Approval of Request to Embargo a Thesis
(Pursuant to AC98/168 (Revised 2), Approved by Academic Board 17/02/99)

Name of Candidate: Shuxiong Chen ID Number: 07202350

Degree: Master of Science Dept/Institute/School: Massey University

Thesis title: Functional protein display on the surface of bio-particles produced by recombinant Escherichia coli

Name of Chief Supervisor: Bernd Rehm Telephone Ext: 7890

As author of the above named thesis, I request that my thesis be embargoed from public access until (date) 21/03/2015 for the following reasons:

☒ Thesis contains commercially sensitive information.

☐ Thesis contains information which is personal or private and/or which was given on the basis that it not be disclosed.

☐ Immediate disclosure of thesis contents would not allow the author a reasonable opportunity to publish all or part of the thesis.

☐ Other (specify):

Please explain here why you think this request is justified:

The results are sensitive & will be part of the industry products (Polybatics)

Signed (Candidate): Date: 28/3/2013

Endorsed (Chief Supervisor): Bernd Rehm Date: 28/3/2013

Approved/Not Approved (Representative of VC): Date: 28/06/2013

Note: Copies of this form, once approved by the representative of the Vice-Chancellor, must be bound into every copy of the thesis.

Abstract

Polyhydroxyalkanoic acids (PHAs) are biopolyesters produced by various bacteria. They are deposited as spherical water-insoluble cytoplasmic inclusions (beads) containing an amorphous hydrophobic polyester core and surrounded by a phospholipid monolayer and embedded proteins, including PHA synthase (PhaC), the key enzyme required for PHA bead formation. Although inactive PhaC cannot produce PHA beads, fusing inactive PhaC to green fluorescent protein (GFP) leads to GFP protein bead formation. Both PHA and protein beads could serve as a versatile platform for display of desired proteins suitable for various biotechnological and medical applications.

The tuberculin skin test (TST) for diagnosing bovine tuberculosis (TB) in cattle uses the purified protein derivative (PPD) that is prepared from *Mycobacterium bovis*. However, some antigens in the PPD are also present in environmental mycobacteria. Therefore, the TST lacks specificity if animals are exposed to non-pathogenic environmental mycobacteria. In this study, three specific TB antigens, CFP10, ESAT6, and Rv3615c — which are present in pathogenic but absent in most non-pathogenic mycobacteria — were displayed on the surface of PHA beads. The results demonstrated that these triple antigen-displaying PHA beads can differentiate TB-infected from non-infected cattle, making this an attractive alternative to current skin test diagnostic reagents.

IgG binding domains displayed on GFP protein beads have a higher IgG binding ability when compared to their counterpart displayed on PHA beads. However, it is unclear whether an enhancement of IgG binding ability due to GFP protein beads could be achieved by immobilization on other fluorescent protein (FP) beads. The results showed that other FP (including yellow, red and cyan) beads displaying IgG binding domains have an approximately 1.5–2 fold greater IgG binding ability when compared to PHA beads displaying the same binding domains. To investigate whether protein beads displaying iron-binding peptides could be magnetized while maintaining IgG binding function, an iron binding peptide was displayed. The results demonstrated that protein beads displaying both IgG and iron binding peptides can be magnetised by iron oxide and retain a strong IgG binding ability. Finally, this study revealed that different cell disruption techniques could affect the morphology and functionality of FP protein bead.

Acknowledgements

I would like to thank my supervisor, Bernd Rehm, for the opportunity to work under his guidance and supervision and for encouraging my interest in scientific research. I would also like to thank all my colleagues at the Rehm laboratory for their support and assistance. Special thanks go to Jason Lee and Jinping Du, whose support and advice made my research go smoothly. Next, I would like to thank Yajie Wang and Mark Piers Venning-Slater for their support, patience, and valuable advice. The TB skin test study was facilitated by the Hopkirk Institute at Massey University, Palmerston North. I would like to thank Natalie Parlane for her advice and support with the assessment of TB antigen PHA beads reactivity *in vitro*. Special thanks, too, to Neil Wedlock and Bryce Buddle for their time and help when required. I am grateful to Dr Anika Jahns for creating various plasmid constructs for protein bead production. I would also like to acknowledge her assistance with completing the functionality test of protein beads. I thank Polybatics Ltd. for providing access to equipment and materials as well as assistance when needed. My special gratitude goes to my family, especially my parents, Ruchao Chen and Yuxia Sun, for their constant love and assistance. My final thanks go to my lovely girlfriend, Shamyee Chan, for her endless encouragement and support.

Table of Contents

List of abbreviations

A full list of abbreviations used

^{o}C	Degree Celsius
3xFe	Triple iron-binding peptides
AGE	Agarose gel electrophoresis
Ap	Ampicillin
APS	Ammonium persulfate
BL21/	*E. coli* production strain
BL21 69/	*E. coli* production strain harbours plasmid pMCS69, encoding PhaA and PhaB enzymes
BSA	Bovine serum albumin
BCG vaccine strain	Live-attenuated *Mycobacterium bovis* Bacile Calmette-Guerin vaccine strain
CFP10	The 10-kDa culture filtrate protein
CFP10-PhaC	The 10-kDa culture filtrate protein–PHA synthase
CFP10-Rv3615c-PhaC-ESAT6	The 10-kDa culture filtrate protein-Rv3615c-PHA synthase-the 6-kDa early secretory antigenic target
Cm	Chloramphenicol
DMSO	Dimethylsulfoxide
DNA	Deoxyribonucleic acid
DNAase	Deoxyribonuclease
dNTPs	Deoxyribonucleotide triphosphates
DTH	Delayed-type hypersensitivity
ECFP	Enhanced cyan fluorescent protein
ECFP-PhaC(C319A)-[GB1]3	Enhanced cyan fluorescent protein-inactive PHA synthase-triple IgG binding domain of protein G
ELISA	Enzyme-linked immunosorbent assay
EtOH	Ethanol
ESAT6	The 6-kDa early secretory antigenic target
ESAT6-PhaC	The 6-kDa early secretory antigenic target–PHA synthase

EYFP	Enhanced yellow fluorescent protein
EYFP-PhaC(C319A)-[GB1]3	Enhanced yellow fluorescent protein-inactive PHA synthase-triple IgG binding domain of protein G
FPs	Fluorescent proteins
FP beads	Fluorescent protein beads
FP-PhaC(C319A)	Fluorescent protein-inactive PHA synthase
g	Gravity/gram
[GB1]3	Triple IgG binding domains of protein G
GFP	Green fluorescent protein
GFP beads	Green fluorescent protein beads
GFP-PhaC(C319A)	Green fluorescent protein-inactive PHA synthase
HcR	Far red protein HcRed
HcR-PhaC(C319A)-[GB1]3	Far red protein HcRed-inactive PHA synthase-triple IgG binding domains of protein G
HRP	Horseradish peroxidase
IFNγ	Interferon-γ
IgG	Immunoglobulin G
IPTG	Isopropyl â-D-1-thiogalactopyranoside
kDa	Kilo Daltons
λ-DNA	Phage lambda DNA
LacZ	β-galactosidase
LB	Luria-Bertani (broth)
MalE	Maltose binding domain
Maldi-TOF/MS	Matrix-assisted laser desorption ionization time-of-flight mass spectrometry
OD	Optical density
OpdA	Organophosphohydrolases
PCR	Polymerase chain reaction
PhaA	β-ketothiolase
PHAs	Polyhydroxyalkanoic acids
PHA_{SCL}	Short chain length PHAs
PHA_{MCL}	Medium chain length PHAs

PhaB	Acetoacetyl-CoA reductase
PhaC	PHA synthase
PhaC-[GB1]3	PHA synthase-triple IgG binding domains of protein G
PhaC(C319A)	Inactive PHA synthase
PhaE	Type III PHA synthase subunit
PhaP	Phasin
PhaR	Phasin regulatory protein
PHB	Poly(3-hydroxybutyric acid)
PPDs	Purified protein derivatives
PPD-A	Avian PPD
PPD-B	Bovine PPD
REs	Restriction endonucleases
Rv3615c-PhaC	Rv3615c–PHA synthase
SD	Standard deviation
SEM	Scanning Electron Microscopy
SDS-PAGE	Sodium dodecyl sulphate polyacrylamide gel electrophoresis
TB	Tuberculosis
TBE	Tris-Borate-EDTA buffer
TEM	Transmission and Electron Microscopy
TEMED	Tetramethylethylenediamine
Tet	Tetracycline
TST	Tuberculin skin test
Tris	Trishydroxymethylaminomethane
v/v	Volume per volume
w/v	Weight per volume
x	AVTS tetrapeptide extension
X-Gal	5-bromo-4-chloro-3-indolyl-beta-D-galactopyranoside
xECFP-PhaC(C319A)-[GB1]3	AVTS tetrapeptide extension-enhanced cyan fluorescent protein-inactive PHA synthase-triple IgG binding domain of protein G

xEYFP-PhaC(C319A)-[GB1]3	AVTS tetrapeptide extension-enhanced yellow fluorescent protein-inactive PHA synthase-triple IgG binding domain of protein G
xGFP-PhaC(C319A)-MalE	AVTS tetrapeptide extension-green fluorescent protein-inactive PHA synthase-maltose binding domain
xGFP-PhaC-MalE	AVTS tetrapeptide extension-green fluorescent protein- PHA synthase-maltose binding domain
xGFP-PhaC(C319A)-ZZ	AVTS tetrapeptide extension-green fluorescent protein-inactive PHA synthase-double IgG binding domains of protein A
xGFP-3xFe-PhaC(C319A)-ZZ	AVTS tetrapeptide extension-green fluorescent protein-triple iron-binding peptides-inactive PHA synthase-double IgG binding domains of protein A
xGFP-PhaC(C319A)-ZZ-3xFe	AVTS tetrapeptide extension-green fluorescent protein-inactive PHA synthase-double IgG binding domains of protein A-triple iron-binding peptides
xHcR-PhaC(C319A)-[GB1]3	AVTS tetrapeptide extension-far red protein HcRed-inactive PHA synthase-triple repeats of IgG binding domain of protein G
XL1-Blue	*E. coli* cloning strain
ZZ	Double IgG binding domain of protein A
ZZPhaC	Double IgG binding domain of protein A-active PHA synthase

List of Figures

List of Tables

Chapter 1: Introduction

Polyhydroxyalkanoic acids (PHAs) are naturally occurring bacterial polyesters which serve as a carbon and energy storage for bacteria (Grage et al., 2009; Rehm, 2003). Active PHA synthase, PhaC, is the key enzyme required for PHA biosynthesis and PHA bead self-assembly in the presence of a suitable substrate (Qi & Rehm, 2001; Rehm, 2007; Taguchi & Doi, 2004). PhaC remains covalently attached to the surface of PHA beads during the self-assembly process (Grage et al., 2009; Rehm, 2003). A variety of foreign proteins have been successfully displayed on the surface of PHA beads by using protein engineering of PhaC and other PHA-surface-associated proteins (Blatchford, Scott, French, & Rehm, 2012; Brockelbank, Peters, & Rehm, 2006; Parlane et al., 2011). PHA beads could act as bio-beads for protein display due to their various properties, including biodegradability, biocompatibility, and non-toxicity (Grage et al., 2009). The PHA-based protein production and immobilization technology provides a self-assembly, one-step, and cost-effective protein production system (Blatchford, Scott, French, & Rehm, 2012; Grage et al., 2009; Parlane et al., 2011).

Class I PHA synthase can be inactivated by the replacement of cysteine residue 319 with alanine. The inactive synthase PhaC (C319A) is unable to mediate PHA bead formation. However, expressing a recombinant gene cassette, encoding a green fluorescent protein-PhaC (C319A)-a foreign protein fusion, leads to the self-assembly of functionalized green fluorescent protein beads (GFP beads) (Jahns et al., 2013). Similar to protein immobilization on PHA beads, many foreign proteins can be displayed on the surface of protein beads by genetic engineering of genes encoding the GFP-PhaC (C319A) fusion (Jahns et al., 2013). Indeed, it has been shown that PHA and protein beads are suitable for a variety of applications by displaying the protein of interest on the beads' surface (Blatchford, Scott, French, & Rehm, 2012; Grage et al., 2009; Jahns et al., 2013; Parlane et al., 2012; Rasiah & Rehm, 2009).

In this chapter, PHAs (Section 1.1), PHA synthases (Section 1.2), PHA bead formation (Section 1.3), and protein immobilization on PHA beads (Section 1.4) will be reviewed. The inactivation (C319A) of PHA synthase PhaC (Section 1.5), a fluorescent reporter protein GFP (Section 1.6), the formation of GFP beads by engineering of the GFP-PhaC

(C319A) fusion (Section 1.7), and protein immobilization on fluorescent protein beads (Section 1.8) will also be described. Finally, the main objective of this study, which was to assess the functionality of target proteins, including specific bovine tuberculosis (TB) antigens, IgG binding domains, and iron-binding peptides, displayed on the surface of different types of bio-beads facilitating the generation of various diagnostic reagents (Section 1.9), will be introduced.

1.1 Polyhydroxyalkanoate

PHAs are naturally occurring biopolyesters, consisting of hydroxyalkanoic acids linked by oxoester bonds. PHAs are synthesized by a variety of bacteria and some Archaea (Hezayen, Steinbuchel, & Rehm, 2002; Rehm, 2007) during imbalanced nutrient conditions when an excess of carbon source is available (Campisano, Overhage, & Rehm, 2008; Grage et al., 2009). They are deposited as spherical water-insoluble inclusions in the cytoplasm and serve as an energy and carbon source (Grage et al., 2009; Rehm, 2003). PHA beads are comprised of an amorphous hydrophobic polyester core surrounded by a phospholipid monolayer and embedded proteins, including PHA synthase and depolymerase, as well as structural proteins (Grage et al., 2009; Rehm, 2003). The size of PHA beads ranges between 100 to 500 nm in diameter (Grage et al., 2009; Steinmann, Christmann, Heiseler, Fritz, & Kolmar, 2010). Poly(3-hydroxybutyric acid) (PHB) synthesized from 3-hydroxybutyrate is the most common form of PHA isolated from bacteria (Campisano, Overhage, & Rehm, 2008; Kikkawa et al., 2005) and was the first PHA polymer identified by Lemoigne in 1926 in *Bacillus megaterium* (Lemoigne, 1926). In general, each bacterial cell produces 5 to 10 PHA beads (Grage et al., 2009; Koller, Salerno, Dias, Reiterer, & Braunegg, 2010), the mass of which can accumulate more than 80% of cellular dry weight (Lee, 1996; Madison & Huisman, 1999).

PHAs are valued for their biodegradable and thermoplastic properties which are greatly influenced by the length and composition of its hydroxyl fatty acids. So far, over 150 different hydroxyalkanoic acids have been identified as constituents of PHAs (Keshavarz & Roy, 2010; Rehm, 2003, 2007). These biopolyesters are classified into two major classes based on their chemical structure: short chain length PHAs (PHA_{SCL})

which contain 3-5 carbon atoms, and medium chain length PHAs (PHA_{MCL}) which contain 6-14 carbon atoms. PHA_{SCL} are hard and brittle, and have a high level of crystallinity and a high melting temperature. However, PHA_{MCL} are more elastomeric, and have a low degree of crystallinity and low melting temperature (Hazer & Steinbuechel, 2007; Rehm, 2003, 2007).

PHAs have been extensively studied and exploited in industrial and medical fields due to their characteristic properties, such as being biodegradable, renewable, elastomeric, biocompatible, and modifiable (Blatchford, Scott, French, & Rehm, 2012; Grage et al., 2009; Hazer & Steinbuechel, 2007; Legat, Gruber, Zangger, Wanner, & Stan-Lotter, 2010; Rehm, 2003, 2006). For example, in industrial fields, petroleum-based plastics are not biodegradable, which could be a major environmental issue. However, biologically produced PHAs are from renewable sources and are biodegradable, which makes them favorable alternatives for use in the packaging industry (Keshavarz & Roy, 2010; Kikkawa et al., 2005; Zheng et al., 2006). In addition, their biocompatibility makes PHAs suitable materials for medical applications without inducing unwanted immune responses. Furthermore, PHAs are generally well tolerated by mammalian systems (Chung, Kim, Kim, & Rhee, 2003; Hazer & Steinbuechel, 2007; Legat, Gruber, Zangger, Wanner, & Stan-Lotter, 2010). This has allowed PHAs to be used in implants, such as bone scaffolding in medical applications, due to their biocompatibility and elastomeric properties (Hazer & Steinbuechel, 2007). These biopolyesters have also been extensively applied in recombinant DNA technologies. In particular, many foreign proteins, for instance organophosphohydrolase, can be displayed on the surface of PHA beads by genetic engineering of embedded proteins such as PHA synthase or phasin (Blatchford, Scott, French, & Rehm, 2012; Grage et al., 2009). Moreover, these foreign protein–displaying PHA beads have been successfully synthesized by recombinant *Escherichia coli* (Blatchford, Scott, French, & Rehm, 2012; Peternel & Komel, 2011).

1.2 PHA synthases

Active PHA synthases are the key enzyme required for PHA biosynthesis and PHA bead formation in the presence of a suitable substrate. These enzymes catalyze the polymerization of different (*R*)-hydroxyacyl-CoA thioester monomers to generate PHAs

with the release of CoA (Grage et al., 2009; Rehm, 2003). Currently, more than 88 PHA synthase genes from 68 different bacteria have been identified (Rehm, 2007). Below, I describe the classification and structural features of PHA synthases.

1.2.1 Classification of PHA synthases

PHA synthases have been classified into four different classes based on their substrate specificity, subunit composition, and primary structure (Table 1) (Rehm, 2003, 2007; Yuan et al., 2001).

Table 1.

PHA Synthases Are Assigned into Four Major Classes

Class	Subunits	Species	Substrate
I	PhaC ~60-73 kDa	*Cupriavidus necator*	$3HA_{SCL}$-CoA (~C3-C5) $4HA_{SCL}$-CoA, $5HA_{SCL}$-CoA, $3MA_{SCL}$-CoA
II	PhaC ~60-65 kDa	*Pseudomonas aeruginosa*	$3HA_{MCL}$-CoA (~≥C5)
III	PhaC PhaE ~40 kDa ~40 kDa	*Allochromatium vinosum*	$3HA_{SCL}$-CoA ($3HA_{MCL}$-CoA [~C6-C8], 4HA-CoA, 5HA-CoA)
IV	PhaC PhaR ~40 kDa ~22 kDa	*Bacillus megaterium*	$3HA_{SCL}$-CoA

(Source: Rehm, 2003, p. 17).

Class I and II PHA synthases consist of a single subunit (PhaC) with a molecular mass between 61 kDa and 73 kDa, while Class III and IV PHA synthases have an additional subunit PhaE and PhaR, respectively (Qi & Rehm, 2001). Class I PHA synthases are mainly found in *Cupriavidus necator* (also known as *Ralstonia eutropha*), and preferentially use short-chain length 3-hydroxy fatty acids for PHA production. In contrast, Class II PHA synthases, mostly found in *Pseudomonas aeruginosa*, preferentially utilize medium-chain length 3-hydroxy fatty acids for PHA synthesis (Rehm, 2003; Ren, de Roo, Kessler, & Witholt, 2000). In comparison, Class III PHA

synthases, mainly found in *Allochromatium vinosum*, are comprised of two subunits, PhaC and PhaE, which are of similar molecular weight (MW = 40 kDa), and utilize both short and medium-chain length 3-hydroxy fatty acids for PHA production. In spite of these similarities, PhaC and PhaE of Class III synthases are very different at the primary structural level. The PhaC subunit of Class III synthases exhibits 21%–28% amino acid similarity to Class I and II PhaC, but the subunit PhaE does not show any amino acid similarity to PhaC (Qi & Rehm, 2001; Rehm, 2007). Class IV PHA synthases, mainly found in *Bacillus megaterium*, are similar to Class III synthases in which PhaE is replaced with PhaR, a protein with a MW of 22 kDa. Class IV synthases also prefer the same substrate as Class I synthases (short-chain length 3-hydroxy fatty acids) for PHA production (Rehm, 2003, 2007).

1.2.2 Structural features of PHA synthases

Alignments of the amino acid sequence of the 88 PHA synthases from a variety of bacteria have shown that although the N-terminal region is highly variable, there are at least six conserved amino acid blocks throughout the protein (Figure 1) (Rehm, 2007). Truncation analysis of the Class I PHA synthase of *C. necator* has revealed that the first 100 amino acids of its highly variable N-terminal region are dispensable for PHA production (Rehm, 2003). In contrast, the C-terminal region is highly conserved, suggesting its critical role in synthase activity (Rehm, Antonio, Spiekermann, Amara, & Steinbuchel, 2002; Schubert, Kruger, & Steinbuchel, 1991). In particular, the C-terminus of Class I and II PHA synthases is highly hydrophobic and functions as a binding domain to mediate the contact of the synthase with the hydrophobic polyester core (Rehm, 2003). Contrastingly, no hydrophobic C-terminal region has been identified in the PhaC subunit of Class III and IV PHA synthases. However, the second subunit, PhaE or PhaR, of these two classes has been suggested to replace the hydrophobic C-terminus of the PhaC subunit and might facilitate the binding of synthases to the hydrophobic polyester core (Jahns & Rehm, 2009; Rehm, 2003).

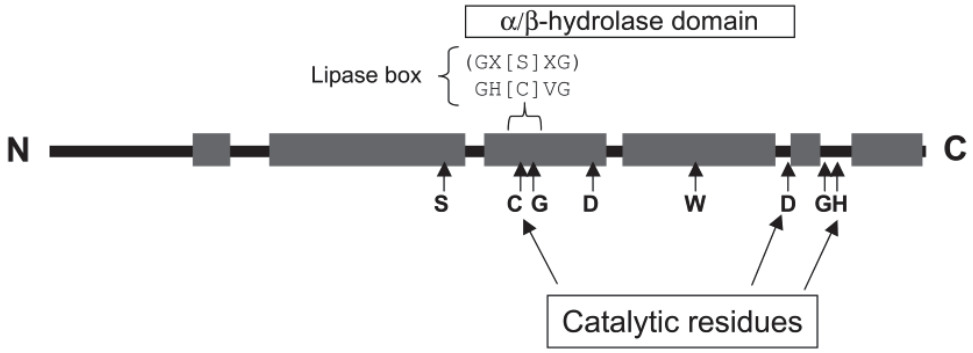

***Figure 1*. Primary structure of Class I PHA synthase PhaC of *C. necator*.** Six conserved blocks, eight amino acids and a conserved α/β-hydrolase domain are indicated by grey rectangles, arrows, and the upper rectangle, respectively (Source: Rehm, 2007, p. 44).

Sequence alignments of PHA synthases also show that they are homologous to lipases, members of the α/β-hydrolase superfamily. The α/β hydrolase domain, located at the C-terminus of PHA synthases (Figure 1), is essential for the synthase function (Rehm, 2003, 2007). The core of the α/β hydrolase fold is a α/β sheet composed of eight β-sheets connected by α-helices (Ollis et al., 1992). Enzymes of this superfamily contain highly conserved catalytic triads consisting of an active site nucleophile (serine, cysteine, or aspartate), acidic amino acid (aspartate or glutamate), and histidine residue (Carr & Ollis, 2009). The nucleophile is typically located at a conserved elbow-like structure between β strand and α helix (Ollis et al., 1992). Furthermore, all the PHA synthases contain a highly conserved lipase box (GX[S/C]XG) in the C-terminal region in which the active site nucleophile serine of the lipase is replaced by a cysteine residue (Figure 1) (Grage et al., 2009; Rehm, 2007).

PHA synthases exist in equilibrium as monomers and dimers, and the dimeric forms have been shown to be the active form (Rehm, 2007; Zhang, Kolvek, Lenz, & Goodwin, 2003). The presence of substrate induces dimerization of PHA synthases, which polymerize available substrates, forming PHA beads (Rehm, Qi, Beermann, Hinz, & Steinbuchel, 2001). Mutagenic analysis shows that the highly conserved tryptophan-425 of the Class I PHA synthase from *C. necator* is required to generate a hydrophobic surface for dimerization of PhaC subunits by mediating protein-protein interactions (Gerngross et al., 1994; Jia et al., 2001). Class I and II PHA synthases form homodimers. The dimerized PHA synthase is the key enzyme required for the formation

of PHA beads (Jia et al., 2001). However, Class III and IV PHA synthases involve the formation of multimeric heterodimers (Rehm, 2007).

1.3 Formation of PHA beads

PHA biosynthesis occurs as soon as the substrate (*R*)-3-hydroxyacyl-CoA thioesters are made available in the cytoplasm (Philip, Keshavarz, & Roy, 2007; Rehm, 2007; Rehm et al., 2002). As described in Section 1.1, PHAs are categorized into two major classes: PHA_{SCL} and PHA_{MCL} (Hazer & Steinbuechel, 2007; Rehm, 2003, 2007), which are mainly determined by the substrate specificity of the PHA synthases (Rehm, 2007). The biosynthesis of PHA_{SCL} and PHA_{MCL} has been extensively studied in *C. necator* and *P. aeruginosa,* which produce Class I and II PHA synthases, respectively (Grage et al., 2009; Philip, Keshavarz, & Roy, 2007; Rasiah & Rehm, 2009; Rehm, 2007). The formation of PHA beads is a self-assembly process (Rehm, 2003, 2007) and starts at discrete cytoplasmic regions in bacteria (Jendrossek, 2005; Peters & Rehm, 2005).

1.3.1 Biosynthesis of PHA

PHA biosynthesis relies on three key enzymes: PHA synthase (PhaC), β-ketothiolase (PhaA), and acetoacetyl-CoA reductase (PhaB), which are encoded by genes *phaC*, *phaA*, and *phaB,* respectively (Qi & Rehm, 2001; Rehm, 2007; Taguchi & Doi, 2004). Class I and II PHA synthases are encoded by *phaC*. In contrast, Class III and IV synthases require expression from both *phaC* and *phaE/phaR* (Table 1) (Rehm, 2007). These PHA biosynthetic genes are always clustered together in bacterial genomes. For instance, the *phaA*, *B,* and *C* genes in *C. necator* are located in the *phaCAB* operon (Grage et al., 2009; Rehm, 2007; Rehm et al., 2002), and the synthase gene *phaC* is constitutively expressed at low levels (Rehm, 2007). Enzymes PhaA and PhaB synthesize (*R*)-3-hydroxyacyl-CoA thioesters, which are polymerized, forming PHAs by an active synthase, PhaC dimer (or PhaC and PhaE/PhaR for Class III/IV PHA synthases, Peoples, 1989a, 1989b).

The biosynthesis of PHA_{SCL} and PHA_{MCL} is dependent on the carbon source and the class of PHA synthase. An example of PHAs composed of short-chain length 3-hydroxy fatty acid is PHB, which is commonly found in *C. necator*–producing Class I PHA synthase (Campisano, Overhage, & Rehm, 2008; Kikkawa et al., 2005). In particular, PhaA condenses two acetyl CoA molecules to generate acetoacetyl-CoA, which is then reduced to (*R*)-3-hydroxybutyryl-CoA by NADPH–dependent enzyme PhaB. Ultimately, dimerized PhaC catalyzes the polymerization of monomeric (R)-3-hydroxybutyryl-CoA to generate PHB with the release of CoA (Figure 2) (Peoples, 1989a, 1989b). *P. aeruginosa*–producing Class II PHA synthase has been shown to produce PHA_{MCL} (Rehm, 2003; Ren, de Roo, Kessler, & Witholt, 2000). Indeed, various intermediates produced from the fatty acid *de novo* synthesis and/or fatty acid β-oxidation pathways act as precursor molecules, which are converted into (*R*)-3-hydroxyacyl-CoA thioesters, the substrates of PhaC. These substrates are finally polymerized into PHA_{MCL} (Figure 2) (Grage et al., 2009; Rehm, 2007).

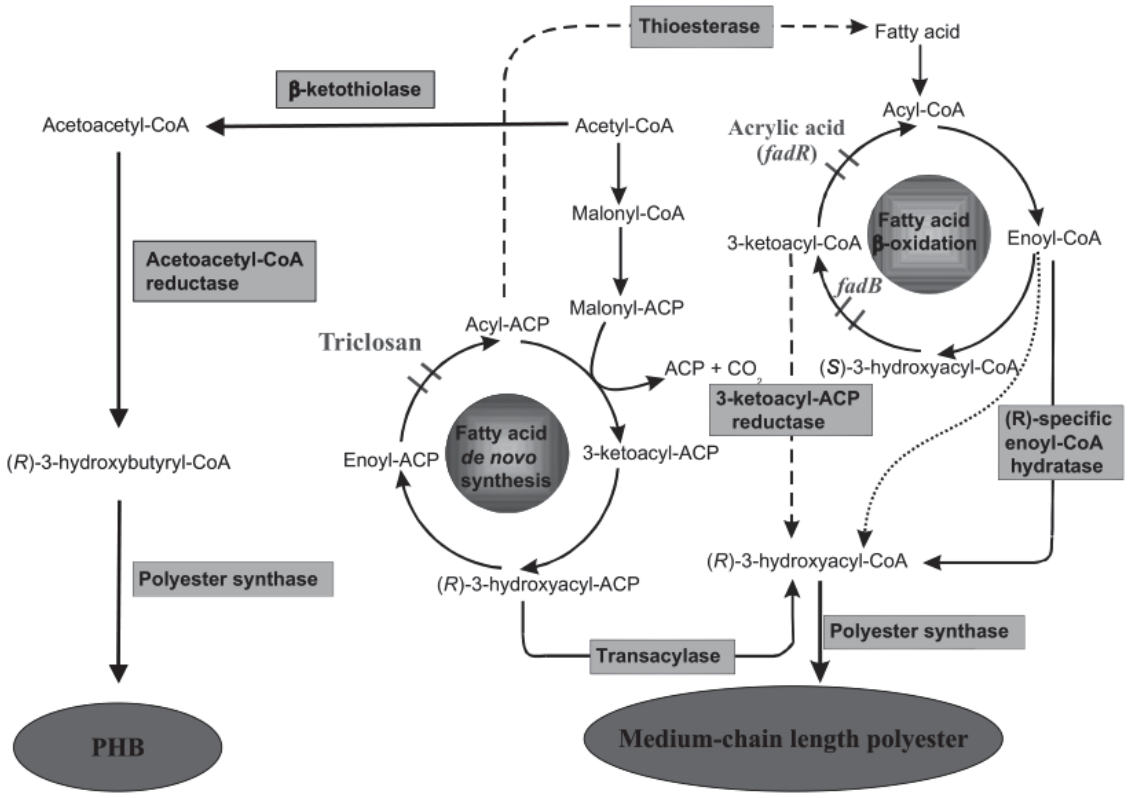

Figure 2. **The biosynthesis pathways of PHAs composed of short-chain length or medium-chain length 3-hydroxy fatty acids** (Source: Rehm, 2007, p. 52).

1.3.2 Self-assembly of PHA beads

Gerngross and Martin first demonstrated *in vitro* synthesis of PHAs and self-assembly of spherical beads in 1995 by utilizing purified PHA synthases and substrates. This *in vitro* study shows that the PHA synthases are able to carry out the self-assembly process of PHAs into spherical beads (Gerngross & Martin, 1995). The exact mechanism of PHA bead assembly is not fully understood; however, two models of bead assembly, the micelle model and the budding model (Figure 3), have been proposed.

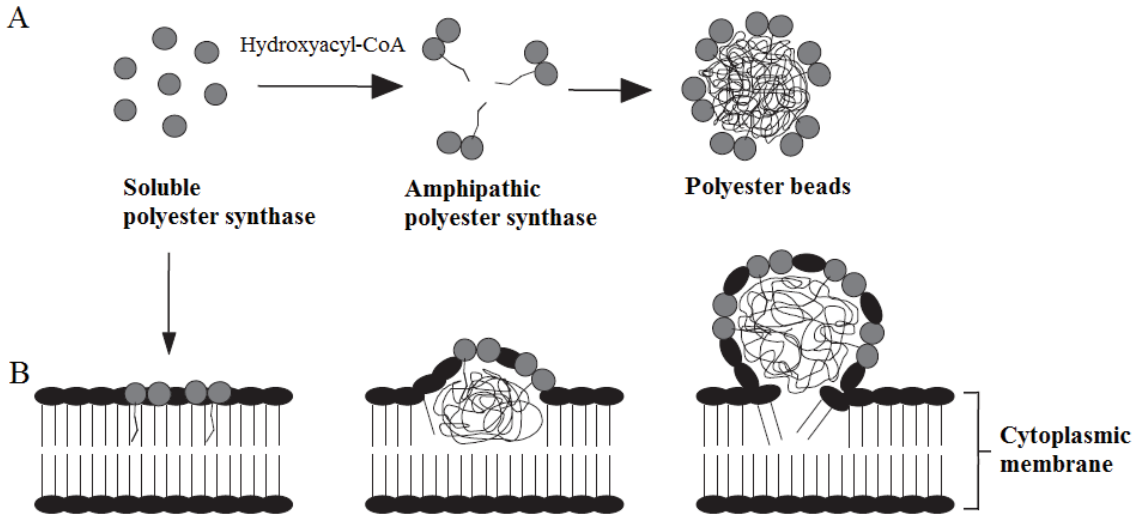

Figure 3. **Models of PHA bead formation.** (A) Bead formation by micelle model. (B) Bead formation by budding model from cytoplasmic membrane (Source: Rehm, 2007, p. 50).

The micelle model is based on the property of an amphipathic molecule containing an elongated PHA chain with a dimerized synthase. In particular, the growing PHA chain remains covalently attached to the PHA synthase (Hezayen, Steinbuchel, & Rehm, 2002; Rehm et al., 2002), and increased hydrophobicity of the chain converts the soluble synthase into an amphipathic molecule (Grage et al., 2009; Rehm, 2007). The growing PHA chains aggregate to form the hydrophobic core of the beads, while the active synthases remain attached at the surface (Grage et al., 2009; Rehm, 2007). Currently, the micelle model is supported by PHA beads formation *in vitro* and in the absence of the cytoplasmic membrane (Rehm, 2007). However, some studies using electron microscopy have shown that a lipid membrane-like structure can be found at the surface of isolated PHA beads (Lundgren, Merrick, & Pfister, 1964; Mayer & Hoppert, 1997)

and beads in intact cells, implying that PHA bead assembly occurs via the budding mode (Dunlop & Robards, 1973; Jensen & Sicko, 1971).

The budding model suggests soluble PHA synthases are associated with the inner cytoplasmic membrane (Thomson, Summers, & Sivaniah, 2010), and growing PHA chains are synthesized and assembled into spherical beads between the phospholipid bilayer (Rehm, 2007). Eventually, intracellular PHA beads are formed through budding from the cytoplasmic membrane and surrounded by a phospholipid monolayer with PHA synthases and other proteins attached (Grage et al., 2009; Rehm, 2007). Recently, the budding model of PHA bead formation has been supported by newly emerging evidence. For instance, time course studies have indicated that PHA beads are not randomly distributed in the cytosol and are close to the cytoplasmic membrane in the early stage of bead formation (Tian, Sinskey, & Stubbe, 2005). Fluorescence microscopy has also shown that emerging PHA beads are located at the cell poles and the cell division sites, which are associated with the cytoplasmic membrane (Jendrossek, 2005; Peters & Rehm, 2005).

1.4 Immobilization of functionalized proteins on PHA beads

Protein purification is often required to purify proteins from a complex mixture without denaturing their biological activity or irreversibly altering the protein structure (Grage et al., 2009). This could be achieved by using affinity-based purification techniques that are dependent on a highly specific interaction between a target protein and an immobilization matrix (Arnau, Lauritzen, Petersen, & Pedersen, 2006). This interaction generally requires the fusion of a purification tag, such as polyHis-tag or a polyArg-tag, to the target protein. However, the addition of a purification tag may alter the intrinsic properties of the target protein, including solubility, net charge, and protein folding (Arnau, Lauritzen, Petersen, & Pedersen, 2006; Waugh, 2005). This problem may be overcome by cleaving the affinity tag enzymatically from the target protein after purification (Esposito & Chatterjee, 2006). However, removal of the tag can cause soluble proteins to revert to their insoluble form. It is possible that some proteins might not be present in their true, native, soluble form, but exist as ‘soluble aggregates’ through interactions with the purification tag (Nomine et al., 2001; Waugh, 2005). Thus,

the affinity-based protein purification must be optimized individually for each desired protein. Expensive enzymatic cleavage and multiple separation steps also make this method very costly and time-consuming (Grage et al., 2009).

Protein immobilization is used to attach a desired protein to a solid support. Studies have shown that immobilization could increase the stability of the target proteins and enhance protein activity due to the increased stability (Brady & Jordaan, 2009; Steinmann, Christmann, Heiseler, Fritz, & Kolmar, 2010). However, many conventional protein immobilization techniques require reagents to purify proteins and their matrices, and subsequently use non-specific absorption or chemical cross-linking to display proteins on solid supports (Hanefeld, Gardossi, & Magner, 2009). Hence, the cost and multiple immobilization steps make conventional approaches cumbersome. Therefore, it would be desirable to have a technique in which the target protein and microbead (immobilization matrix) are produced by the same microbial cell, and the protein is intracellularly immobilized directly to the surface of the bead. Subsequently, the beads displaying the target protein can be simply purified from lysed cells by centrifugation (Steinmann, Christmann, Heiseler, Fritz, & Kolmar, 2010).

The large-molecular-weight of PHA beads with the surface-associated proteins (for example, PHA synthase PhaC or phasin PhaP) and the cost-effective production make the beads a suitable tool for protein purification and immobilization (Grage et al., 2009; Grage, Peters, & Rehm, 2011; Parlane et al., 2011). Banki, Gerngross, and Wood (2005) developed a protein purification method which exploits two technologies: intracellular PHA bead production and intein-mediated self-splicing. In this method, the target protein is fused to the C-terminus of PhaP, which acts as an affinity tag and attaches to the PHA beads. Both the fusion protein and the PHA beads are coproduced in recombinant *E. coli* cells, and the target protein binds to the beads via the affinity tag PhaP. This strategy eliminates the need for a further cross-linking step because the target protein is directly immobilized on the surface of PHA beads by one step (Banki, Gerngross, & Wood, 2005). The PHA beads displaying the target protein are purified by cell disruption and centrifugation. The target protein can then be released by intein self-cleavage. Other proteins, including the maltose binding protein and β-galactosidase (LacZ) and chloramphenicol acetyltransferase, have been successfully purified by the same technique (Banki, Gerngross, & Wood, 2005). Other similar methods have been

described to purify and immobilize foreign proteins by using PHA beads with surface-associated proteins. For instance, Grage, Peters, and Rehm (2011) demonstrate that PhaC acts as an affinity tag to attach the target protein on the surface of PHA beads. After isolation of the beads, the target protein can be liberated by using a cleavable site which is recognized by an enterokinase. Overall, the use of PHA beads for protein purification and immobilization is relatively cheaper than conventional methods. Moreover, the cost-effective one-step generation and isolation of foreign proteins displaying PHA beads could be very useful for large-scale industrial protein production, purification, and immobilization (Grage et al., 2009).

1.4.1 Application of PHA beads as bio-beads for various protein display

PHA beads could act as bio-beads due to their various characteristics. PHA beads are fully biodegradable and non-toxic (Grage et al., 2009). In addition, they are unlikely to activate an immune response, and are well tolerated by mammalian systems due to their biodegradability and biocompatibility (Chung, Kim, Kim, & Rhee, 2003; Hazer & Steinbuechel, 2007; Legat, Gruber, Zangger, Wanner, & Stan-Lotter, 2010). PHA beads are small, ranging between 100 to 500 nm in diameter (Grage et al., 2009; Steinmann, Christmann, Heiseler, Fritz, & Kolmar, 2010). Target proteins, such as galactose oxidase, immobilized on the surface of PHA beads have been shown to possess increased stability and activity when compared to non-immobilized proteins. Therefore, PHA beads are able to increase the stability of diagnostic reagents when target proteins are immobilized on their surfaces (Steinmann, Christmann, Heiseler, Fritz, & Kolmar, 2010).

Many studies have shown that PHA beads could serve as a versatile platform for the display of desired proteins, and this could be achieved by fusing them to embedded proteins (Blatchford, Scott, French, & Rehm, 2012; Steinmann, Christmann, Heiseler, Fritz, & Kolmar, 2010). For example, PhaC remains covalently attached to the surface of PHA beads during the self-assembly process (Gerngross, Reilly, Stubbe, Sinskey, & Peoples, 1993; Grage et al., 2009; Rehm, 2003). Thus, target proteins can be covalently displayed on the surface of PHA beads via PhaC (Blatchford, Scott, French, & Rehm, 2012). Protein engineering of PhaC has shown that variable regions of the N- and C-terminus of PhaC are dispensable and can be functionally replaced by foreign

proteins without affecting PHA bead formation (Atwood & Rehm, 2009). This has allowed foreign protein functions, such as enzymes, binding domains, and antigens, to be successfully displayed on the surface of PHA beads (Blatchford, Scott, French, & Rehm, 2012; Brockelbank, Peters, & Rehm, 2006; Parlane et al., 2011). Multiple fusion of several target proteins and the co-production of different PhaC fusion proteins allow different protein functions to be co-displayed on the same PHA bead (Atwood & Rehm, 2009; Jahns, Haverkamp, & Rehm, 2008; Jahns & Rehm, 2009; Mullaney & Rehm, 2010). As described in Section 1.4, foreign proteins can be immobilized on the surface of PHA beads for subsequent cleavage and purification (Backstrom, Brockelbank, & Rehm, 2007; Grage, Peters, & Rehm, 2011; Hooks, Blatchford, & Rehm, 2013; Peters & Rehm, 2005). PHA bead-displaying antigens have been found to be immunogenic *in vivo* and can activate specific Th1 and Th2 immune responses, leading to protective immunity (Parlane et al., 2011, 2012; Parlane, Wedlock, Buddle, & Rehm, 2009).

Hence, PHA beads are suitable for a variety of applications by displaying the protein of interest on the beads' surface (Grage et al., 2009; Steinmann, Christmann, Heiseler, Fritz, & Kolmar, 2010). PHA bead-displaying foreign proteins, such as antigens, are able to serve as various diagnostic reagents in medical fields (Grage et al., 2009; Steinmann, Christmann, Heiseler, Fritz, & Kolmar, 2010). The PHA bead technology can also be applied in other industries. For example, Organophosphohydrolases (OpdA) is able to hydrolyse and detoxify organophosphate pesticides, commonly used in agriculture (Jeyaratnam, 1990). PHA beads have also been used to display amylase, an enzyme that catalyses the hydrolysis of starch into smaller and more soluble compounds (Rasiah & Rehm, 2009; Shewale & Pandit, 2007). Thus, PHA beads displaying these proteins can be applied for bioremediation (OpdA beads) and food production (amylase beads) industries (Blatchford, Scott, French, & Rehm, 2012; Rasiah & Rehm, 2009).

1.5 Inactivation of PHA synthases

As described in Section 1.3, the biosynthesis and self-assembly of PHA beads are based on the presence of active PHA synthases and the availability of substrates (Grage et al., 2009; Rehm, 2007). Recently, it was also shown that the formation of intracellular PHA

beads is completely inhibited when amino acid residiues of the conserved catalytic triad are replaced in PHA synthases (Jahns et al., 2013).

The conserved catalytic triad plays an important role in the activity of all PHA synthases. Structural models of the four Classes of PHA synthase have been established, based on the α/β-hydrolase fold (Figure 4) (Rehm, 2003; Valappil, Boccaccini, Bucke, & Roy, 2007). Site-specific mutagenesis has shown that the residues cysteine-319, aspartate-480, and histidine-508 of the Class I synthase PhaC from *C. necator* are directly involved in covalent catalysis (Jia et al., 2001; Qi & Rehm, 2001; Rehm, Antonio, Spiekermann, Amara, & Steinbuchel, 2002). The general base catalyst histidine-508 is thought to activate the catalytic nucleophile cysteine-319 (Rehm, 2006). The cysteine residues at 319 from each of the two monomers of the dimerized synthase provide two identical thiol groups to form a single catalytic site for the initiation and elongation reactions of PHA chains. In particular, one thiol group acts as the accepting site for the substrate 3-hydroxybutyryle-CoA, and the second thiol group carries out the priming and elongation (Rehm, 2007; Zhang, Kolvek, Lenz, & Goodwin, 2003). Moreover, the three catalytic triad residues (cysteine-aspartate-histidine) are highly conserved in all PHA synthases, and the catalytic cysteine residue is always located at the nucleophile elbow (Valappil, Boccaccini, Bucke, & Roy, 2007).

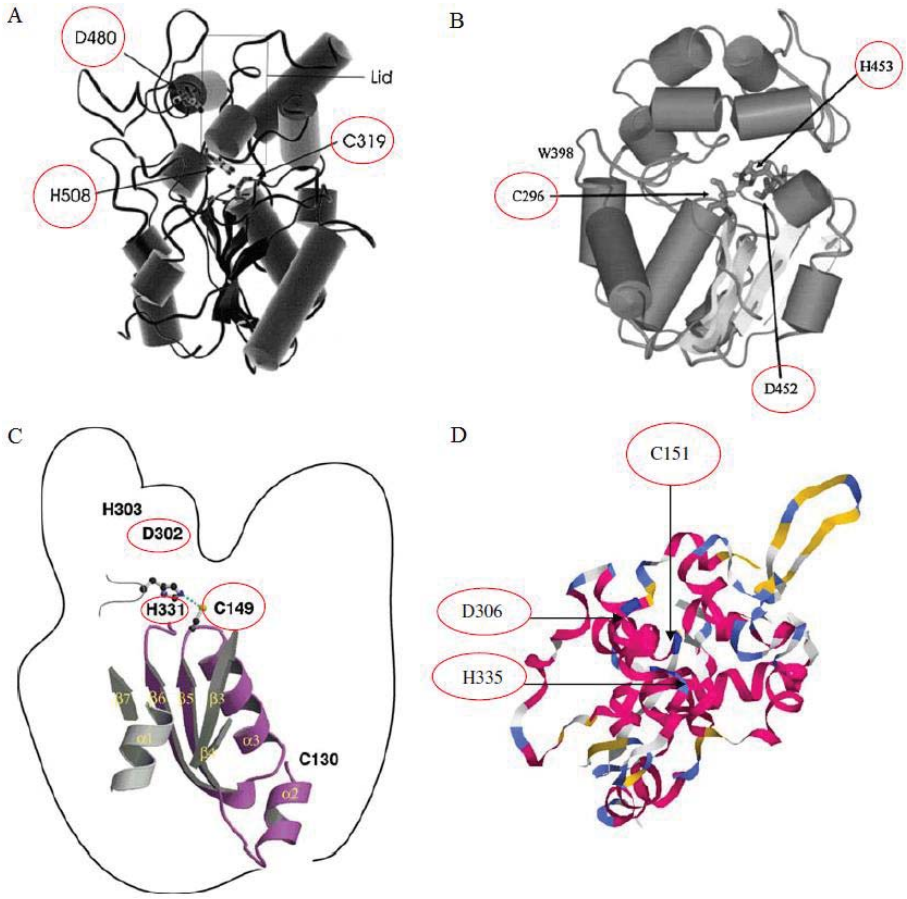

Figure 4. **Threading models of different classes of PHA synthase.** (A) Class I PhaC from *C. necator*; (B) Class II PhaC from *P. aeruginosa*; (C) Class III PhaC from *A. vinosum*; and (D) Class IV PhaC from *Bacillus cereus* SPV. The conserved catalytic triad residues (cysteine-aspartate-histidine) are encircled (Source: Valappil, Boccaccini, Bucke, & Roy, 2007, p. 9).

As described in Section 1.2, the active PHA synthase PhaC from *C. necator* is the key enzyme required for the production of PHB, the most common form of PHA (Peoples, 1989a, 1989b). However, Jahns et al. (2013) have shown that the use of alanine in substitution for the cysteine residue 319 of the Class I synthase PhaC from *C. necator* leads to inactivation of the synthase and completely inhibits the formation of PHA beads. Moreover, they have demonstrated that genetic engineering of inactive PhaC (C319A) could lead to the self-assembly of protein beads, while active PhaC tends to inhibit protein bead formation. For example, overproduction of a fusion protein containing GFP and inactive PhaC (C319A) results in the formation of large GFP protein beads only. In contrast, overproduction of a green fluorescent fusion protein containing active PhaC leads to the production of protein/PHA hybrid beads (Jahns et al., 2013).

1.6 Green fluorescent protein

Green fluorescent protein (GFP) is frequently used in scientific research due to its ability to emit green fluorescence. It was discovered in the 1950s in the jellyfish *Aequorea victoria* during a chemiluminescence study (Shimomura, Johnson, & Saiga, 1962). This fluorescent protein is also found in many other bioluminescent organisms (Zimmer, 2002). The structure of the GFP fold is an 11-stranded β-barrel with a coaxial α-helix. Located at the center of the β-barrel is a *p*-hydroxybenzylidene-imidazolidone chromophore (Ormo et al., 1996; Zimmer, 2002). The properly folded structure of GFP and molecular oxygen are required for the autocatalytic formation of chromophore and fluorescence emission. In particular, the chromophore is generated by the spontaneous cyclization and oxidation of the tripeptide Ser65-Tyr66-Gly67 of the native GFP fold (Cody, Prasher, Westler, Prendergast, & Ward, 1993; Heim, Prasher, & Tsien, 1994; Ormo et al., 1996).

GFP possesses a variety of interesting properties that can be exploited for many scientific applications. For instance, GFP is resistant to treatment with heat, alkaline pH, detergents, chaotropic salts, organic solvents, and a number of proteases (Ehrmann, Scheyhing, & Vogel, 2001). Moreover, GFP is an autofluorescent protein; thus, specific substrates or cofactors are not required (Naylor, 1999; Zimmer, 2002). It has also been shown that GFP does not alter the activity or localization of recombinant gene products and is not toxic to host cells in most cases (Zimmer, 2002).

1.7 Formation of GFP bead *in vivo*

GFP has been involved in the formation of protein inclusion bodies, which are large insoluble protein aggregates (beads) (de Groot, Espargaro, Morell, & Ventura, 2008; Garcia-Fruitos et al., 2005). Initially, these protein beads were thought to contain only misfolded and inactive proteins (de Groot, Espargaro, Morell, & Ventura, 2008). However, recently, it has been found that protein beads produced in recombinant bacteria contain properly folded and biologically active proteins (de Groot & Ventura, 2006; Garcia-Fruitos et al., 2005; Peternel, Jevsevar, Bele, Gaberc-Porekar, & Menart, 2008). Thus, bacterial protein beads are comprised of improperly folded proteins as well

as a significant amount of correctly folded and biologically active proteins (Garcia-Fruitos et al., 2012; Peternel & Komel, 2011). Protein beads possess some biological functions, such as fluorescence activity in terms of fluorescent proteins, due to the native structure of incorporated polypeptides which can be exploited for various biomedical and biotechnological applications (Garcia-Fruitos et al., 2009).

The schematic overview of PHA and GFP bead formation in recombinant *E. coli* is shown in Figure 5. As described in Section 1.2, active PHA synthases PhaC are responsible for the biosynthesis and self-assembly of PHA beads when suitable substrates are available (Figure 5A) (Grage et al., 2009; Rehm, 2003). However, PhaC activity is not specifically required for protein bead self-assembly (Jahns et al., 2013). In addition, a recent study has shown that a GFP-PhaC (C319A) fusion can be genetically engineered to self-assemble into biologically active GFP beads displaying various protein functionalities, such as IgG binding domains ZZ of protein A and GB1 of protein G (Jahns et al., 2013). Generally, the formation of GFP beads is found when recombinant genes are overexpressed by using a strong promoter, such as a T7 promoter (Jahns et al., 2013; Peters & Rehm, 2005). Protein beads are oval-shaped and are 0.5–1.5 μm in size, which is approximately 10 times larger than PHA beads (Jahns et al., 2013). The factors required for GFP bead formation are described below.

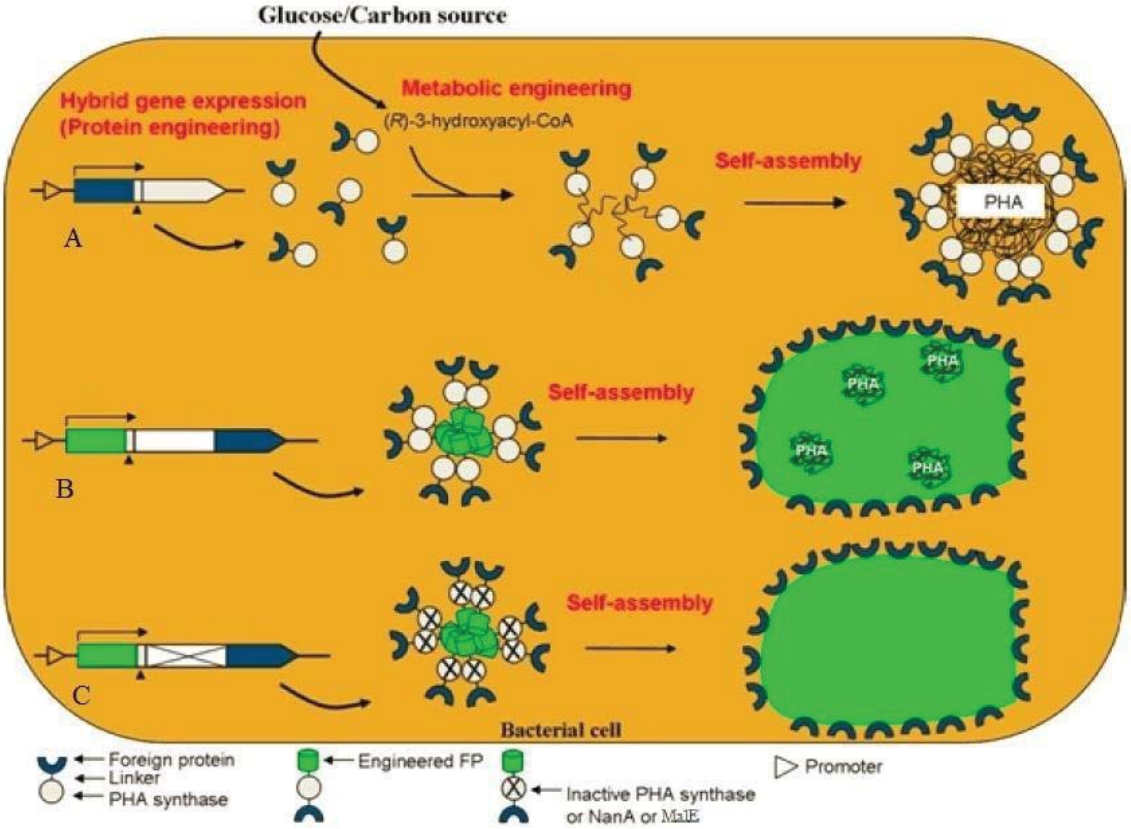

Figure 5. **Schematic overview of PHA and fluorescent protein bead formation in *E. coli*.** (A) Overproduction of fusion proteins containing active PhaC lead to self-assembly of PHA beads. (B) Overproduction of fusion proteins comprising N-terminally extended GFP, active PhaC, and a C-terminal fusion partner (for example, ZZ or GB1) lead to the formation of protein/PHA hybrid beads. (C) Overproduction of fusion proteins containing N-terminally extended GFP, inactive PhaC (indicated by the cross in the white box), and a C-terminal fusion partner lead to the self-assembly of GFP beads only. All protein domains displayed on the surface of bead varieties as described here are functional (Source: Jahns et al., 2013, p. 1316).

1.7.1 The effect of an N-terminal extension and the C-terminal fusion PhaC on GFP bead formation

N-terminal peptide extensions (such as AVTS) as well as C-terminal fusion partners (such as PhaC) of GFP are important for the formation of GFP beads (Jahns et al., 2013). The AVTS tetrapeptide extension at the N-terminus of GFP is generated by the use of an alternative start codon upstream of the *gfp* gene. The extension at the N-terminus of the GFP-PhaC fusion has been found to enhance protein aggregate formation and repress PHA bead assembly when compared to the non-extended version. Thus, the GFP-PhaC fusion containing this extension at its N-terminus could stimulate the

formation of protein beads (Jahns et al., 2013). However, in the absence of the C-terminal PhaC fusion, overproduction of direct GFP and N-terminally extended GFP does not lead to the formation of protein beads. Therefore, the fusion partner PhaC at the C-terminus of the N-terminally extended GFP is also important for the formation of GFP protein beads (Jahns et al., 2013).

1.7.2 The effect of PhaC activity on GFP bead formation

A GFP recombinant fusion containing active PhaC inhibits the formation of protein beads. It has been shown that overproduction of a fusion protein containing active PhaC can lead to the formation of protein/PHA hybrid beads in the presence of PhaA and PhaB, which mediate provision of precursors for PHA synthesis (Figure 5B). However, when PhaA and PhaB are absent, overproduction of the fusion could only lead to protein bead formation (Jahns et al., 2013). As described in Section 1.5, PhaC can be inactivated by the replacment of cysteine residue 319 by alanine. Jahns et al. (2013) have demonstrated that, in the absence or presence of PhaA and PhaB background, overproduction of a GFP recombinant fusion containing inactive PhaC(C319A) only leads to the formation of protein beads and always inhibits the formation of PHA beads (Figure 5C). Thus, the formation of protein beads is not initiated by small PHA beads, and PhaC activity is not required for protein bead formation (Jahns et al., 2013). Notably, the combination of N-terminally extended GFP and an inactive PhaC could significantly induce the formation of protein beads when compared to the non-extended versions (Jahns et al., 2013).

1.7.3 The effect of exchanging PhaC (C319A) on GFP bead formation

Jahns et al. (2013) have shown that inactive PHA synthase PhaC (C319A) in a GFP recombinant fusion can be replaced by other proteins, such as *N*-acetyl-D-neuraminic acid aldolase and maltose-binding domain (MalE). They have also found that this replacement does not impair the formation of GFP beads. Therefore, PhaC (C319A) might function as a larger linker region between GFP and foreign proteins. In summary, the formation of GFP beads requires overexpression of a structured gene cassette: a fluorescence gene linked to foreign genes by a large linker (Jahns et al., 2013).

Moreover, fluorescent protein beads (FP beads) could also be formed by using other types of fluorescent proteins (FPs) (Jahns et al., 2013).

1.7.4 Formation of various fluorescent protein beads

Various FPs, including enhanced yellow fluorescent protein (EYFP), enhanced cyan fluorescent protein (ECFP), and far red protein HcRed (HcR), have been shown to be capable of forming different types of FP beads in a manner similar to GFP. EYFP and ECFP are GFP-derivatives, which are derived from point mutations (Stuurman et al., 2000; Tsien, 1998), while HcR, a dimeric red FP, is derived from the Anthozoa species *Heteractis crispa* (Gurskaya et al., 2001). These FPs are able to mediate the self-assembly of their respective FP beads when linked to an inactive PhaC (C319A). In a similar fashion to GFP, extending the N-terminus of FP fusion proteins enhances the formation of protein beads when compared to the non-extended versions (Jahns et al., 2013). Jahns et al. have shown that although the respective FP alone is not capable of producing FP protein beads, providing an N-terminal extension in combination with a large C-terminal fusion partner significantly stimulates the formation of FP protein beads. They have also shown that a further similarity to GFP is that fusing an active PhaC to the C-terminus of FP leads to the formation of protein/PHA hybrid beads and, thus, inhibits protein bead formation. However, the inactivation (C319A) or replacement of PhaC dramatically stimulates the protein bead formation. Furthermore, various FP beads have the potential to display desired proteins, such as IgG binding domains ZZ or GB1, and perform their designated functions (Jahns et al., 2013).

1.8 Immobilization of protein function on protein beads

As described in Section 1.4, protein immobilization on the PHA bead surface can be performed by using its surface-associated proteins, including PhaC. In a manner similar to PHA beads, the protein immobilization on the surface of FP beads is conducted by genetic engineering of the FP-PhaC (C319A) fusion (Jahns et al., 2013). Jahns et al. have shown that the target protein production and immobilization is part of the protein bead self-assembly process, which occurs intracellularly in the same microbial cells. Thus, there is no need to synthesize and purify the protein of interest and then

immobilize it on the bead surface. They have also demonstrated that the beads displaying the protein of interest can be simply purified by centrifugation after cell disruption. Therefore, target protein production and immobilization on the surface of protein beads can be performed by a one-step production system which is cost effective and time saving (Jahns et al., 2013).

1.8.1 Application of protein beads as bio-beads for various protein display

Using FP beads as a platform for displaying various proteins is a new, emerging technology. Jahns et al. (2013) have shown that protein beads have the potential to act as a versatile platform for the display of various proteins. For example, target proteins, such as MalE and the IgG binding domains ZZ or GB1, have been displayed on the surface of protein beads by the engineering of the FP-PhaC (C319A) fusion. They also demonstrate that these domains can be detected at the surface of protein beads using ELISA. Although Jahns et al. did not measure the activity of MalE, their study still demonstrates the potential of protein beads for displaying functional foreign proteins. The IgG-binding domains displayed on the surface of protein beads have shown a strongly increased level of IgG-binding capacity when compared to their counterparts displayed on the surface of PHA beads. Therefore, target proteins immobilized on the surface of protein beads might have a higher activity than the proteins displayed on the surface of PHA beads (Jahns et al., 2013).

1.9 Aims and objectives of this study

The primary aim of this study was to assess the functionality of foreign proteins displayed on the surface of different types of biobeads (including PHA, protein, and magnetic beads) to facilitate the generation of various cost-effective diagnostic reagents. Briefly, this research was divided into four parts:

- Design and preparation of a specific bovine TB diagnostic reagent by developing antigen-displaying PHA beads;
- Assessment of the IgG binding ability of the [GB1]3 domains displayed on the surface of various FP protein beads;

- Development of a method to generate functionalized, super-paramagnetic protein beads; and
- Characterization of the morphology and funcationality of protein beads generated via different cell disruption methods.

Section I: Development of a specific bovine TB diagnostic reagent by developing antigen displaying PHA beads

TB is primarily an infectious disease of the lungs caused by various pathogenic strains of mycobacteria. Bovine TB is a worldwide health problem for animals with approximately 50 million cattle infected with *Mycobacterium bovis*, the causative agent of this disease (Waters, Palmer, Buddle, & Vordermeier, 2012). Meat and milk products of TB-infected cattle are not edible as *M. bovis* can be detected in their tissue and milk samples. This could lead to significant financial loss (Cornejo et al., 1998). Infected cattle are considered as potential sources of TB infection; therefore, it is important to restrict bovine TB transmission (Costello, Doherty, Monaghan, Quigley, & O'Reilly, 1998). Currently, control of this disease is predominantly achieved by testing cattle regularly using the tuberculin skin test (TST), which uses the purified protein derivatives (PPDs) isolated from cell lysates of *M. bovis* (Andersen, Doherty, Pai, & Weldingh, 2007; Brock, Weldingh, Lillebaek, Follmann, & Andersen, 2004).

The TST distinguishes TB-infected from non-infected cattle based on the delayed-type hypersensitivity (DTH) immune responses. For instance, after intradermal injection of the TST reagent into cattle, TB-infected cattle show raised skin at the injection site due to the presence of DTH. In contrast, non-infected cattle have no skin changes at the injection site due to the absence of DTH (Pollock & Andersen, 1997). However, the TST generally lacks specificity due to the cross-reactivity of antigens in the non-specific bovine PPDs with the antigens in Live-attenuated *Mycobacterium bovis* Bacile Calmette-Guerin (BCG) vaccine strain or non-pathogenic environmental mycobacteria. Due to its low specificity, the TST is not able to accurately distinguish TB-infected from non-infected cattle (Brock, Weldingh, Lillebaek, Follmann, & Andersen, 2004; Vinton et al., 2009; Vordermeier et al., 2001). Therefore, a new differential diagnostic reagent containing specific TB antigens is required to improve the specificity of bovine TB skin tests (Vordermeier et al., 2001). Three specific TB antigens, the 10-kDa culture

filtrate protein (CFP10), the 6-kDa early secretory antigenic target (ESAT6), and Rv3615c from *M. tuberculosis*, have been identified. Their orthologues have also been detected in other tuberculous mycobacteria, including *M. bovis*, but are absent in the majority of non-tuberculous mycobacteria or the BCG vaccine strain (Millington et al., 2011; Waters et al., 2004).

The biological actions of CFP10, ESAT6, and Rv3615c play an important role in TB pathogenesis. Indeed, CFP10 and ESAT6 are co-expressed and secreted as a heterodimer. The specific binding of the functional heterodimer CFP10:ESAT6 to the surface receptor of target cells functions as a signalling molecule. CFP10 specifically binds onto the membrane of target cells, while ESAT6 contributes to the disruption of planar membranes (Kamath et al., 2004; Renshaw et al., 2005). Thus, the main signalling role of the CFP10:ESAT6 complex in TB pathogenesis is to modulate the behavior of target cells to benefit the pathogens and promote their dissemination (Pym, Brodin, Brosch, Huerre, & Cole, 2002; Renshaw et al., 2005). In addition, the immunodominant antigen Rv3615c is critical for the early stage of TB infection as it facilitates the secretion of CFP10 and ESAT6. Tuberculous mycobacteria increase the expression of *Rv3615c* in response to host infection. Consequently, the increased level of Rv3615c enhances the secretion of the heterodimer CFP10:ESAT6 during TB infection (MacGurn, Raghavan, Stanley, & Cox, 2005).

These immunodominant TB antigens are highly immunogenic and able to induce a specific and strong T cell-mediated immune response in cattle with both active and long-term latent TB infections (MacGurn, Raghavan, Stanley, & Cox, 2005; Millington et al., 2011; Sidders et al., 2008). These three TB antigens are strong inducers of interferon-γ (IFNγ)-producing T cells. Particularly, CD4+ and CD8+ T cells are able to specifically bind to the processed antigens CFP10, ESAT6, and Rv3615c, which are associated with MHC molecules on the surface of antigen presenting cells (Kamath et al., 2004; Millington et al., 2011; Ravn et al., 2005; Sidders et al., 2008). IFNγ assay, a diagnostic test for TB, is based on measuring the release of IFNγ from T cells in cattle blood samples after re-induction *in vitro* with specific TB antigens (Mori et al., 2004). These three immunodominant antigens have been evaluated in a IFN-γ test for the diagnosis of TB in cattle, and results have shown that a diagnostic reagent containing CFP10, ESAT6, and Rv3615c is capable of distinguishing TB-infected from

non-infected (BCG-vaccinated and non-pathogenic environmental mycobacteria-sensitized) cattle (Buddle et al., 1999; Millington et al., 2011; Sidders et al., 2008; Vordermeier et al., 2001).

The main focus and aim of this section was to display CFP10, Rv3615c, and ESAT6 on the surface of PHA beads individually or in combination to produce four functionalized diagnostic reagents. Section I tested two hypotheses:

(1) The triple TB antigens displayed on the surface of PHA beads would have a higher specificity and sensitivity than single antigens displayed on the beads.

(2) The triple TB antigens on beads would be better able to differentiate TB-infected from non-infected cattle to act as a cost-effective diagnostic test.

The objectives of section I are described below:

- **Plasmid construction and expression:** Clone four plasmid constructs containing single gene or the triple TB genes, which are subsequently transformed into recombinant *E. coli* for expression;
- **Bead isolation:** Isolate and purify the PHA beads displaying TB antigens from the *E. coli* strains;
- **Protein characterization:** Characterize and evaluate the proteins of interest by Sodium dodecyl sulphate polyacrylamide gel electrophoresis (SDS-PAGE) and matrix-assisted laser desorption ionisation time-of-flight mass spectrometry (Maldi-TOF/MS); and
- **Assessment *in vitro* and *vivo*:** Reactivity of PHA bead displaying TB antigens *in vitro* will be assessed by using Enzyme-linked immunosorbent assay (ELISA) and *in vivo* by using a cattle model (conducted in collaboration with Natalie Parlane, Neil Wedlock, and Bryce Buddle of the Hopkirk Research Institute, AgResearch, Palmerston North, New Zealand).

Section II: Assessment of the IgG-binding ability of [GB1]3 on various FP beads

A variety of bacterial surface proteins can bind to the Fc region of immunogluobulin molecules and have been critical for immunoglobulin purification (Bjorck & Kronvall, 1984; Huse, Bohme, & Scholz, 2002). Two of the most common bacterial cell surface proteins used for antibody purification are Staphylococcal protein A and Streptococcal

protein G. Protein A is a cell-wall-bound adhesin from *Staphylococcus aureus* (Forsgren, 1970; Tashiro et al., 1997), which can strongly bind to immunoglobulin G through its Z domain that has a three-helix-bundle structure (Zheng, Aramini, & Montelione, 2004). The anti-parallel nature of these helices, along with the flexibility of the first helix, allows them to bind immunoglobulin G (Tashiro et al., 1997; Zheng, Aramini, & Montelione, 2004). In contrast, protein G is isolated from the cell walls of various Streptococcal species and is able to recognize mouse, goat, and all subclasses of human IgG (Bjorck & Kronvall, 1984). Although this protein does not have intra-chain disulfide bonds, it contains a stable IgG-binding domain B1 (GB1), comprising of a α helix and two β hairpins (Akerstrom & Bjorck, 1986; Blanco & Serrano, 1995). A recent study has shown that a tandem repeat of the IgG-binding domains immobilized on a protein bead platform significantly increased IgG-binding capacity (Jahns et al., 2013).

Jahns et al. have further demonstrated that immobilization of the triple IgG-binding domain of protein G, [GB1]3, on GFP protein beads or protein/PHA hybrid beads yielded a significantly higher IgG-binding capacity compared to immobilization on PHA beads (Jahns et al., 2013). Despite this, it is not clear whether an enhancement of IgG-binding capacity can be achieved by immobilization on other FP protein beads. Thus, the aim of this section is to test the IgG-binding capacity of the [GB1]3 domains displayed on the surface of FP beads made of EYFP, ECFP, or HcR. The hypothesis of Section II was that the [GB1]3 domains displayed on the surface of these three different FP beads would show a higher IgG-binding ability than the domains displayed on the surface of PHA beads.

The objectives of section II are described below:

- **Transformation**: Transform the available plasmids containing the genes encoding EYFP/ECFP/HcR and the [GB1]3 domains into recombinant *E. coli* for expression;
- **Bead isolation:** Isolate and purify the various protein beads displaying the [GB1]3 domains from their respective *E. coli* strains; and
- **IgG binding assessment**: Assess IgG-binding capacity of the [GB1]3 domains displayed on the surface of PHA and FP beads.

Section III: Development of a method for generation of functionalized super-paramagnetic protein beads

E. coli can specifically adhere to iron oxide but not other metal oxides. The iron-binding peptide (Fe), RRTVKHHVN, is present in the λ receptor on the outer membrane of *E. coli* and contributes to the specific binding of iron oxide (Brown, 1992). Nanobeads displaying this peptide are not magnetic. The magnetism is only obtained when the iron-binding peptide on beads adheres to iron oxide in the presence of a magnetic field (Ito, Shinkai, Honda, & Kobayashi, 2005). Furthermore, the magnetism of beads is correlated with the number of the iron-binding peptides (Johnson, Zawadzka, Deobald, Crawford, & Paszczynski, 2008). Johnson et al. (2008) have further shown that a recombinant fusion, containing haloalkane dehalogenase and three consecutive copies of the iron-binding peptide (3xFe), is successfully purified by uncoated iron oxide nanoparticles.

It is unknown whether protein beads displaying iron-binding peptides could be magnetized while maintaining the IgG-binding function. The aim of this section is to assess the magnetism and IgG-binding ability of GFP protein beads displaying the 3xFe and ZZ domains after magnetization using ferrofluid. This solution is colloidal suspension-containing surfactants and iron oxide particles, which are used to prevent iron oxide particle aggregation and to magnetize protein beads, respectively (Berger et al., 1999). Section III tested two hypotheses:

(1) Protein beads displaying 3xFe would become magnetic after mixing with ferrofluid.
(2) The immobilized IgG-binding domains ZZ on the surface of super-paramagnetic GFP protein beads would maintain a strong IgG-binding capacity.

The objectives of section III are described below:

- **Plasmid construction and expression:** Clone two plasmids (pET-14b xGFP-3xFe-PhaC(C319A)-linker-ZZ and pET-14b xGFP-PhaC(C319A)-linker-ZZ-3xFe) containing 3xFe between xGFP and PhaC(C319A)-ZZ and at the C-terminus of the xGFP-PhaC(C319A)-ZZ fusion. These plasmids will then be transformed into recombinant *E. coli* for expression;
- **Bead isolation:** Isolate and purify the GFP protein beads displaying the 3xFe and ZZ domains from respective *E. coli* strains; and

- **Functional assessment:** Assess magnetism and IgG-binding capacity of GFP protein beads after magnetization.

Section IV: Characterization of the morphology and functionality of protein beads displaying the ZZ domains obtained through different cell disruption methods

The aim of this section was to determine the effect of using different cell disruption techniques on the morphology and functional activity of FP beads displaying the ZZ domains. The hypothesis of Section IV was that protein beads isolated by various methods would show different morphologies and functional activities.

The objectives of section IV are described below:

- **Bead isolation:** Isolate and purify GFP beads displaying the MalE and ZZ domains from their respective *E. coli* strains; and
- **IgG-binding assessment**: Assess IgG-binding capacity of the ZZ displaying GFP beads isolated via different cell disruption methods.

Chapter 2: Materials and Methods

Unless indicated, all reagents were purchased from Sigma-Aldrich, Ajax Finechem, and Merck. Ultracentrifugation was performed using a Sorvall WX Ultra 80 (Thermo Scientific).

2.1 Bacterial strains and plasmids

The bacterial strains and plasmids used in this study are listed in Tables 2, 3, 4, and 5 below.

2.1.1 Bacterial strains

Table 2.

Bacterial Strains Used in this Study

***E.coli* strains**	**Relevant characteristics**	**References**
BL21 (DE3)	F- *dcm ompT hsdS*(r_B^- m_B^-) gal λ(DE3)	Stratagene
XL1-Blue	*recA1 endA1 gyrA96 thi-1 hsdR17 supE44 relA1 lac* [*F´ proAB lacI*^{q}*ZΔM15 Tn10* (Tet^r)]	Stratagene

Tet^r, tetracycline resistance

2.1.2 Plasmids

Table 3.

Plasmids Used in the Development of a Specific TB Diagnostic Reagent by developing antigen displaying PHA Beads

Plasmid name	Relevant characteristics	References
pET-14b	Ap^r; T7 promoter	Novagen
pET-14b phaC	pET-14b derivative containing *phaC* gene fragment	(Peters & Rehm, 2005)
pET-14b cfp10-phaC	pET-14b derivative containing *Nde*I fragment gene *cfp10* fused to the 5' end of *phaC*	Jason Lee
pET-14b rv3615c-phaC	pET-14b derivative containing *Nde*I fragment gene *Rv3615c* fused to the 5' end of *phaC*	Jason Lee
pET-14b esat6-phaC	pET-14b derivative containing *Nde*I fragment gene *esat6* fused to the 5' end of *phaC*	Jason Lee
pET-14b cfp10-linker-rv3615c-phaC-linker-malE	pET-14b derivative containing *Spe*I fragment genes *cfp10*-linker-*Rv3615c* fused to the 5' end of *phaC* and *Xho*I/*Bam*HI fragment gene *malE* fused to the 3' end of *phaC* via a linker sequence	Jason Lee
pET-14b cfp10-linker-rv3615c-phaC-linker-esat6	pET-14b derivative containing *Spe*I fragment genes *cfp10*-linker-*Rv3615c* fused to the 5' end of *phaC* and *Xho*I/*Bam*HI fragment gene *esat6* fused to the 3' end of *phaC* via a linker sequence	This study
pMCS69	Cm^r; T7 promoter, pBBR1MCS derivative containing the genes *phaA* and *phaB* from *C. necator* co-linear *to lac* promoter	(Amara & Rehm, 2003)
pUC57-esat6	Cloning vector, ColE1 origin, Ap^r ,	Jason Lee

*Xho*I/*Bam*HI fragment gene *esat6*

Ap^r, ampicillin resistance

Cm^r, chloramphenicol resistance

Table 4.

Plasmids Used in the Assessment of IgG-binding Abilities of [GB1]3 on Various FP Beads

Plasmid name	**Characteristics**	**References**
pET-14b eyfp-phaC(C319A) -linker-(gb1)3	pET-14b derivative containing *eyfp* fused to the 5' end of *phaC(C319A)* and *[gb1]3* fused to 3' end of *phaC(C319A)* via a linker sequence	(Jahns et al., 2013)
pET-14b xeyfp-phaC(C 319A)-linker-(gb1)3	pET-14b derivative containing x*eyfp* fused to the 5' end of *phaC(C319A)* and *[gb1]3* fused to 3' end of *phaC(C319A)* via a linker sequence	(Jahns et al., 2013)
pET-14b ecfp-phaC(C319 A)-linker-(gb1)3	pET-14b derivative containing *ecfp* fused to the 5' end of *phaC(C319A)* and *[gb1]3* fused to 3' end of *phaC(C319A)* via a linker sequence	(Jahns et al., 2013)
pET-14b xecfp-phaC(C31 9A)-linker-(gb1)3	pET-14b derivative containing x*ecfp* fused to the 5' end of *phaC(C319A)* and *[gb1]3* fused to 3' end of *phaC(C319A)* via a linker sequence	(Jahns et al., 2013)
pET-14b HcR-phaC(C319 A)-linker-(gb1)3	pET-14b derivative containing *HcR* fused to the 5' end of *phaC(C319A)* and *[gb1]3* fused to 3' end of *phaC(C319A)* via a linker sequence	(Jahns et al., 2013)
pET-14b xHcR-phaC(C31 9A)-linker-(gb1)3	pET-14b derivative containing *xHcR* fused to the 5' end of *phaC(C319A)* and *[gb1]3* fused to 3' end of *phaC(C319A)* via a linker sequence	(Jahns et al., 2013)
pET-14b xgfp-phaC-linker-malE	pET-14b derivative containing *xgfp* fused to the 5' end of *phaC* and *malE* fused to 3' end of *phaC* via a linker sequence	(Jahns et al., 2013)
pET-14b phaC-linker-(gb1)3	pET-14b derivative containing *[gb1]3* fused to 3' end of *phaC*	(Jahns et al., 2013)

pET-14b zz(-)phaC	pET-14b derivative containing *Xba*I/*Bam*HI gene fragment *zz-phaC* without a signal sequence-encoding region	(Backstrom, Brockelbank, & Rehm, 2007)

x, AVTS tetrapeptide extension

Table 5.

Plasmids Used in the Generation of Super-paramagnetic Protein Beads

Plasmid name	**Characteristics**	**References**
pGEM-T Easy	Ap^r, T7 and SP6 RNA promoter, *lacZ*	Promega
pET-14b 3×Fe-linker-zz -phaC	pET-14b derivative containing *3×Fe*-linker-*zz* fused to 5' end of *phaC*	Anika Jahns
pET-14b xgfp-phaC(C319A)-linker-malE	pET-14b derivative containing *xgfp* fused to the 5' end of *phaC(C319A)* and *malE* fused to 3' end of *phaC(C319A)* via a linker sequence	(Jahns et al., 2013)
pET-14b xgfp-phaC(C319A)-linker-zz	pET-14b derivative containing *xgfp* fused to the 5' end of *phaC(C319A)* and *zz* fused to 3' end of *phaC(C319A)* via a linker sequence	(Jahns et al., 2013)
pET-14b xgfp-phaC(C319A)-linker-zz-3×Fe	pET-14b derivative containing *xgfp* fused to the 5' end of *phaC(C319A)* and *zz-3×Fe* fused to 3' end of *phaC(C319A)* via a linker sequence	This study
pET-14b xgfp-3×Fe-phaC(C319A)-linker-zz	pET-14b derivative containing *xgfp-3×Fe* fused to the 5' end of *phaC(C319A)* and *zz* fused to 3' end of *phaC(C319A)* via a linker sequence	This study

3×Fe, triple iron-binding peptides

2.2 Primers

Primers used in this study are listed in Tables 6, 7, and 8 below. All primers were synthesized by Invitrogen.

Table 6.

Primers Used in the Development of a Specific TB Diagnostic Reagent by developing antigen displaying PHA Beads

Primer name	Restriction site (underlined)	Sequence from 5' to 3'	References
cfp10_fwd	*Nde*I	AACATATGGCAGAAATGAAA ACGGATGCGGC	Jason Lee
cfp10_rev	*Nde*I	TTCATATGGAAACCCATTTG AGAGCTCAGAGCC	Jason Lee
rv3615c_fwd	*Nde*I	AACATATGACCGAAAACCTG ACGGTTCAGCCGG	Jason Lee
rv3615c_rev	*Nde*I	TTCATATGGGTGAACAGGCC GTCGATTGCTTTAC	Jason Lee
esat6_fwd	*Nde*I	AACATATGACGGAACAACAA TGGAACTTTGCTGGC	Jason Lee
esat6_rev	*Nde*I	TTCATATGTGCGAACATGCC CGTGACATTGCCTTC	Jason Lee

Table 7.

Primers Used in the Generation of Super-paramagnetic Protein Beads

Primer name	Restriction site (underlined)	Sequence from 5' to 3'	References
N-3×Fe_fwd	*Not*I	TAGCGGCCGCGATGCGCCGTACCGTGAAAC	Jinping Du
N-3×Fe_rev	*Not*I	CTGCGGCCGCGTTAACATGATGTTTCACGGTGC	Jinping Du
C-3×Fe_fwd	*Bam*HI	TAGGATCCGATGCGCCGTACCGTGAAAC	Jinping Du
C-3×Fe_rev	*Bam*HI	CCGGATCCGTTAACATGATGTTTCACGGTGC	Jinping Du

Table 8.

Sequencing Primers Used in this Study

Primer name	Restriction site	Sequence from 5' to 3'	References
N-phaC_rev	N/A	CGATCTTGACGCCTGCCAGC	Anika Jahns
C-phaC_fwd	N/A	AGCCACTGGACTAACGATGC	Anika Jahns
T7_fwd	N/A	TAATACGACTCACTATAGGG	Allan Wilson Centre
M13_fwd	N/A	CCCAGTCACGACGTTGTAAAACG	Allan Wilson Centre
M13_rev	N/A	AGCGGATAACAATTTCACACAGG	Allan Wilson Centre
C-GFP_fwd	N/A	TGCTGGGATGACACATGGCAT	This study

2.3 Liquid media

Luria-Bertani (LB) medium (Invitrogen) was prepared by adding 20 g per litre of Milli-Q water and autoclaved at 121^{o}C for 20 minutes.

2.4 Solid media

LB-agar medium was made by adding 1.5 g agar (Oxoid) per 100 ml LB medium and autoclaved at 121˚C for 20 minutes.

2.4.1 X-Gal medium

X-Gal medium was made by adding supplements (Table 9) to the sterile LB-agar medium (Section 2.4).

Table 9.

X-Gal Medium Supplements Stock and Final Concentrations

Supplements	Stock concentration	Final concentration
IPTG	1 M in Milli-Q water	1 mM
X-Gal	4% (w/v) in DMSO	4×10^{-3}%

2.5 Antibiotic stock solutions and concentrations

Antibiotics were prepared as previously described (Rasiah & Rehm, 2009). These solutions were sterilized by filtration through a 0.22 µm filter and stored at -20°C for future use. When required, antibiotics were added to autoclaved nutrient solid media (Section 2.4.) after cooling the media to approximately 50ºC. Antibiotics used in this study are shown in Table 10.

Table 10.

Antibiotic Stocks and Final Concentrations

Antibiotics	Stock solution (mg/ml)	Final concentration (µg/ml)
Ampicillin (Sodium salt)	75 in Milli-Q water	75
Chloramphenicol	50 in 95% EtOH	50
Tetracycline	12.5 in 70% EtOH	12.5

2.6 Cultivation conditions of *E. coli*

The *E. coli* cell cultivation condition has been described elsewhere (Blatchford, Scott, French, & Rehm, 2012). *E. coli* strains were grown in Erlenmeyer flasks containing liquid LB medium (Section 2.3) supplemented with appropriate antibiotics, carbon source, and supplements. These bacterial cultures were incubated at 37°C and shaken at 200–250 rpm. The ratio of flask volume to liquid medium was approximately 5:1 to maximize aeration.

2.6.1 PHA and FP protein bead production conditions

The PHA bead production conditions were performed as described previously (Parlane et al., 2011). Recombinant pET expression vectors were transformed into *E. coli* (Section 2.9) production strain BL21 (DE3, Stratagene, Section 2.1.1), harboring pMCS69. Four millilitres of an overnight culture was used to inoculate 400 ml of liquid LB medium (Section 2.3) containing 1% (v/v) glucose and the appropriate antibiotics 75 µg/ml ampicillin and 50 µg/ml chloramphenicol. The cultures were incubated at 37°C on a TR/Novotron shaker (INFORS HT, Switzerland) for two to three hours until the OD600 reached 0.4–0.5. The *E. coli* cell cultures were then grown at 25°C for 48 hours after the addition of IPTG at a final concentration of 1 mM to induce gene expression. Protein bead production conditions were similar to PHA beads as described by Jahns et al. (2013).

2.7 Long-term storage and revival of bacterial strains

2.7.1 Storage of *E. coli* strains

The *E. coli* strains were incubated overnight in a sterile LB liquid medium (Section 2.3) in the presence of appropriate antibiotics at 37°C on a thermoline orbital shaker TLM510 (N.S.W., Australia; Section 2.6). Subsequently, 1 ml of the overnight culture was mixed with 70 µl of sterile dimethylsulfoxide (DMSO) in a 2 ml cryovial tube to give a final concentration of 6.5% (v/v) and stored at -80°C for future use.

2.7.2 Revival of *E. coli* strains

The *E. coli* strains were revived by using a sterile pipette tip to remove a small chip of frozen stock, which was used to inoculate the sterile LB liquid medium (Section 2.3) containing appropriate antibiotics. This medium was grown on a thermoline orbital shaker TLM510 (NSW, Australia) at 37^{o}C overnight (Section 2.6).

2.8 Preparation of competent *E. coli* cells

Competent *E. coli* cells were prepared as described elsewhere (Hanahan, 1983). Fifty millilitres of LB liquid medium (Section 2.3) was inoculated with 0.5 ml inoculum of an overnight culture and incubated at 37^{o}C until the OD_{600} reached approximately 0.35. Subsequently, the cell culture was stored on ice for about 15 minutes and then harvested using centrifugation at 8,000 x g (Heraeus multifuge 1 S-R, Sorvall) for 15 minutes. The harvested cells were re-suspended in 16 ml of RF1 solution and further incubated on ice for 30 minutes. Cells were harvested again using centrifugation at 8,000 x g for 15 minutes and then re-suspended in 4 ml of RF2 solution. Finally, 200 µl of these competent cells were aliquoted into 1.5 ml microfuge tubes and stored at -80^{o}C for future use. The composition of RF1 and RF2 solutions which were sterilized by filtration through a 0.22 µm filter are outlined below:

RF1 solution:

100 mM	RbCl
50 mM	$MnCl_2$
30 mM	Potassium acetate
10 mM	$CaCl_2 \cdot 6H_2O$

Adjust the pH to 5.8 using acetic acid

RF2 solution:

10 mM	RbCl
10 mM	MOPS
75 mM	$CaCl_2 \cdot 6H_2O$
15 mM	Glycerol

Adjust the pH to 5.8 using NaOH

2.9 Transformation of *E. coli* cells

The transformation of *E. coli* cells has been described elsewhere (Sambrook, Fritsch, & Maniatis, 1989). A microfuge tube containing 200 µl of frozen competent cells (Section 2.8) was thawed on ice for 40 minutes. Subsequently, they were mixed thoroughly with 3 µl of purified plasmid DNA or 10 µl of a ligation mix and then incubated on ice for 20 minutes to allow plasmid DNA to be adsorbed at the cell surface. To promote the uptake of the adsorbed plasmid DNA, the competent *E. coli* cells were gently mixed and heat-shocked at 42^{o}C for 90 seconds and then immediately incubated on ice for a further five minutes. Cells were regenerated by the addition of 800 µl liquid LB medium (Section 2.3) and incubated at 37^{o}C for one hour. To select and isolate recombinant clones, 100 µl of the cells was spread-plated on solid LB-agar medium (Section 2.4) containing appropriate antibiotics. The remaining cells were harvested using centrifugation at 6,000 x g (Heraeus Pico 17, Thermo Scientific) for two minutes. Finally, the cell sediments were re-suspended in 100 µl of LB medium, plated on a solid LB-agar medium and incubated at 37^{o}C overnight.

2.10 Molecular cloning

2.10.1 Plasmid isolation and concentration

2.10.1.1 High Pure Plasmid Isolation Kit

Plasmid isolation from recombinant *E. coli* was performed using the High Pure Plasmid Isolation Kit (Roche, Switzerland) according to the manufacturer's instructions.

2.10.1.2 Plasmid Clean and Concentrator Kit

Due to low plasmid concentrations or impure plasmid preparations, the Clean and Concentrator Kit (Zymo Research, USA) was applied according to the manufacturer's instructions to prepare a suitable plasmid solution for DNA cloning and sequencing.

2.10.1.3 Determination of plasmid concentration

Plasmid concentration was determined using one of the two techniques as described below. First, plasmid concentration was measured by the Qubit™ fluorometer (Invitrogen, USA) in conjunction with the Quant-iT DNA BR Assay Kit (Invitrogen, USA) according to the manufacturer's instructions. Second, NanoDrop 1000 (Thermo Scientific) was used to measure plasmid concentration according to the manufacturer's instructions.

2.10.2 DNA hydrolysis

The DNA digestion methods used in this study were according to laboratory protocols (Sambrook, Fritsch, & Maniatis, 1989). Plasmid DNA was digested with restriction endonucleases (REs) to clone and analyze plasmid DNA. All REs were purchased from Roche, Invitrogen, and New England Biolabs and used according to the manufacturers' instructions. For DNA hydrolysis with one RE, a typical 20 µl digestion reaction containing the following reagents was performed: 16 µl of plasmid, 2 µl of 10x RE buffer, and 2 µl of RE. For DNA hydrolysis with two REs using compatible buffers (100% activity for both REs), plasmid DNA and two REs were combined with a compatible buffer in a single digestion reaction. For DNA hydrolysis with two REs using incompatible buffers, isopropanol precipitation (Section 2.10.2.1) was required to allow individual enzyme digestion.

2.10.2.1 Isopropanol precipitation of DNA

Isopropanol precipitation of DNA was performed as described elsewhere by Sambrook, Fritsch, and Maniatis (1989). Plasmid DNA was precipitated by incubating it with three volumes of isopropanol on ice for five minutes. Centrifugation at 16,200 x g for 30 minutes (Heraeus Pico 17, Thermo Scientific) was performed to sediment precipitated DNA, and the supernatant fraction was carefully removed by pipetting. The sedimented DNA was subsequently washed once with three volumes of 70% (v/v) ethanol to remove traces of isopropanol and then air dried.

2.10.3 Polymerase chain reaction

Polymerase chain reaction (PCR) was used to amplify target DNA fragments (Sambrook, Fritsch, & Maniatis, 1989). The reaction was performed by repeated steps of denaturing, annealing, and replication/elongation. The denaturation step separates the double-stranded DNA into single strands, while the annealing step allows the primers to bind to the single stranded DNA template. In the replication step, the DNA polymerase synthesizes a new DNA strand complementary to the DNA template. When required, Platinum® *Pfx* DNA polymerase (Invitrogen Corporation, USA) was employed to achieve high fidelity. A typical PCR reaction mixture using *Pfx* DNA polymerase is shown in Table 11.

Table 11.

PCR Reaction Mix Using Pfx *DNA Polymerase*

Reagents	**Amounts**
10x *Pfx* reaction buffer	10 µl
$MgSO_4$ (50 mM)	5 µl
DMSO	5 µl
Forward primer (10 pmoles/µl)	10 µl
Reverse primer (10 pmoles/µl)	10 µl
dNTPs (10 mM of dATP, dTTP, dCTP and dGTP)	10 µl
Template DNA	5–10 ng
Pfx DNA polymerase (2.5 U/µl)	0.5 µl
Autoclaved distilled water	To 100 µl

PCR reaction was conducted in a Biometra Tpersonal thermocycler (Whatman Biometra, Germany). A typical PCR reaction program using *Pfx* DNA polymerase is shown in Table 12.

Table 12.

PCR Reaction Condition Using Pfx *DNA Polymerase*

Steps	Conditions
1. Denature	94°C for two minutes
2. Denature	94°C for 15 seconds
3. Anneal	An optimal annealing temperature* for 30 seconds
4. Replicate/elongate	68°C for one minute
5. Repeated cycles	Repeat steps two to four for 33 cycles
6. Hold	10°C

* An optimal annealing temperature is dependent on the melting temperatures of the primer-DNA template hybrid. Generally, the annealing temperature is performed at approximately 5°C below the melting temperature of primers. However, optimization may be required.

2.10.4 Agarose gel electrophoresis

Agarose gel electrophoresis (AGE) was carried out as outlined elsewhere (Sambrook, Fritsch, & Maniatis, 1989). Digested DNA or PCR products were separated by AGE performed in a 1x TBE buffer, using a horizontal slab gel electrophoresis apparatus. In this study, 1–3% agarose gels were made in a 1x TBE buffer, based on the size of DNA fragments. Generally, 1% agarose gel was used to resolve DNA fragments larger than 1000 bp; 2% agarose gel was used for DNA fragments smaller than 1000 bp; and 3% agarose gels were used for DNA fragments below 90 bp. DNA samples were mixed with 6x DNA loading dye before loading on the agarose gels. Electrophoresis conditions were dependent on the size of the AGE chamber and the level of separation required among DNA fragments. Typically, 1–2% agarose gels were run for 45–60 minutes at 100–120 V, and 3% agarose gels were run for 90–120 minutes at 80–90 V. Agarose gels were stained in an ethidium bromide solution for 20 minutes and distained in distilled water for one minute. The gels were visualized using a UV transilluminator at a wavelength of 254 nm (Bio-Red, Gel Doc 2000). When DNA fragments were required for cloning, SYBR safe DNA gel stain (Invitrogen, USA) was used according to the manufacturer's instructions, and DNA fragments were visualized using a Safe Imager™ 2.0 Blue-Light Transilluminator (Invitrogen). The compositions of the 10x TBE buffer and 6x DNA loading dye are outlined below:

TBE buffer (10x):

500 mM	Tris-HCl
500 mM	Boric acid
25 mM	EDTA
Adjust to about pH8.5 using HCl	

DNA loading dye (6x):

4 M	Urea
50% (v/v)	Sucrose
50 mM	EDTA
0.1%	Bromophenol Blue

2.10.4.1 DNA ladder standards

A suitable DNA ladder was used to estimate the size of DNA fragments on AGE. Phage lambda DNA (λ-DNA) (Invitrogen, USA) was digested with the RE *Pst*I (Section 2.10.2) to generate the fragments with known sizes (Table 13). The digested λ-DNA was mixed with 6x DNA loading dye and stored at -20^{o}C for future use. GeneRuler 100 bp DNA ladder plus (Fermentas, Canada) was another DNA ladder used in this study to determine the size of DNA fragments. It was used according to the manufacturer's instructions, and the sizes of the DNA fragments are shown in Table 13.

Table 13.

*DNA Ladders: λ/*Pst*I and GeneRuler 100bp DNA Ladder Plus*

DNA ladders	Sizes (bp)
λ/*Pst*I	11490, 5077, 4749, 4507, 2838, 2560, 2449, 2443, 2140, 1986, 1700, 1159, 1093, 805, 514, 468, 448, 339, 264, 216, 211, 200, 164, 160, 94, 72, 15
GeneRuler 100bp DNA ladder plus	3000, 2000, 1500, 1200, 1000, 900, 800, 700, 600, 500, 400, 300, 200, 100

2.10.5 Recovery of DNA fragments from agarose gels

DNA fragments separated by AGE with SYBR safe DNA gel stain (Section 2.10.4) were recovered using the Zymoclean™ Gel DNA Recovery Kit (Zymo Research, USA), according to the manufacturer's instructions.

2.10.6 pGEM-T Easy vector system

2.10.6.1 A-tailing reaction and pGEM-T Easy ligation

The Thymine-Adenine (T-A) cloning technique has been described elsewhere (Hengen, 1995; Marchuk, Drumm, Saulino, & Collins, 1991). This efficient technique was applied to ligate blunt-ended PCR products to the pGEM-T Easy vector (Promega, USA), an intermediate cloning vector. The A-tailing reaction (Table 14) was used to add a 3' terminal adenine overhang onto blunt-ended PCR products and performed in a Biometra T-personal thermocycler (Whatman Biometra, Germany) at 70°C for 30 minutes. An aliquot of the A-tailed PCR product was then used in an overnight ligation reaction with the pGEM-T Easy vector at 4°C (Table 14).

Table 14.

A-tailing and pGEM-T Easy Ligation Reaction Mix

A tailing reaction mix	pGEM-T Easy ligation mix
1 µl dATP (0.2mM)	5 µl pGEM-T Easy 2x ligase buffer
1 µl *Taq* DNA polymerase (Invitrogen)	0.5 µl pGEM-T Easy vector
1 µl 10x *Taq* reaction buffer without $MgCl_2$	1 µl pGEM-T Easy ligase
1 µl $MgCl_2$	3.5 µl A-tailed PCR product
6 µl PCR product	

2.10.6.2 Blue and white selection

Blue and white selection was performed as described previously (Sambrook, Fritsch, & Maniatis, 1989). This selection method was applied to detect a successful ligation between A-tailed PCR products and a pGEM-T Easy vector. After overnight ligation (Section 2.10.6.1), the pGEM-T Easy ligation mix (Section 2.10.6.1) was transformed

into *E. coli* (Section 2.9) cloning strain XL1-Blue (Stratagene, Section 2.1.1) and plated on a X-Gal medium (Section 2.4.1) containing 75 µg/ml of ampicillin. These plates were then incubated at 37°C overnight. White colonies contain pGEM-T Easy plasmids that have their β-galactosidase encoding gene insertionally inactivated by the DNA fragment of interest. Therefore, a single white colony was selected and spread-plated on a new X-Gal medium to confirm the presence of the desired insert and loss of β-galactosidase activity.

2.10.7 DNA ligation

T4 DNA ligase (Invitrogen, USA) was applied in the ligation reaction between inserts of interest and linearized expression vectors (Sambrook, Fritsch, & Maniatis, 1989). These linearized DNAs were obtained from DNA hydrolysis using suitable REs (Section 2.10.2) or DNA fragment recovery from agarose gels (Section 2.10.5). A molar ratio of 6:1 between the insert and linearized vector was used to maximize ligation efficiency. Ligation reactions were prepared in 1.5 ml microfuge tubes according to the manufacturer's instructions. These reactions were incubated at 4°C in a floating water bath overnight.

2.10.8 DNA sequencing

DNA sequencing of recombinant plasmids was performed by the Allan Wilson Centre Genome Service (Massey University, Palmerston North) using a capillary ABI3730 Genetic Analyzer (Applied Biosystems Inc., USA). DNA sequencing reactions were prepared in a sterile 0.2 ml thin-walled PCR tube (Axygen, USA) containing 300 ng of DNA template and 3.2 pmol/µl of primer in a total volume of 15 µl. The results presented in ABI format were analysed by Vector NTI version 10.

2.11 Isolation of PHA and protein beads

Bead isolation was performed through cell harvesting, cell disruption (Section 2.11.1), and then bead purification (Section 2.11.2).

2.11.1 Cell disruption

Approximately 400 ml cell cultures were harvested after 48 hours growth at 25°C (Section 2.6.1) using centrifugation at 6,000 x g for 20 minutes in a Sorvall RC-5B (Du Pont instruments). The cell pellet was washed once by re-suspending it in a suitable buffer solution (50 mM potassium phosphate buffer, pH7.5, for PHA bead isolation, and 1x PBS buffer, pH7.5, for protein bead isolation). Cells were transferred into 50 ml falcon tubes and harvested again using centrifugation at 6000 x g for 15 minutes in a Heraeus Multifuge 1 S-R (Sorval, Germany). Cell sediments were then prepared for cell disruption using various methods as described in Sections 2.11.1.1 and 2.11.1.2. The compositions of the 50 mM potassium phosphate buffer and 1x PBS buffer are outlined below:

50 mM potassium phosphate buffer:

50mM	K_2HPO_4 (Alkaline solution)
50mM	KH_2PO_4 (Acidic solution)

Adjust the pH of K_2HPO_4 solution to 7.5 using KH_2PO_4 solution

1x PBS buffer:

137mM	NaCl
2.7mM	KCl
10.0mM	Na_2HPO_4
1.76mM	KH_2PO_4

Adjust pH to 7.5 using HCl

2.11.1.1 Chemical cell disruption

Bugbuster® Protein Extraction Reagent (Merck, Germany) was used to isolate PHA or protein beads according to the manufacturer's instructions. Briefly, 5 ml of Bugbuster® reagent (1x) was mixed with 1 g of cells (wet weight). The re-suspended cells were then mixed with 2–5 mg of lysozyme (Sigma-Aldrich, USA) and incubated at room temperature for 20 minutes with shaking. Next, DNase (Sigma-Aldrich, USA) and $MgCl_2$ (to a final concentration of 5 mM) were added in the mixture and incubated as described above. After incubation, the crude cell lysate was sedimented using

centrifugation at 8,000 x g for 10 minutes at 4°C (Heraeus Multifuge 1 S-R, Sorval). To ensure remaining cells were lysed, the pellet was re-suspended in the same volume of Bugbuster® reagent containing lysozyme as described here. The mixture was then incubated at room temperature for 10 minutes with shaking. This final cell lysate containing PHA (or protein) beads was harvested using centrifugation at 4,000 x g for 15 minutes at 4°C (Heraeus multifuge 1 S-R, Sorvall). The pellet was washed once and re-suspended in 2–5 ml of phosphate (for PHA beads) or 1x PBS buffer (for protein beads). Bead samples in the pellet were purified by ultracentrifugation as described in Section 2.11.2.

2.11.1.2 Mechanical cell disruption

Cells were disrupted using two methods of mechanical disruption as described below:

Cell disruptor method

To disrupt cells using the cell disruptor method, the cell pellet (Section 2.11.1) was re-suspended in a 50 mM potassium phosphate buffer or 1x PBS buffer. To inhibit protease activity, suspension buffers were supplemented (one tablet per 10 ml of buffer) with a Complete Mini EDTA-free protease inhibitor cocktail (Roche, Switzerland). To the cell suspension, 2–5 mg of lysozyme (Sigma-Aldrich, USA) and DNase (Sigma-Aldrich, USA) were added and the mixture was subjected to two passes of mechanical cell disruption at 20 kPsi (Constant Cell Disruption Systems, UK). Disrupted crude cell lysates were centrifuged at 4,000 x g for 15 minutes at 4°C (Heraeus multifuge 1 S-R, Sorvall). Sediment containing beads, unlysed cells, and insoluble cell debris were then re-suspended in 2–5 ml phosphate (for PHA beads) or 1x PBS buffer (for protein beads) and subjected to further purification steps (Section 2.11.2).

Microfluidizer method

Microfluidizer (Alphatech Systems) was another mechanical cell disruption method applied in this study, and it could disrupt cells with high efficiency. Cell sediment (Section 2.11.1) was re-suspended in a 50 mM of potassium phosphate buffer or 1x PBS buffer. To this suspension, 2–5 mg of lysozyme (Sigma-Aldrich, USA) and DNase (Sigma-Aldrich, USA) was added. The mixture was then subjected to 10–25 passes of

mechanical cell disruption at 1,000 bar (Alphatech Systems). The crude cell lysate was harvested using centrifugation at 4,000 x g for 15 minutes at 4°C (Heraeus multifuge 1 S-R, Sorvall). The pellet was washed once and re-suspended in 2–5 ml of phosphate or 1x PBS buffer, depending on the bead type as described in Section 2.11.1. Bead samples in the sediment were purified by ultracentrifugation in combination with glycerol gradients (Section 2.11.2).

2.11.2 Purification of PHA and protein bead from crude cell lysate

PHA and protein beads were purified from crude cell lysates as described previously using glycerol gradients and ultracentrifugation (Jahns, Haverkamp, & Rehm, 2008; Jahns et al., 2013). Two types of glycerol gradients made in a 50 mM potassium phosphate buffer (pH7.5) were used. PHA beads were isolated using a glycerol gradient containing an upper 44% and a lower 88% glycerol layer. In contrast, protein beads were purified using a glycerol gradient containing an upper 49.75% and a lower 99.5% glycerol layer. After ultracentrifugation (35,000 rpm for two hours at 10°C), purified PHA and protein beads formed a layer at the interface of 44%-88% glycerol and 49.75%-99.5% glycerol, respectively. The process for isolating and purifying PHA and protein beads from crude cell lysate is shown in Figure 6.

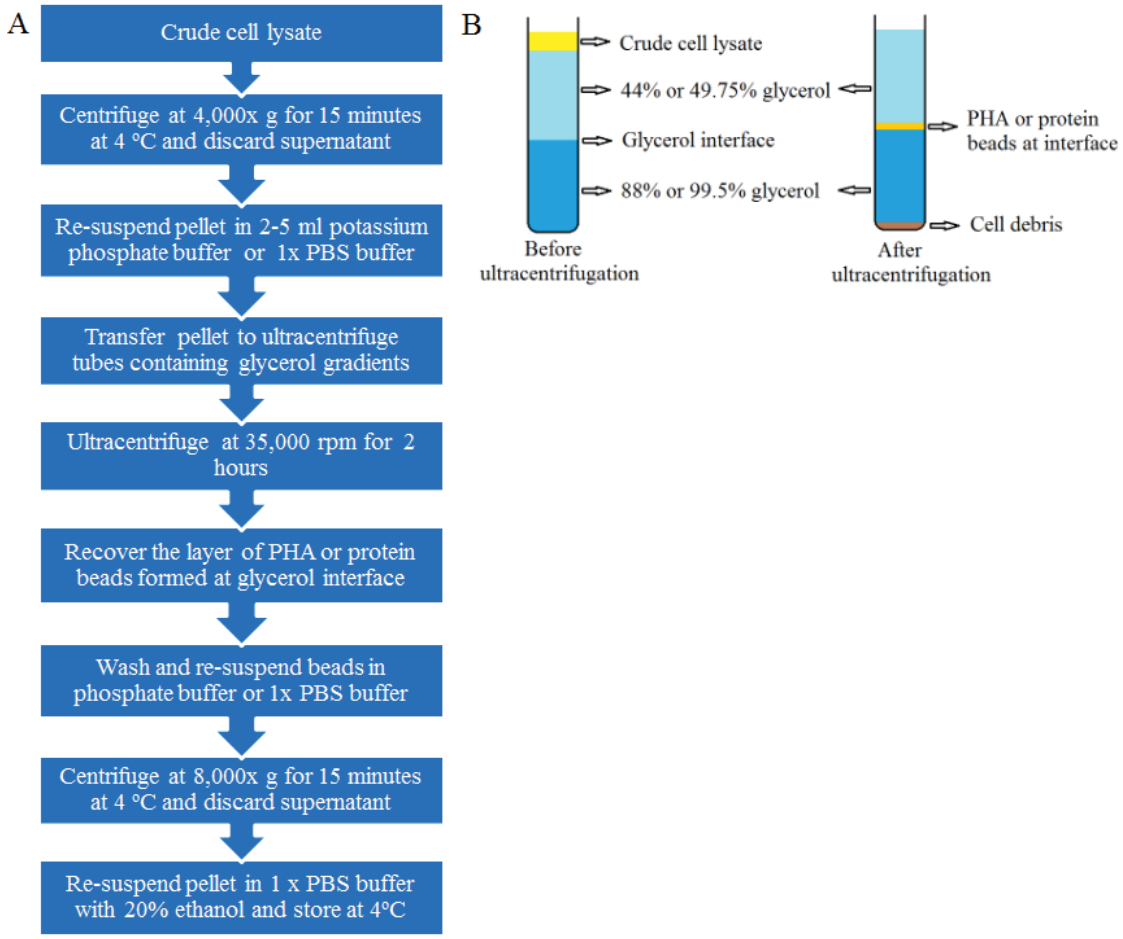

Figure 6. **Schematic overview of the PHA and protein beads isolation after cell disruption**. (A) The process of extracting and purifying PHA and protein beads from disrupted crude cell lysate using ultracentrifugation and glycerol gradients. (B) PHA or protein bead layer in glycerol gradients before and after ultracentrifugation.

2.12 Analysis of PHA and protein beads

2.12.1 Detection of PHA and FP protein beads

Nile-red staining (Section 2.12.1.1) and fluorescent microscopy (Section 2.12.1.2) were used to analyze cells producing PHA beads. Intracellular FP protein beads were detected using fluorescent microscopy (Section 2.12.1.2).

2.12.1.1 Nile-red staining

Nile-red staining was used to analyze PHA-accumulating cells in a liquid LB medium (Section 2.3) as described previously (Spiekermann, Rehm, Kalscheuer, Baumeister, & Steinbuchel, 1999). Briefly, 1 ml of cell culture was harvested using centrifugation (Heraeus Pico 17, Thermo Scientific) at 6000 x g for one minute, and the supernatant fraction was carefully removed by pipetting. Ten microlitres of Nile-red solution (0.25 mg/ml in DMSO) was added to the cell pellet and mixed thoroughly. Then, 1 ml of 50 mM potassium phosphate buffer (pH7.5) was added, and the mixture was incubated in the dark at room temperature for 15 minutes. Cells were harvested again after the incubation and washed once with 1 ml of 50 mM potassium phosphate buffer. The cell pellet was re-suspended in 1 ml of 50 mM potassium phosphate buffer, spotted onto a glass slide, covered with a coverslip and, finally, analyzed using fluorescent microscopy (Section 2.12.1.2).

2.12.1.2 Fluorescent microscopy

Fluorescent microscopy was applied to analyze the presence of PHA beads and FP beads in *E. coli* cells (Peters, Becher, & Rehm, 2007). A glass slide containing Nile-red stained PHA bead-accumulating cells (Section 2.11.3.1) was examined through a fluorescent light microscope (Olympus, Japan) using filter 4 under 1000x magnification. Meanwhile, FP bead-accumulating cells were directly spotted onto a glass slide without staining and covered with a coverslip. This glass slide was analyzed through a fluorescent light microscope (Olympus, Japan) using filter 3 under 1000x magnification. All images were captured using Magnafire^{TM} 2.1 (Optronics, USA).

2.12.2 Gas chromatography-mass spectrometry

Gas chromatography-mass spectrometry (GC-MS) was used to determine the PHA content of cells quantitatively, as described previously (Brandl, Gross, Lenz, & Fuller, 1988). The PHA standards (ranging from 2–80 mg, Sigma-Aldrich, USA) and lyophilized cell samples (75 mg) were suspended in GC-MS bottles containing 2 ml of chloroform with 105 µg/ml undecane, respectively. These samples were then methanolyzed by adding 2 ml of 15% (v/v) methanolic sulphuric acid, followed by

incubation at 100^{o}C for five hours in a heated oil bath. After incubation, the tubes containing the methanolyzed samples were allowed to cool at room temperature before the addition of 2 ml of distilled water. These samples were then vortexed thoroughly for one minute and left at room temperature for phase separation. Methyl esters of the corresponding fatty acid in the bottom organic layer were recovered and analyzed by GC-MS for 3-hydroxyalkanoate methyl esters. All GC-MS experiments were conducted at Plant and Food (Palmerston North, New Zealand). The solutions required for GC-MS sample preparation are outlined below:

Chloroform with 105 µg/ml undecane:

100 ml	Chloroform
14.2 µl	Undecane

15% (v/v) methanolic sulphuric acid:

85 ml	Methanol
15 ml	Sulphuric acid

2.12.3 Transmission and Scanning Electron Microscopy

All Transmission Electron Microscopy (TEM) and Scanning Electron Microscopy (SEM) samples were processed at the Manawatu Microscopy and Imaging Centre (MMIC, Massey University, Palmerston North, New Zealand). Samples for TEM and SEM processing were sent to the MMIC as 20 mg sediments in 1.5 ml microfuge tubes.

2.12.4 Determination of bead size

qNano (Izon Science Ltd) was used to analyse the size of bead varieties. All measurements were performed by PolyBatics (Palmerston North, New Zealand).

2.13 General methods for protein analysis

2.13.1 Determination of protein concentration

The Bradford method was used to determine the concentration of proteins in purified bead fractions, as previously performed elsewhere (Bradford, 1976). Ten microlitres of serially-diluted bead samples were prepared in a high-binding capacity microtitre plate (Greiner bio-one). Ten microlitres of bovine serum albumin (BSA, Sigma-Aldrich) or IgG (GE life sciences) with known protein concentrations were used as standards for the Bradford assay. To each well containing a sample or standard, 200 µl of filtered Bradford reagent (Bio-Rad laboratories, USA) was loaded and incubated for five minutes in the dark at room temperature for colour development. After incubation, the absorbance was measured at 595 nm using an ELx808iu ultra microtiter plate reader (BIO-TEK Instruments Inc., USA). Protein concentrations in bead samples were determined by a prepared standard curve, based on absorbance readings of known protein concentrations of BSA (0.05–0.4 mg/ml) or IgG (0.05–0.8 mg/ml).

2.13.2 Sodium dodecylsulfate Polyacrylamide Gel Electrophoresis

Sodium dodecylsulfate Polyacrylamide Gel Electrophoresis (SDS-PAGE) has been outlined previously (Sambrook, Fritsch, & Maniatis, 1989). This method was performed in a 1x electrode buffer using a vertical slab gel electrophoresis apparatus to characterize and evaluate protein samples. Each Tris-glycine gel typically consists of two layers: a lower resolving gel layer (8–10%, w/v, pH 8.9) and an upper stacking gel layer (4%, w/v, pH 6.8). The gel was made in a pre-cast cassette (8cm×8cm) yielding a gel thickness of 1.5 mm (Invitrogen, USA). The electrode buffer used for SDS-PAGE preparation is outlined below:

Electrode buffer:

14.4 g	Glycine
3.0 g	Tris
1 g	SDS

Make up to 1 L with distilled Milli-Q water and adjust to pH 8.5 with HCl

The resolving gel solution was prepared and degassed by adding 2–5 mg of Na_2SO_3 to avoid the formation of air bubbles. The polymerization of the gel solution was initiated by adding 20 µl of N, N, N', N'-tetramethylethyl-endiamin (TEMED) and 40 µl of a 40% (w/v) ammonium persulfate (APS) solution. The mixture was then gently poured into the pre-cast cassette and immediately overlaid with isopropanol. After allowing one hour for polymerization, the isopropanol layer was poured off. The compositions of resolving gel buffer and revolving gels are shown below:

Resolving gel buffer:

54.45 g	Tris/HCl
1.2 g	SDS
300 ml	Distilled Milli-Q water
Adjust to pH 8.9 with HCl	

Resolving gel:

8% (w/v)	**10% (w/v)**	
10.4 ml	10.4 ml	Resolving buffer
11.1 ml	13.9 ml	Acrylamide (30%)
20.1 ml	17.3 ml	Distilled Milli-Q water
41.6 ml	41.6 ml	Total volume

The stacking gel solution was prepared and also degassed using Na_2SO_3. Similarly, 4.4 µl TEMED and 8.8 µl APS (40% w/v) was added to begin the polymerization process. This solution was gently poured on the top of the resolving gel in the pre-cast cassette. A plastic comb was immediately inserted into the cassette to allow the formation of wells. The gel was then left at room temperature for 30 minutes. The compositions of the stacking gel buffer and stacking gel are outlined below:

Stacking gel buffer:

18.14 g	Tris/HCl
1.2 g	SDS
300 ml	Distilled Milli-Q water
Adjust to pH6.8 with HCl	

Stacking gel (4%, w/v):

3.12 ml	Stacking gel buffer
1.88 ml	Acrylamide (30%)
7.50 ml	Distilled Milli-Q water
12.5 ml	Total volume

2.13.2.1 Protein sample preparation for SDS-PAGE and electrophoresis condition

Generally, 10–20 µl of protein solution containing 5–20 µg proteins was used in the preparation of protein samples for SDS-PAGE. Two volumes of protein solution was mixed with one volume of SDS denaturing buffer (3x) in a 1.5 ml microfuge tube and incubated for 15 minutes at 95^{o}C. The denatured protein samples were allowed to cool to room temperature before they were loaded onto the gel. A molecular weight standard, Mark 12 (Invitrogen, USA; Table 15), was also loaded onto the gel and used to estimate the molecular weight of proteins on SDS-PAGE. The electrophoresis conditions were 15 mA and 25 mA for proteins running through the stacking and resolving gels, respectively. The compositions of the denaturing buffer used for SDS-PAGE protein sample preparation are shown below:

Denaturing buffer (3x):

8.0 g	SDS
37.2 mg	EDTA
40.0 ml	Glycerol
20.0 ml	β-mercaptoethanol
10.0 mg	Bromothymol blue

Make up to 100 ml with Tris/HCl (100 mM, pH 6.8)

Table 15.

Protein Marker

Protein marker	**Molecular weights (kDa)**
Mark 12	200, 116.3, 97.4, 66.3, 55.4, 36.5, 31, 21.5, 14.4, 6, 3.5, 2.5

2.13.2.2 Protein staining and destaining solution

The SDS-PAGE gel was carefully removed and stained by incubating with Coomassie Brilliant Blue Staining solution for 15 minutes on a tilt-shaker (Labnet International, USA) on a slow setting. After staining, the gel was washed with distilled water and destained by incubating with destaining solution for three to four hours with shaking until protein bands were visible and the background colour from the staining solution was removed. Gel images were obtained using the GEL-DOC 2000 (Bio-Rad Laboratories, USA) and Image Lab Software (Version 3.0 build 11, Bio-Rad Laboratories, USA). The compositions of staining and destaining solutions are outlined below:

Coomassie Brilliant Blue Staining solution:

4 g	Coomassie blue R-250
450 ml	Ethanol
90 ml	Acetic acid
460 ml	Distilled water

Destaining solution:

660 ml	Ethanol
200 ml	Acetic acid
1,140 ml	Distilled water

2.13.3 Densitometry

Densitometry was used to determine a fusion protein percentage of the total protein in bead fractions by analyzing the gel images of SDS-PAGE (Section 2.13.2) through myImageAnalysis Software (Thermo Scientific).

2.13.4 Maldi-TOF mass spectrometry

Protein bands of interest on SDS-PAGE were excised and subjected to protein identification using matrix-assisted, laser desorption, ionization time-of-flight mass spectrometry (Maldi-TOF/MS) (Jahns & Rehm, 2009). Protein sample preparation and

Maldi-TOF/MS analysis were performed by The Centre for Protein Research (Otago University, Dunedin, New Zealand).

2.13.5 Determination of fusion protein activity on PHA and protein beads

2.13.5.1 Enzyme-linked immunosorbent assay

Specific activity of the PHA beads displaying the TB antigens was determined using Enzyme-linked immunosorbent assay (ELISA) as previously described (Parlane, Wedlock, Buddle, & Rehm, 2009). A high-binding capacity microtitre plate (Greiner bio-one) was coated at 4°C overnight with 100 µl of control beads or purified PHA beads displaying TB antigens. These bead samples were diluted in a carbonate-bicarbonate coating buffer, pH 9.6 (Sigma-Aldrich), at protein concentrations ranging from 100 µg/ml to 0.05 µg/ml over serial dilutions. As positive controls for the ELISA assay, the microtitre plates were also coated with 100 µl of free single or a mixture of the three single TB antigens, provided by Dr H.M. Vordermeier (AHVLA, UK) at 4^{o}C and left overnight and diluted in a carbonate-bicarbonate coating buffer at protein concentrations ranging from 1 µg/ml to 0.125 µg/ml. Plates were washed three times with 1x PBS (Section 2.11.1.) containing 0.05% (vol/vol) Tween 20 (PBST) and then blocked with 3% (wt/vol) BSA for one hour at room temperature to prevent non-specific binding of antibodies to the well's surface. Plates were washed three times with PBST to remove unbound BSA. The plates were then incubated with 100 µl of mouse monoclonal antibody (1:1,000 dilutions) to CFP-10 or ESAT-6 (both antibodies were from Abcam, Cambridge, UK), or poly-clonal rabbit sera (1:1,000 dilutions) produced against recombinant Rv3615c (AgResearch, Hamilton, New Zealand) or pre-immune rabbit serum (1:100 dilutions) for one hour at room temperature. Following washing with PBST, the plates were incubated with 100 µl of anti-mouse IgG-horseradish peroxidase (HRP) conjugate (1:5,000 dilutions) or anti-rabbit HRP-conjugate (1:5,000 dilutions) for one hour at room temperature. After further washing, 100 µl of substrate, *o*-pheylenediamine, as prepared according to the manufacturer's instructions (Abbott Diagnostics, IL, USA) was added and incubated for 15 minutes at room temperature. The reaction was stopped by adding 50 µl of 1 N H_2SO_4, and the absorbance was measured at 490 nm on an ELx808iu ultra microtiter

plate reader (BIO-TEK Instruments Inc., USA) (Jahns, Haverkamp, & Rehm, 2008). Results were expressed as optical density units at 490 nm.

2.13.5.2 TB skin test on cattle

A TB skin test on cattle was performed by the Hopkirk Research Institute, AgResearch (Palmerston North, New Zealand). Ten 15-month-old Friesian-cross cattle were experimentally infected with a dose of approximately 5×10^3 colony forming units of *M. bovis* intratracheally, as previously described (Buddle et al., 1995). These infected cattle were kept on pasture in an isolation unit that was completely separated from the paddocks where 14 control cattle of an equivalent age and breed were grazing. All cattle involved in this test were sourced from TB-free herds and located in TB-free regions of New Zealand. Before the *M. bovis* inoculation, the cattle tested negative in the IFNγ test (BOVIGAM™ test; Prionics, Switzerland) for bovine TB, and the control cattle were negative in this test throughout the study using the standard interpretation, as described previously (Buddle, Livingstone, & Lisle, 2009). At 27 weeks after *M. bovis* infection, the infected and control cattle were tested in a comparative cervical skin test. These tests compared responses for PHA beads displaying triple TB antigen and control PHA beads with those for the PPD from *M. bovis* (PPD-B; 5,000 IU/0.1 ml injection) and *M. avium* (PPD-A; 2,500 IU/0.1 ml injection; AsureQuality, Upper Hutt, New Zealand). The 0.1 ml inoculum of the PHA beads displaying TB antigens contained 3.3 µg fusion protein, consisting of 0.9 µg of the mycobacterial proteins and 2.4 µg PhaC protein, and mixed in PBS. The control PHA beads contained 3.3 µg PhaC protein in 1x PBS. The skin thickness at the injection site was measured using callipers immediately before injection and 72 hours later, and results are expressed as the change in skin thickness (mm). The *M. bovis*-infected animals were killed and necropsied at 28 weeks after infection. Tuberculous lesions, like those typically found in naturally-infected animals, were identified in the lungs and/or pulmonary lymph nodes of the 10 test animals. *M. bovis* was then cultured from the lesions of all these animals using the BACTEC method and confirmed by AccuProbe. The AgResearch Grasslands Animal Ethics Committee approved all animal procedures.

2.13.5.2.1 Statistical analysis

The Kruskall-Wallis test was used to compare the *in vitro* ELISA responses for the antigen activity on PHA beads and analyze the cross-reactivity of the specific antisera with heterologous antigens. ANOVA was used to compare the skin test responses to the PPD-B and the triple TB antigen beads. The correlation between the skin test responses for bovine PPB and the triple antigen bead in the experimentally-infected cattle was undertaken using Spearman's rank correlation test. Statistical analyses were performed using package "agricolae" in R.3.0.1., and statistical significance was denoted when $P < 0.05$.

2.13.5.3 IgG-binding capacity assay

An IgG-binding capacity assay was used to assess the maximum IgG-binding ability of FP and PHA beads displaying the ZZ or [GB1]3 domains on their surface, as previously described (Jahns et al., 2013). For every sample, 50 mg wet weight of IgG-binding beads and control beads was measured in a 1.5 ml microfuge tube. All bead samples were washed twice with 1x PBS buffer (pH7.5) by pipetting. Samples were centrifuged at 6000 x g for four minutes (Heraeus Pico 17, Thermo Scientific) between each wash in order to remove storage ethanol. All samples were re-suspended in 500 µl 1x PBS buffer, and 5 mg purified goat IgG (Innovative Research, USA) or human IgG (Sigma-Aldrich, USA) was added to each sample and incubated at 25^{o}C for 30 minutes with agitation to allow IgG binding to occur. The tubes were centrifuged at 6,000 x g for four minutes after incubation, and the supernatants containing the unbound fraction of IgG were aliquoted and analyzed. The sediment was washed three times with a 1x PBS buffer by pipetting, followed by centrifugation at 6,000 x g for four minutes between each wash. Bound IgG from PHA and FP protein beads was eluted by re-suspending the sediment in 0.5 ml of 50 mM Glycine (pH 2.7) and incubated at room temperature for five minutes with agitation. All samples were centrifuged at 16,200 x g for four minutes and the supernatant (approximately 0.5 ml) containing eluted IgG was transferred into a new 1.5 ml microfuge tube. Supernatants with a low pH were immediately neutralized by adding 10 µl of 1 M K_2HPO_4 and stored at -20^{o}C so that further analysis could be performed.

2.13.5.4 IgG-binding condition test

The IgG-binding method described in Section 2.13.5.3 was also used to test IgG-binding ability under different conditions of temperatures and pH. Briefly, FP beads displaying the [GB1]3 or ZZ domains were re-suspended in 1x PBS buffer (pH 7.5) and incubated with purified IgG for 30 minutes at 4, 25, 35, 45, 55, and 65^{o}C in a Digital Dry Bath (Labnet Intenational, USA) with shaking. All bead samples were also re-suspended in a 1x PBS buffer and incubated with IgG for 30 minutes with different pHs (4, 5, 6, 7, 8, 9, 10, and 11) at 40^{o}C (for beads displaying ZZ) and 45^{o}C (for beads displaying the [GB1]3 domains) with agitation.

2.13.5.5 Purification of IgG from human serum

Purification of IgG from human serum (Sigma-Aldrich, USA) was used to assess the IgG purification ability of FP and PHA beads displaying the ZZ or [GB1]3 domains on their surface (Jahns et al., 2013). Approximately 50 mg wet weight of beads was measured per sample in a 1.5 ml microfuge tube. All bead samples were washed as described below:

- Twice with TBS (5 mM Tris/HCl, 150 mM NaCl, pH 7.4);
- Once with 50 mM Tris/HCl, 500 mM NaCl, pH 7.4;
- Once with 50 mM Tris/HCl, 37.5 mM NaCl, pH 7.4; and
- Once with TBS.

Samples were centrifuged at 6000 x g for four minutes between each wash and supernatants were discarded. After washing, all bead samples were incubated with an excess of human serum (the stock human serum was diluted four fold, and then added 200 µl diluted serum to 50 mg beads and made the volume up to 1 ml by adding 1x PBS buffer) for 30 minutes at room temperature with agitation. After incubation, the tubes were centrifuged at 6,000x g for four minutes (Heraeus Pico 17, Thermo Scientific) and aliquots of the supernatant (the unbound fraction) were taken for further analysis. The sediments were then washed as outlined below:

- Once with TBS;
- Twice with 50 mM Tris/HCl, 500 mM NaCl, pH 7.4; and
- Twice with 50 mM Tris/HCl, 37.5 mM NaCl, pH 7.4.

Bound proteins were then eluted by re-suspending the sediment in 0.5 ml of 50 mM Glycine (pH 2.7) and incubated at room temperature for five minutes with agitation. All bead samples were centrifuged at 16,200 x g for four minutes and the supernatant (the elution fraction) was transferred into a 1.5 ml microfuge tube. The supernatant was immediately neutralized to approximately pH 7.0 by adding 10 µl of 1 M K_2HPO_4 and stored at -20^{o}C for analysis.

2.13.5.6 IgG-binding assay of magnetized protein beads

For each sample, 20–40 mg wet weight of FP protein beads was measured in a 1.5 ml microfuge tube. All bead samples were washed twice with 1x PBS buffer by pipetting. Samples were then centrifuged at 6000 x g for four minutes (Heraeus Pico 17, Thermo Scientific) after each wash. Freshly prepared ferrofluid (Section 2.13.5.6.1) was thoroughly mixed with the plain beads at a ratio of 20:1 (volume, µl: wet weight, mg) and then incubated at 25^{o}C for 30 minutes with agitation. After incubation, the tubes were centrifuged at 6,000 x g for four minutes and supernatant was discarded. The pellet (magnetized beads) was washed three times with 1x PBS buffer by incubating on a magnetic rack for two minutes. To bind IgG to the beads, all samples were then re-suspended in 500 µl of 1x PBS buffer and 2-4 mg purified human IgG (Sigma-Aldrich, USA) was added to each sample and incubated at 25^{o}C for 30 minutes with agitation. The tubes were then incubated on a magnetic rack for two minutes, and aliquots of the supernatant (the unbound IgG fraction) were taken for further analysis. The sediment was washed three times with 1x PBS buffer by incubating on a magnetic rack for two minutes. Bound IgG was eluted by re-suspending the sediment in 0.5 ml of 50 mM Glycine (pH 2.7) and incubated at room temperature for five minutes with agitation. All samples were centrifuged at 16,200 x g for four minutes, and the supernatants (eluted IgG fraction) were transferred into 1.5 ml microfuge tubes. Supernatants with a low pH were immediately neutralized by adding 10 µl of 1 M K_2HPO_4. Samples were stored at -20^{o}C for further analysis.

2.13.5.6.1 Ferrofluid solution

Ferrofluid solution, containing surfactants and iron oxide particles, was used to magnetize various beads displaying iron-binding peptides as previously described (Berger et al., 1999) and prepared by PolyBatics (Palmerston North, New Zealand). Briefly, 1 ml of $FeCl_3$ (in 2 M HCl) was slowly mixed with 4 ml of $FeCl_2$ (in 2 M HCl) by stirring, while 50 ml of 0.7 M liquid ammonia was also added dropwise to the mix. The solution was then transferred into falcon tubes and centrifuged at 1,000 rpm for one minute in a Heraeus Multifuge 1 S-R (Sorval, Germany). The sediment was re-suspended into 8 ml of 25% $(CH_3)_4NOH$ and the excess of ammonia were evaporated with a vacuum filtration flask for 30 minutes. Distilled Milli-Q water was added to bring up the volume to 50 ml. This ferrofluid was highly alkaline, with a pH of 14. For neutralizing this solution, glacial acetic acid was added (30 µl per 1 ml of ferrofluid) and thoroughly mixed by vortexing, and then incubated on a magnetic rack for two minutes. After neutralization, the sediment was re-suspended in 1x PBS buffer, which brought the pH down to approximately 7.5.

Chapter 3: Results

3.1 Development of a specific bovine TB diagnostic reagent by developing antigen-displaying PHA beads

To develop a specific bovine TB diagnostic test, antigens CFP10, Rv3615c, and ESAT6 were displayed on the surface of PHA beads individually or in combination to produce four functionalized reagents. To achieve this, the following four plasmids were constructed: (1) pET-14b cfp10-phaC; (2) pET-14b rv3615c-phaC; (3) pET-14b esat6-phaC; and (4) pET-14b cfp10-linker-rv3615c-phaC-linker-esat6 (Table 3, Section 2.1.2). The first three plasmids carrying individual genes (*esat6*, *cfp10,* or *Rv3615c*) were constructed by Jason Lee (IFS, Massey University, Palmerston North, New Zealand), while I constructed the final plasmid harbouring all three genes as described in Section 3.1.1.

The hypotheses for this TB study were that PHA beads displaying all three antigens would show a better performance than beads displaying single antigens. Furthermore, the triple antigen beads would be capable of differentiating TB-infected from non-infected cattle. In order to test these hypotheses, the reactivity of the beads displaying either individual or a combination of all three antigens was assessed, both *in vitro* and *in vivo*. For *in vitro* assessment of bead reactivity, ELISA (Section 2.13.5.1) was performed to evaluate the accessibility and structural integrity of TB antigens displayed on the surface of PHA beads (Section 3.1.6). For *in vivo* assessment of bead functionality, purified TB antigen beads were tested in a cattle model in collaboration with Natalie Parlane, Neil Wedlock, and Bryce Buddle of the Hopkirk Research Institute, AgResearch, Palmerston North, New Zealand. Results for these experiments are presented in Section 3.1.7.

3.1.1 Construction of pET-14b cfp10-linker-rv3615c-phaC-linker-esat6

The strategy for constructing the plasmid encoding the three TB antigen genes, pET-14b cfp10-linker-rv3615c-phaC-linker-esat6, is presented in Figure 7. The gene fragment encoding the antigen ESAT6 was excised from the pUC57 vector, which was obtained from Genescript Corporation (USA) by DNA hydrolysis (Section 2.10.2) using two restriction enzymes, *Xho*I and *Bam*HI. The *esat6* fragment was then separated from the digestion mixture using AGE with SYBR safe stain (Section 2.10.4) and isolated and purified using gel purification (Section 2.10.5). Meanwhile, the plasmid pET-14b cfp10-linker-rv3615c-phaC-linker-malE (Table 3) was digested (Section 2.10.2) with *Xho*I and *Bam*HI, and the resulting linearized vector backbone fragment, pET-14b cfp10-linker-rv3615c-phaC-linker, was isolated (Section 2.10.4) and purified (Section 2.10.5). Subsequently, the *esat6* gene and linearized vector fragment were ligated together (Section 2.10.7), generating the final plasmid, pET-14b cfp10-linker-rv3615c-phaC-linker-esat6 containing the three TB antigen genes. This plasmid was transformed (Section 2.9) into *E. coli* XL-Blue (Section 2.1.1) and spread-plated onto a LB-agar medium containing ampicillin. Single colonies were selected for plasmid isolation (Section 2.10.1), and DNA sequence was confirmed by the Massey University Genome Service (Section 2.10.8).

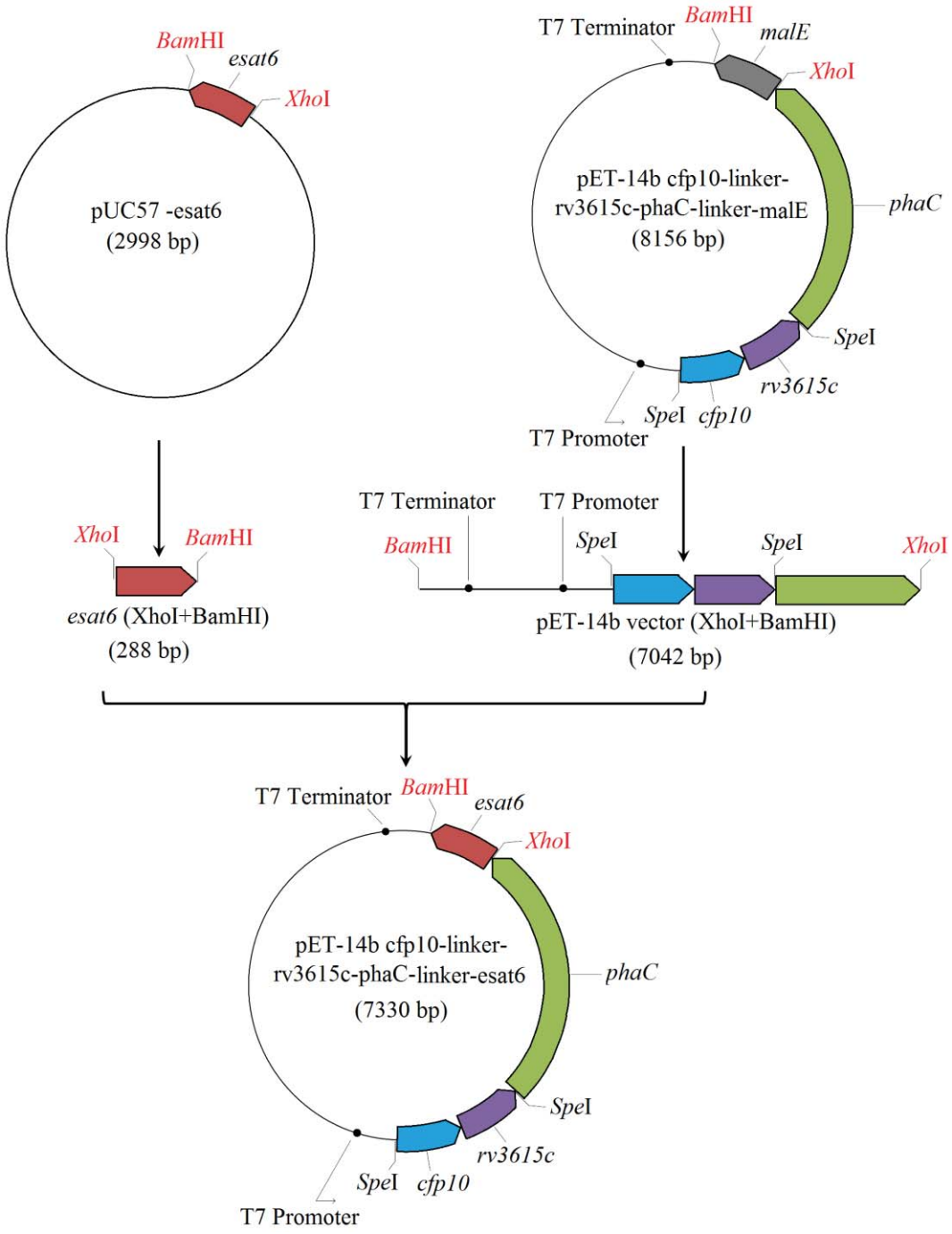

Figure 7. **Construction of pET-14b cfp10-linker-rv3615c-phaC-linker-esat6.** The DNA fragment encoding the *esat6* gene was isolated from pUC57-esat6 by a restriction digest with *Xho*I and *Bam*HI (Section 2.10.2), followed by separation of DNA fragments using agarose gel electrophoresis (Section 2.10.4) and gel purification (Section 2.10.5). The *esat6* gene was ligated into linearized vector pET-14b *cfp10*-linker-*rv3615c-phaC*-linker, generated by restriction digest with *Xho*I and *Bam*HI, using T4 DNA ligase (Section 2.10.7) to generate the final plasmid, pET-14b cfp10-linker-rv3615c-phaC-linker-esat6.

3.1.2 Composition of plasmids encoding PhaC and containing either single or all three mycobacterial genes

The modular compositions of the various hybrid genes and encoded fusion proteins are outlined in Figure 8. These hybrid genes were constructed to encode fusion proteins that mediate intracellular production of PHA beads either displaying single TB antigens or all three TB antigens. To display single TB antigens on the surface of PHA beads, individual antigens were directly fused to the N-terminus of PhaC. In contrast, to display three antigens on PHA beads, the CFP10 and Rv3615c antigens were fused to the N-terminus, while the ESAT6 antigen was fused to the C-terminus of PhaC.

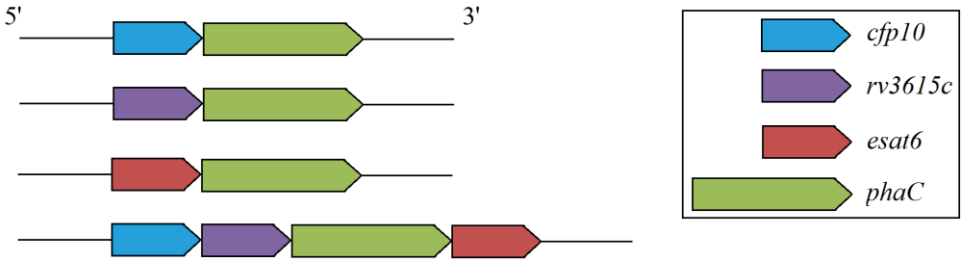

Figure 8. **Schematic representation of hybrid genes encoding fusion proteins mediated production of PHA beads displaying TB antigens.**

3.1.3 Plasmid expression and PHA bead production

The pET expression vector is comprised of several important features: a *lacI* gene (encodes a *lac* repressor), a T7 promoter (specific for T7 RNA polymerase), a *lac* operator, a f1 origin of replication, an ampicillin resistance gene, and a ColE1 origin of replication. The pET expression system allows the overproduction of fusion proteins by enabling high expression of recombinant genes encoded by pET–derived plasmids using the T7 RNA polymerase. This polymerase was provided by *E. coli* production strain BL21 (DE3, Stratagene) in this study.

The gene encoding the Class I PHA synthase PhaC of *C. necator* and the mycobacterial antigens (CFP10, Rv3615c and/or ESAT6) were incorporated into the pET expression vector. These recombinant expression vectors were transformed into *E. coli* (Section 2.9) production strain BL21(DE3), harbouring pMCS69 for *in vivo* PHA bead production. Plasmid pMCS69 contains the genes–encoding enzymes PhaA and PhaB of *C. necator*

(Table 3) that synthesize the precursors for PHA synthesis. *E. coli* cells harboring the various plasmids were cultivated under PHA–accumulating conditions (Section 2.6.1) to produce PHA beads displaying one or three TB antigens. The beads were subsequently isolated (Section 2.11).

3.1.4 Characterization of PHA beads displaying mycobacterial antigens

PHA–accumulating *E. coli* cells were stained with Nile-red (Section 2.12.1.1) and visualized by fluorescent microscopy (Section 2.12.1.2). Fluorescence indicated the presence of intracellular PHA beads in *E. coli* cells and activity of PHA synthase (Figure 9). This observation was further verified by TEM analysis of recombinant *E. coli* cells harbouring various plasmids and of PHA beads isolated from the production host (Figure 10). These TEM images show the formation of PHA beads mediated by the respective fusion protein inside recombinant *E. coli* cells. Accumulation of intracellular PHA beads was further confirmed and quantified by GC-MS (Section 2.12.2). GC-MS analysis shows that cells were accumulating the polyester polyhydroxybutyrate, which contributes to approximately 31.5%, 10%, 30%, 14.3%, and 40% of cellular dry weight when genes encoding PhaC, CFP10-PhaC, Rv3615c-PhaC, ESAT6-PhaC, and CFP10-Rv3615c-PhaC-ESAT6, respectively, were present (data not shown).

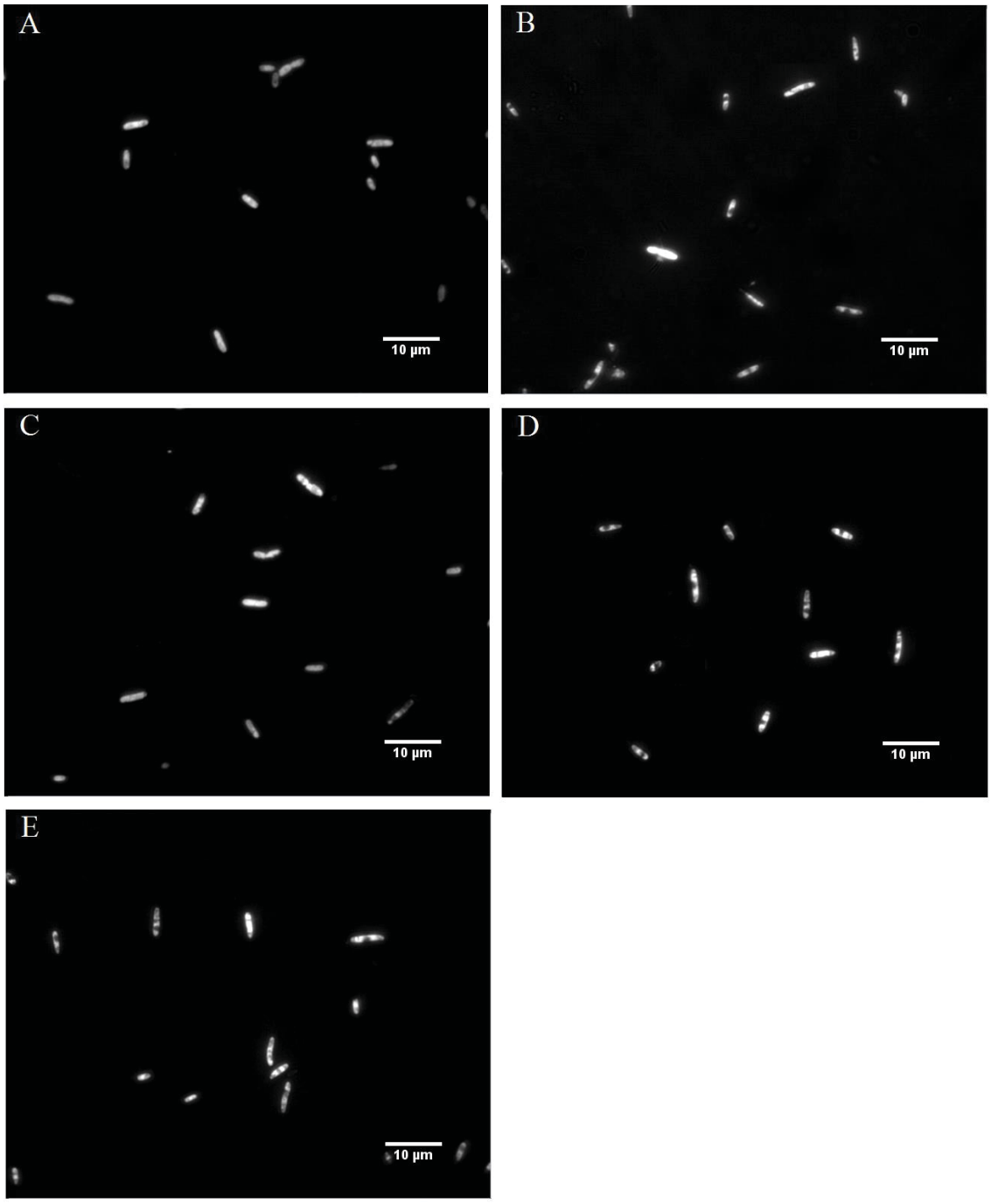

***Figure 9*. Fluorescence microscopy images of PHA beads produced in recombinant *E. coli* BL21 (DE3), harbouring pMCS69 and the various fusion protein-encoding pET expression vectors stained with Nile red.** Detection of PHA beads was described in the Materials and Methods chapter (Section 2.12.1). (A) pET-14b phaC; (B) pET-14b cfp10-phaC; (C) pET-14b rv3615c-phaC; (D) pET-14b esat6-phaC; and (E) pET-14b cfp10-linker-rv3615c-phaC-linker-esat6.

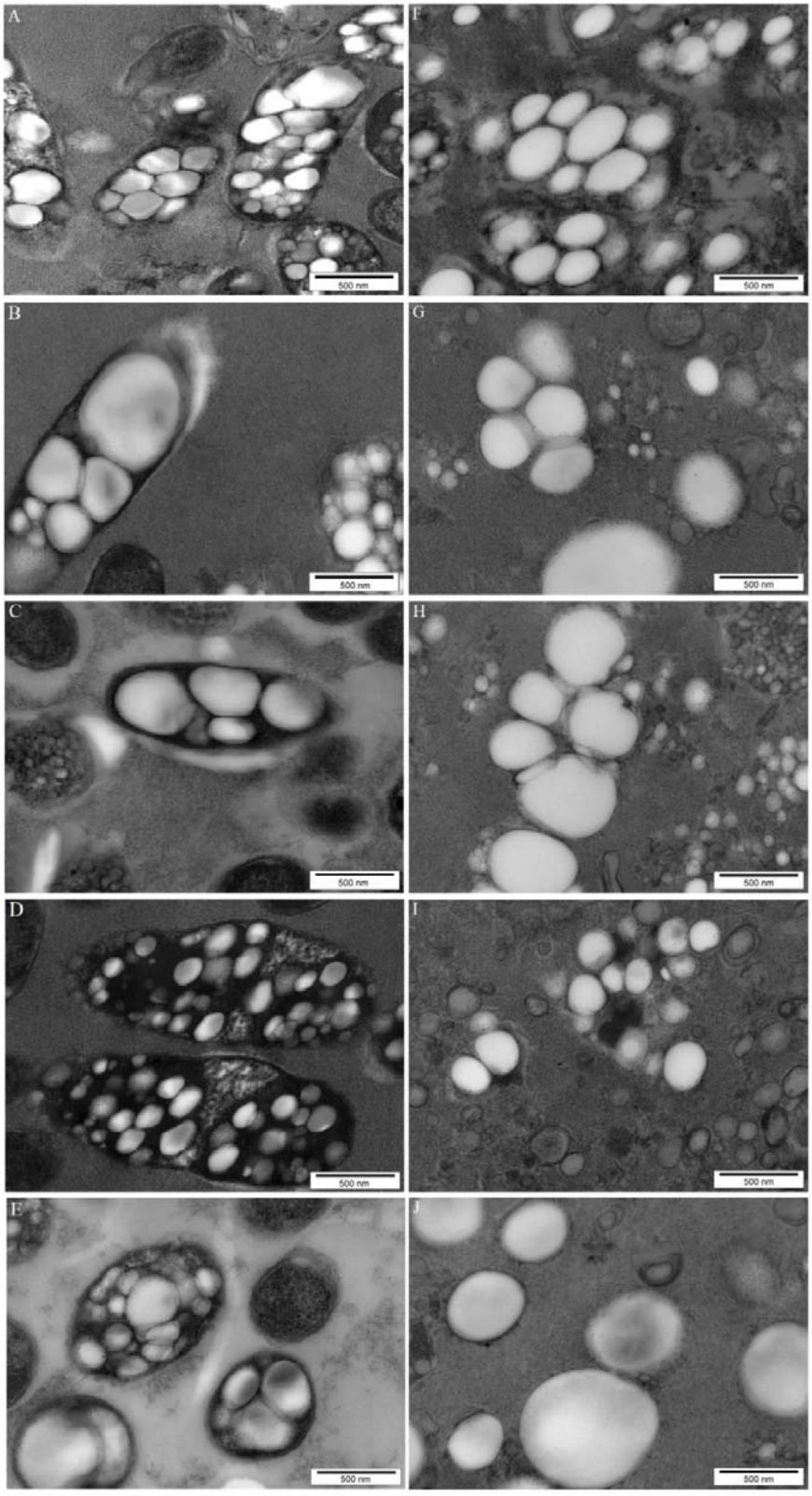

***Figure 10*. TEM analysis of recombinant *E. coli* harboring various plasmids (A-E) and of isolated PHA beads displaying mycobacterial antigens (F-J).** TEM microscopy was described in the Materials and Methods chapter (Section 2.12.3). (A and F) pET-14b phaC; (B and G) pET-14b cfp10-phaC; (C and H) pET-14b rv3615c-phaC; (D and I) pET-14b esat6-phaC; and (E and J) pET-14b cfp10-linker-rv3615c-phaC-linker-esat6.

3.1.5 Display of recombinant PhaC-TB antigen fusion protein on the surface of PHA beads

To test whether recombinant fusion proteins were successfully immobilized on the surface of PHA beads and whether these proteins were susceptible to proteolytic degradation, SDS-PAGE (Section 2.13.2) was used to analyze the PHA bead protein profile (Figure 11). The theoretical molecular weight of recombinant fusion proteins in this study were calculated utilizing the ProtParam tool from the ExPASy Proteomics Server (http://www.expasy.org/). Recombinant fusion protein in purified PHA bead fraction was quantified by Bradford assay (Section 2.13.1) before being loaded onto SDS-PAGE. Dominant protein bands were observed corresponding to proteins with theoretical molecular weights of 63 kDa for PhaC; 74.3 kDa for the ESAT6-PhaC fusion; 75.2 kDa for CFP10-PhaC; 75.2 kDa for Rv3615c-PhaC; and 98.1 kDa for CFP10-Rv3615c-PhaC-ESAT6. These four PhaC-TB fusion proteins (CFP10-PhaC, Rv3615c-PhaC, ESAT6-PhaC, and CFP10-Rv3615c-PhaC-ESAT6) were identified by tryptic peptide fingerprinting using Maldi-TOF/MS (Section 2.13.4, Appendix I). Densitometry analysis (Section 2.13.3) of the SDS-PAGE showed that PhaC accounted for 20% of the total protein in the PhaC bead fraction, while CFP10-PhaC, Rv3615c-PhaC, ESAT6-PhaC, and CFP10-Rv3615c-PhaC-ESAT6 accounted for approximately 26% of the total protein in their corresponding bead fractions (data not shown).

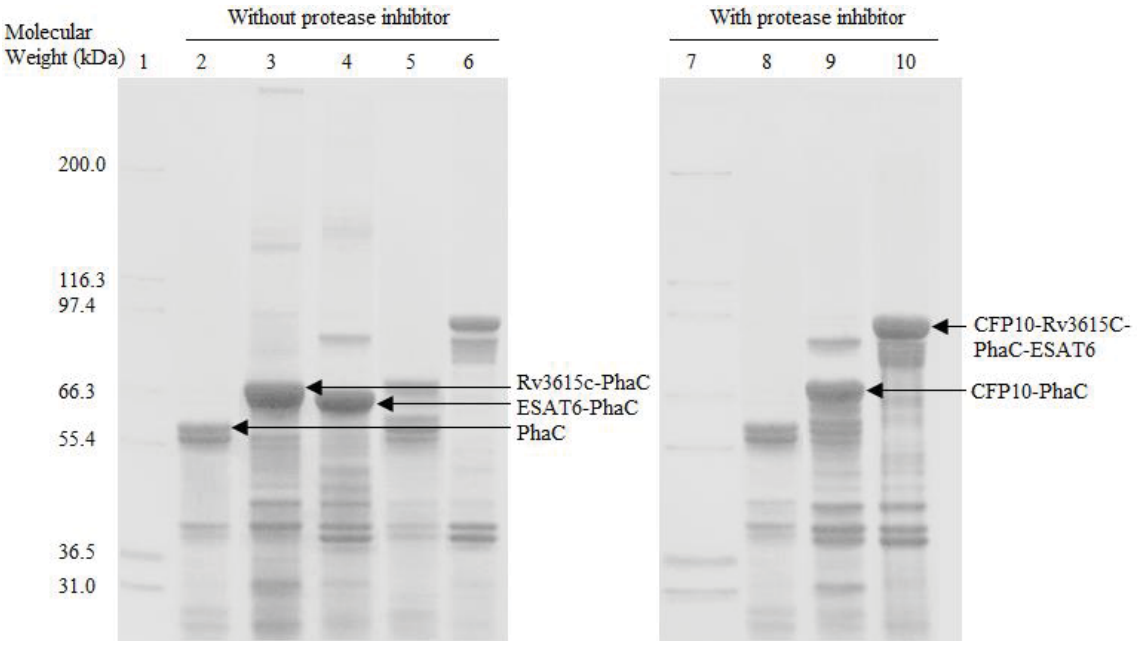

Figure 11. **Protein profiles of PHA beads isolated from recombinant *E. coli* cells harbouring various plasmids with and without a protease inhibitor treatment during the beads' isolation process.** Lanes 2-6, samples without protease inhibitor treatment during bead extraction, and lanes 8-10 with protease inhibitor treatment during bead isolation. Lanes 1 and 7, molecular weight marker (Mark 12, Invitrogen); lanes 2 and 8, PhaC (WT, 63kDa); lane 3, Rv3615c-PhaC (75.2 kDa); lane 4, ESAT6-PhaC (74.3 kDa); lanes 5 and 9, CFP10-PhaC (75.2 kDa); and lanes 6 and 10, CFP10-Rv3615c-PhaC-ESAT6 (98.1 kDa). The presence of PhaC-TB antigen fusion proteins was confirmed by tryptic peptide fingerprinting, utilizing Maldi-TOF/MS (Appendix I).

Degradation of PhaC-TB antigen fusion proteins was also assessed. As shown in Figure 11, the samples on the left panel of the SDS-PAGE were not treated by a protease inhibitor during the bead extraction process. The Rv3615c-PhaC and ESAT6-PhaC fusion proteins were stable and did not show protein degradation (Lanes 3 and 4). However, an increased level of protein degradation was observed in the CFP10-PhaC and CFP10-Rv3615c-PhaC-ESAT6 fusion proteins (Lanes 5 and 6). The samples on the right panel of the SDS-PAGE were treated with protease inhibitor during bead isolation. The presence of protease inhibitor prevented the degradation of the recombinant fusion proteins containing the CFP10 antigen (Lanes 9 and 10). This indicated that the PhaC-TB antigen fusion proteins containing CFP10 were sensitive to protease digestion during bead isolation and purification (Figure 11). A schematic view of the triple TB antigen displaying PHA beads is shown in Figure 12.

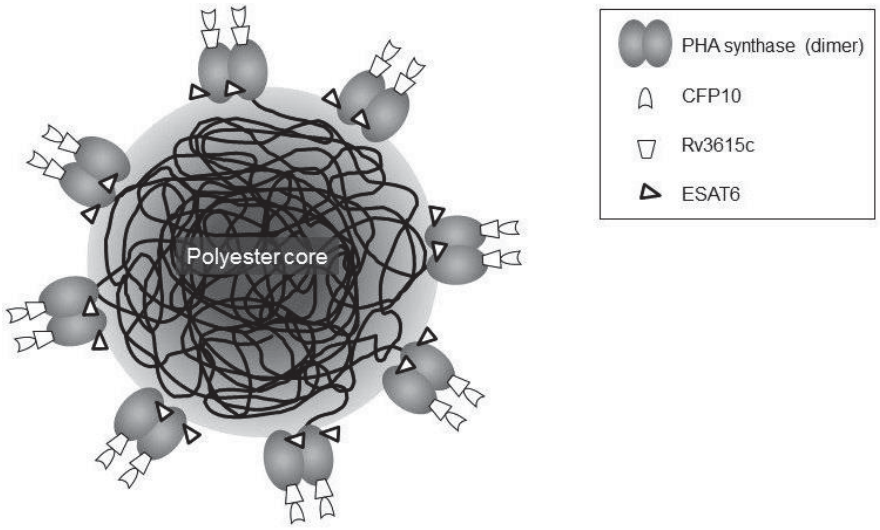

Figure 12. **Model of a triple mycobacterial antigen displaying PHA beads produced by recombinant *E. coli* cells.**

3.1.6 Functional assessment of TB antigen bead reactivity *in vitro*

The applicability of PHA beads displaying single or triple TB antigens as TB diagnostic reagents was assessed by an *in vitro* ELISA assay (Section 2.13.5.1). This allowed us to evaluate the accessibility and structural integrity of TB antigens displayed on the surface of PHA beads (Figure 13). In the reactivity test of the immobilized mycobacterial antigens (Figure 13A), the PHA beads only displaying PhaC served as the negative control (WT). Meanwhile, free recombinant single and a mixture of the three antigens (CFP10, Rv3615c, and ESAT6) were employed as positive controls for this experiment. Various immobilized TB antigens (bead-CFP10, bead-Rv3615c, bead-ESAT6, and bead-CFP10-Rv3615c-ESAT6) were test samples and analyzed. The following three specific antibodies were used: anti-CFP10, anti-Rv3615c, and anti-ESAT6. Results show that there was very low antibody binding in the negative control, suggesting that the naked PHA beads (with no TB antigens displayed) did not have binding sites for the antibodies used. However, a significant increase in the antibody binding of the positive controls was observed. Moreover, the antibody binding of beads displaying triple TB antigens was significantly higher than that for the beads displaying single antigens; this was also observed with the free recombinant single and a mixture of the three antigens (Figure 13A, $P < 0.05$).

In addition, the negative control experiment utilizing rabbit pre-immune sera instead of the three specific antibodies shows that all the samples have very low antibody binding to the rabbit pre-immune serum (Figure 13B). The cross-reactivity test shows that the antibody binding of TB antigens was significantly higher than that for the heterologous antigens when the corresponding antibody was applied (Figure 13C, $P < 0.05$). This suggests that the antibody binding of TB antigens was specific and, thus, the three specific antibodies did not have cross-reactivities with the other two TB antigens.

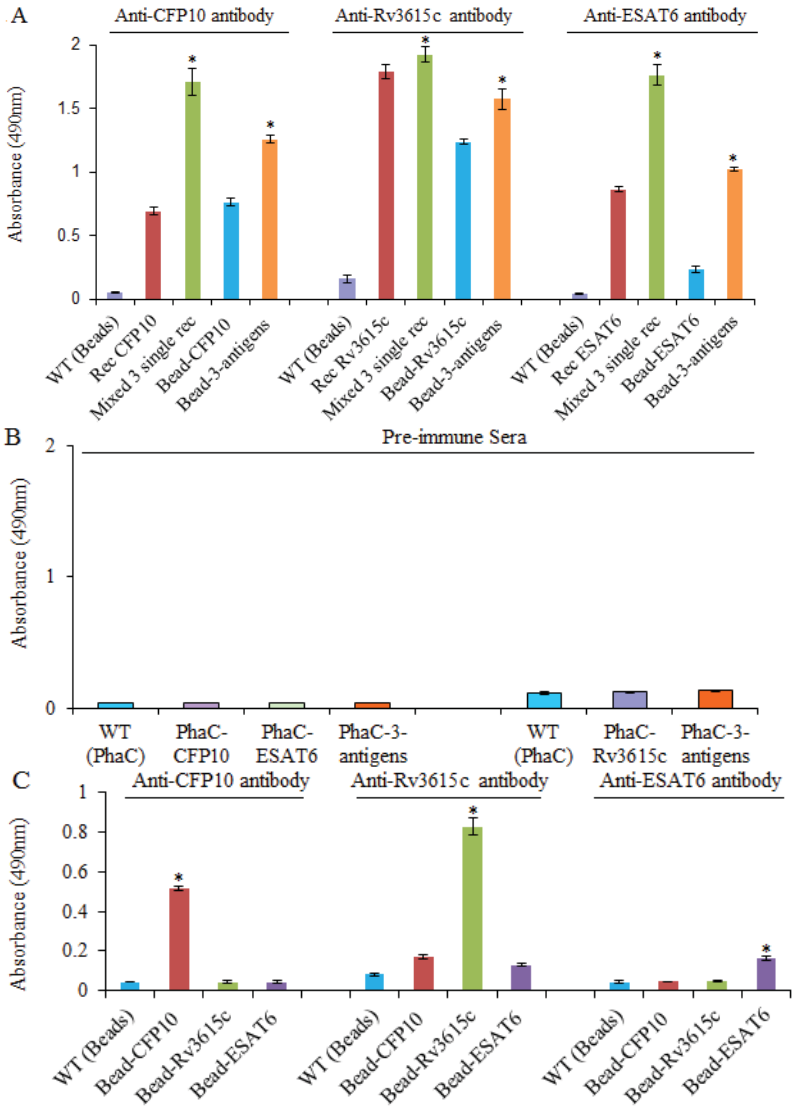

***Figure 13*. Functional assessment of TB antigen reactivity *in vitro*.** The ELISA assay was described in the Materials and Methods chapter (Section 2.13.5.1). All measurements were performed in triplicate. The mean of TB antigen reactivity to a specific antibody is shown ±SD (n=3). (A) Reactivity of TB antigens displayed on the surface of PHA beads. WT (beads) was the negative control, and free recombinant TB antigens (CFP10, Rv3615c, ESAT6, and the mixture of CFP10, Rv3615c and ESAT6) were utilized as positive controls. The testing samples were immobilized TB antigens (bead-CFP10, bead-Rv3615c, bead-ESAT6, and bead-CFP10-Rv3615c-ESAT6). The anti-CFP10 and anti-ESAT6 monoclonal antibodies were produced in a mouse, and the anti-Rv3615c polyclonal antibody was produced in a rabbit.

* Significantly higher than single antigen, $P < 0.05$. (B) Control experiment: the rabbit pre-immune serum was utilized to replace the three specific anti-TB antibodies. (C) Cross-reactivities of specific antibodies with the other two TB antigens. The total protein concentration of control beads, TB antigen beads, and free recombinant antigens in this figure was 1μg/ml, 1μg/ml and 0.125 μg/ml, respectively.

* Significantly higher than all other beads, $P < 0.05$.

3.1.7 Functional assessment of TB antigen bead reactivity *in vivo*

Functional analysis of the TB antigen bead reactivity *in vivo* (Section 2.13.5.2) was described in the Materials and Methods chapter and conducted in collaboration with Natalie Parlane, Neil Wedlock, and Bryce Buddle (Hopkirk Research Institute, AgResearch, Palmerston North, New Zealand). Immunogenicity and specificity of the triple TB antigen displaying beads *in vivo* were tested by injecting the respective beads into cattle intradermally. The TB skin test results are shown in Figure 14. Four diagnostic reagents, beads displaying three TB antigens, control beads, bovine PPD (PPD-B), and avian PPD (PPD-A), were applied for the TB skin tests on cattle. The result was defined as positive if the increase in skin thickness was more than 1 mm. The cattle infected with *M. bovis* (Figure 14A) all responded positively in the skin test to PPD-B alone. Moreover, all PPD-B responses were stronger than those for PPD-A. Responses to the triple antigen beads were all positive. However, there were no significant differences in the skin test responses between PPD-B and the triple antigen beads ($P < 0.05$). One animal showed a weak skin test response (2.5 mm increase in skin thickness) to the control beads, which did not display TB antigens. In contrast, all the non-infected cattle, naturally exposed to environmental mycobacteria (Figure 14B), responded negatively to the triple antigens bead reagents, while 11 cattle responded positively to PPD-A and three cattle to PPD-B.

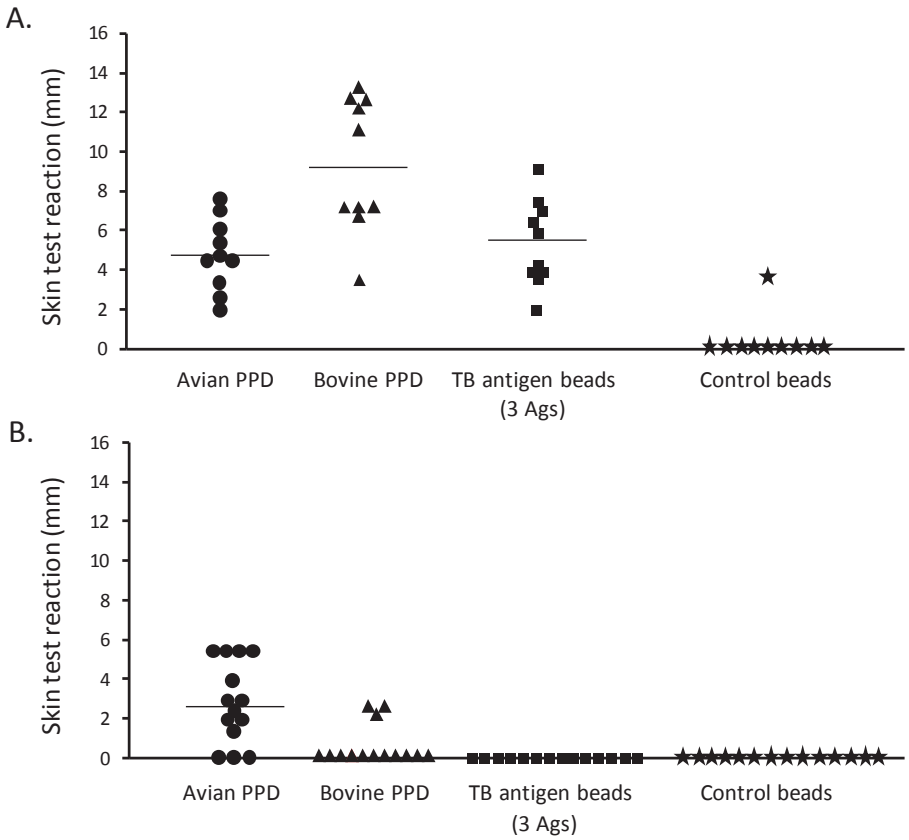

Figure 14. **TB skin test response in cattle.** Four diagnostic reagents, PPD-A, PPD-B, beads displaying the triple TB antigens, and control beads, were utilized for the TB skin tests on cattle. The test result was positive if the increase in skin thickness was more than 1mm. Bar stands for median. (A) Skin test responses of cattle experimentally-infected with *M. bovis*. (B) Skin test responses of non-infected cattle naturally sensitized to environmental mycobacteria.

3.2 Assessment of IgG-binding ability of the [GB1]3 domains on various FP beads

In order to assess the IgG-binding capacity of various FP beads displaying the [GB1]3 domains, the following plasmids were used for this study: pET-14b phaC-linker-[GB1]3; pET-14b eyfp-phaC(C319A)-linker-[gb1]3; pET-14b xeyfp-phaC(C319A)-linker-[gb1]3; pET-14b ecfp-phaC(C319A)-linker-[gb1]3; pET-14b xecfp-phaC(C319A)-linker-[gb1]3; pET-14b HcR-phaC(C319A)-linker-[gb1]3; and pET-14b xHcR-phaC(C319A)-linker-[gb1]3 (Table 4, Section 2.1.2). Jahns et al. (2013) cloned all these pET-14b plasmids containing various FP genes with or without the AVTS tetrapeptide N-terminal extension, and compositions of these plasmids are shown in Section 3.2.1.

As described in Section 1.9, the hypothesis in this section was that the [GB1]3 domains displayed on the surface of various FP beads would show a higher IgG binding ability than those displayed on the surface of PHA beads. In order to test this hypothesis, PHA and various FP beads displaying [GB1]3 were assessed with IgG-binding capacity assay (Section 2.13.5.3), and the results are presented in Section 3.2.4. These functionalized IgG-binding beads were also assessed in terms of testing their IgG bioseparation ability with human blood serum (Section 2.13.5.5), and the results are shown in Section 3.2.5. In addition, the IgG-binding capacity of various FP beads displaying the [GB1]3 domains at different temperatures and pHs were also assessed (Section 2.13.5.4), and the results are shown in Section 3.2.6.

3.2.1 Composition of plasmid – encoding fluorescent genes–PhaC(C319A) and the [GB1]3 domains

The modular compositions of hybrid genes and encoded fusion proteins are outlined in Figure 15. These hybrid genes were constructed to encode fluorescent fusion proteins that mediate intracellular production of protein beads displaying the triple IgG-binding domains [GB1]3. Fluorescent proteins with or without N-terminal extension were fused to the N-terminus of PhaC(C319A). The [GB1]3 domains were directly fused to the C-terminus of PhaC (C319A).

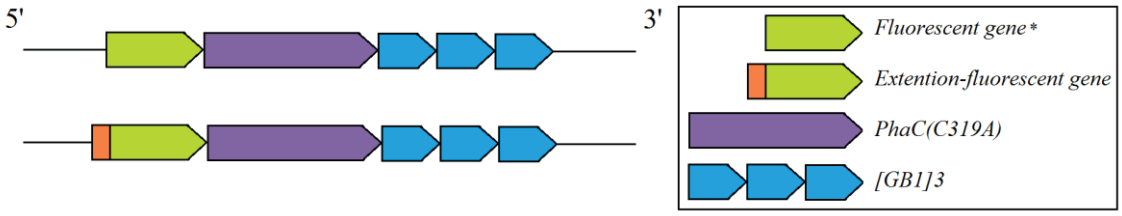

Figure 15. **Schematic representation of various hybrid genes encoding N-terminally extended or non-extended fluorescent protein-PhaC(C319A) fusion mediated production of fluorescent protein beads displaying the [GB1]3 domains.**

* Fluorescent genes including *eyfp* (yellow), *HcRed* (red), and *ecfp* (cyan).

3.2.2 Plasmid expression and FP beads production

The pET expression vectors containing genes encoding various FP, inactive synthase PhaC(C319A), and the [GB1]3 domains for *in vivo* protein bead production were transformed (Section 2.9), either into *E. coli* BL21 or BL21(pMCS69). *E. coli* cells harboring respective plasmids were cultivated under protein bead–accumulating conditions (Section 2.6.1) to produce FP beads displaying [GB1]3. Beads were then isolated (Section 2.11).

Nile-red staining (Section 2.12.1.1) and fluorescent microscopy (Section 2.12.1.2) were carried out to visualize PHA bead–accumulating cells. FP beads in cells were detected directly by fluorescent microscopy (Section 2.12.1.2). Fluorescence shown in Figure 16 indicates the presence of intracellular PHA and FP beads in the *E. coli* cells.

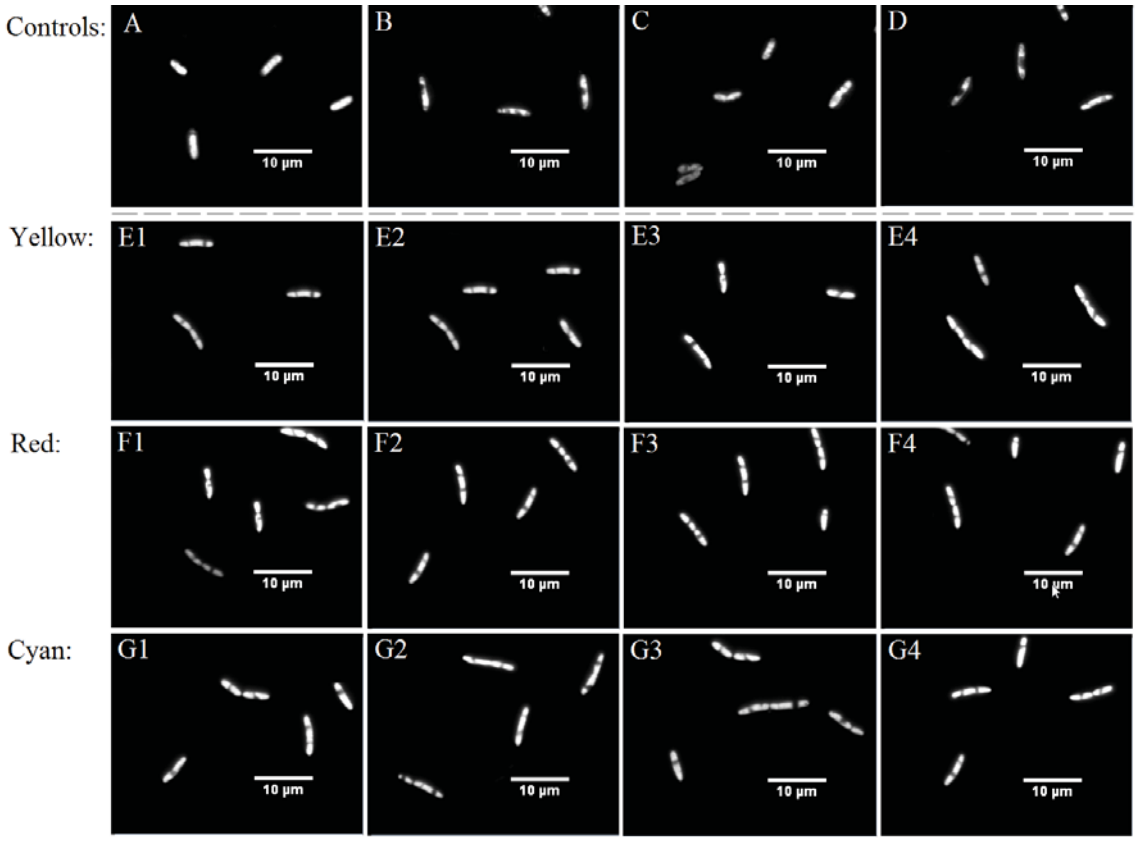

Figure 16. **Fluorescence microscopy images of PHA beads (A-D) or FP beads (E1-G4) produced in recombinant *E. coli* cells.** Detection of PHA or FP beads was described in the Materials and Methods chapter (Section 2.12.1). All beads were produced either in *E. coli* BL21 or BL21(pMCS69), harboring the respective pET plasmid (BL21/; BL21 69/). (A) BL21 69/PhaC; (B) BL21 69/xGFP-PhaC-MalE; (C) BL2169/ZZPhaC; (D) BL21 69/PhaC-[GB1]3; (E1) BL21/EYFP-PhaC(C319A)-[GB1]3; (E2) BL21 69/ EYFP-PhaC(C319A)-[GB1]3; (E3) BL21/xEYFP-PhaC(C319A)-[GB1]3; (E4) BL21 69/xEYFP-PhaC(C319A)-[GB1]3; (F1) BL21/HcR-PhaC(C319A)-[GB1]3; (F2) BL21 69/ HcR-PhaC(C319A)-[GB1]3; (F3) BL21/xHcR-PhaC(C319A)-[GB1]3; (F4) BL21 69/xHcR-PhaC(C319A)-[GB1]3; (G1) BL21/ECFP-PhaC(C319A)-[GB1]3; (G2) BL21 69/ECFP-PhaC(C319A)-[GB1]3; (G3) BL21/xECFP-PhaC(C319A)-[GB1]3; and (G4) BL21 69/xECFP-PhaC(C319A)-[GB1]3.

3.2.3 Display of the IgG-binding domains [GB1]3 on the surface of FP beads

SDS-PAGE (Section 2.13.2) was used to analyse the FP bead protein profile (Figure 17). Dominant protein bands were observed that corresponded to proteins with theoretical molecular weights of 114.7 kDa for EYFP-PhaC(C319A)-[GB1]3; 115.2 kDa for xEYFP-PhaC(C319A)-[GB1]3; 115.9 kDa for HcR-PhaC(C319A)-[GB1]3; 116.4 kDa for xHcR-PhaC(C319A)-[GB1]3; 119.6 kDa for ECFP-PhaC(C319A)-[GB1]3; and 120.1 kDa for xECFP-PhaC(C319A)-[GB1]3. Densitometry analysis (Section 2.13.3) of the SDS-PAGE showed that the fluorescent fusion proteins without the N-terminal extension (EYFP-PhaC(C319A)-[GB1]3, HcR-PhaC(C319A)-[GB1]3 and ECFP-PhaC(C319A)-[GB1]3) accounted for approximately 12% of the total protein in their corresponding bead fraction produced with or without pMCS69 background (data not shown). However, the N-terminally extended versions (xEYFP-PhaC(C319A)-[GB1]3, xHcR-PhaC(C319A)-[GB1]3, and xECFP-PhaC(C319A)-[GB1]3) accounted for about 23% of the total protein in their corresponding protein bead fraction produced in the presence or absence of pMCS69 background (data not shown). These results suggest that pMCS69, harboring the gene–encoding enzymes PhaA and PhaB of *C. necator,* did not have a significant impact on fluorescent fusion protein production. However, the recombinant fusion proteins containing the N-terminal extension (AVTS) significantly enhanced fusion protein production when compared to the non-extended versions.

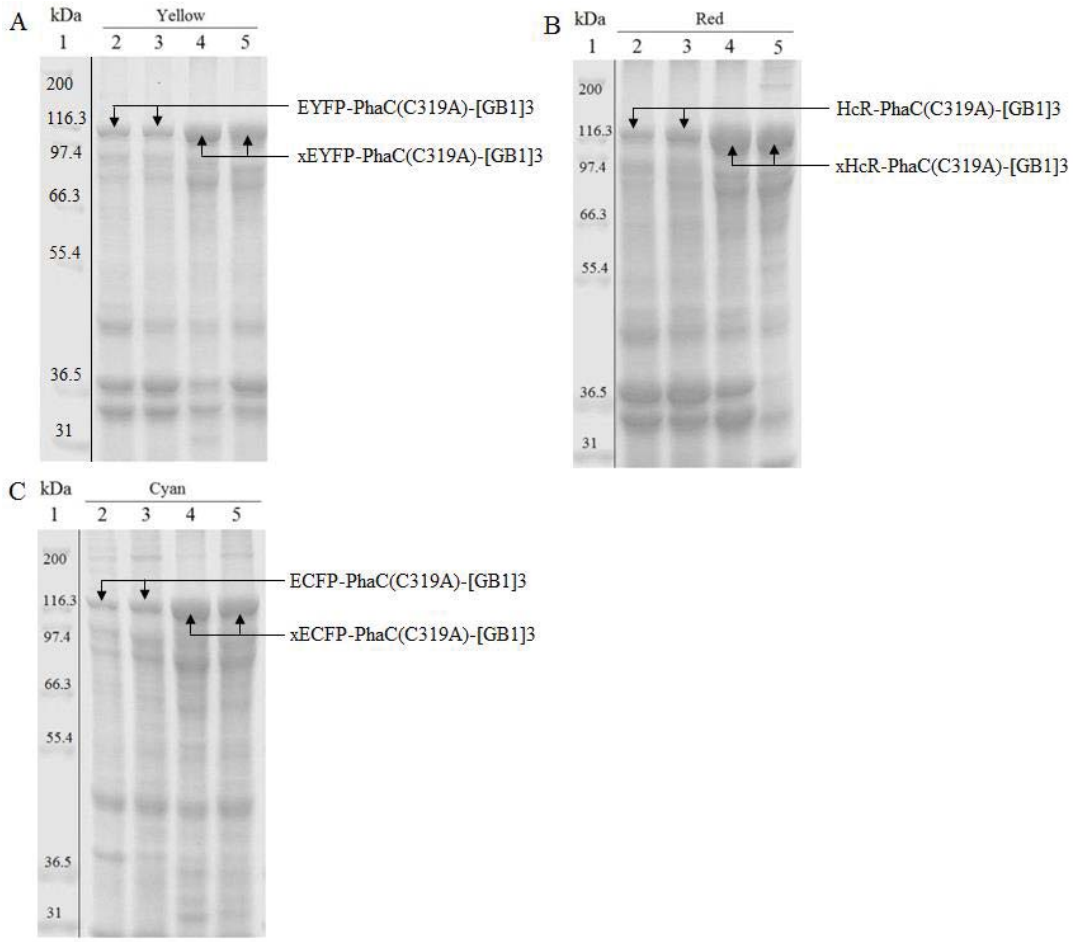

Figure 17. **Protein profiles of FP beads isolated from recombinant *E. coli* cells.** All FP beads were produced either in *E. coli* BL21 or BL21(pMCS69) harboring the respective pET plasmid (BL21/; BL21 69/). **(A)** Protein profiles of EYFP-PhaC(C319A)-[GB1]3 (114.7 kDa) and xEYFP-PhaC(C319A)-[GB1]3 (115.2 kDa) beads. Lane 1, molecular weight marker (Mark 12, Invitrogen); lane 2, FP beads derived from BL21/EYFP-PhaC(C319A)-[GB1]3; lane 3, FP beads derived from BL21 69/EYFP-PhaC(C319A)-[GB1]3; lane 4, FP beads derived from BL21/xEYFP-PhaC(C319A)-[GB1]3; and lane 5, FP beads derived from BL21 69/xEYFP-PhaC(C319A)-[GB1]3. **(B)** Protein profiles of HcR-PhaC(C319A)-[GB1]3 (115.9 kDa) and xHcR-PhaC(C319A)-[GB1]3 (116.4 kDa) beads. Lane 1, molecular weight marker; lane 2, FP beads derived from BL21/HcR-PhaC(C319A)-[GB1]3; lane 3, FP beads derived from BL21 69/HcR-PhaC(C319A)-[GB1]3; lane 4, FP beads derived from BL21/xHcR-PhaC(C319A)-[GB1]3; and lane 5, FP beads derived from BL21 69/xHcR-PhaC(C319A)-[GB1]3. **(C)** Protein profiles of ECFP-PhaC(C319A)-[GB1]3 (119.6 kDa) and xECFP-PhaC(C319A)-[GB1]3 (120.1 kDa) beads. Lane 1, molecular weight marker; lane 2, FP beads derived from BL21/ECFP-PhaC(C319A)-[GB1]3; lane 3, FP beads derived from BL21 69/ECFP-PhaC(C319A)-[GB1]3; lane 4, FP beads derived from BL21/xECFP-PhaC(C319A)-[GB1]3; and lane 5, FP beads derived from BL21 69/xECFP-PhaC(C319A)-[GB1]3.

3.2.4 Functional assessment of the IgG-binding domains [GB1]3 on various FP beads

To test the function of the [GB1]3 domains displayed on the surface of various FP beads, the binding ability of these beads to goat IgG was assessed (Section 2.13.5.3). (IgG binding ability = (Feed – unbound IgG)/Wet weight of protein beads). The unbound and eluted IgG fractions were quantified by the Bradford assay (Section 2.13.1). The IgG binding results are shown in Figure 18. Negative controls were PHA beads with no IgG-binding domains displayed (for example, naked PHA beads and PHA beads displaying MalE). Positive controls were the PHA beads displaying ZZ or [GB1]3 and commercial protein A beads. Recovery rate of IgG binding was between 75% and 90% (data not shown). Recovery rate was used to determine the percentage of IgG obtained from PHA or protein beads after elution (Recovery rate = Eluted IgG/(Feed – unbound IgG) × 100%). As shown in Figure 18, for negative controls, there were very low IgG-binding abilities, suggesting that goat IgG did not specifically bind to the PHA beads lacking IgG-binding domains (ZZ or [GB1]3 domains). Furthermore, protein beads made of the extended EYFP or ECFP displayed a greater goat IgG-binding ability when compared to their non-extended versions. In contrast, protein beads comprised of extended or non-extended HcR behaved similar with respect to goat IgG binding. Generally, FP beads displaying [GB1]3 showed an approximately 1.5- and 2-fold greater IgG-binding ability when compared to PHA beads displaying [GB1]3 and beads varieties displaying ZZ domains (commercial protein A beads and ZZ displaying PHA beads), respectively.

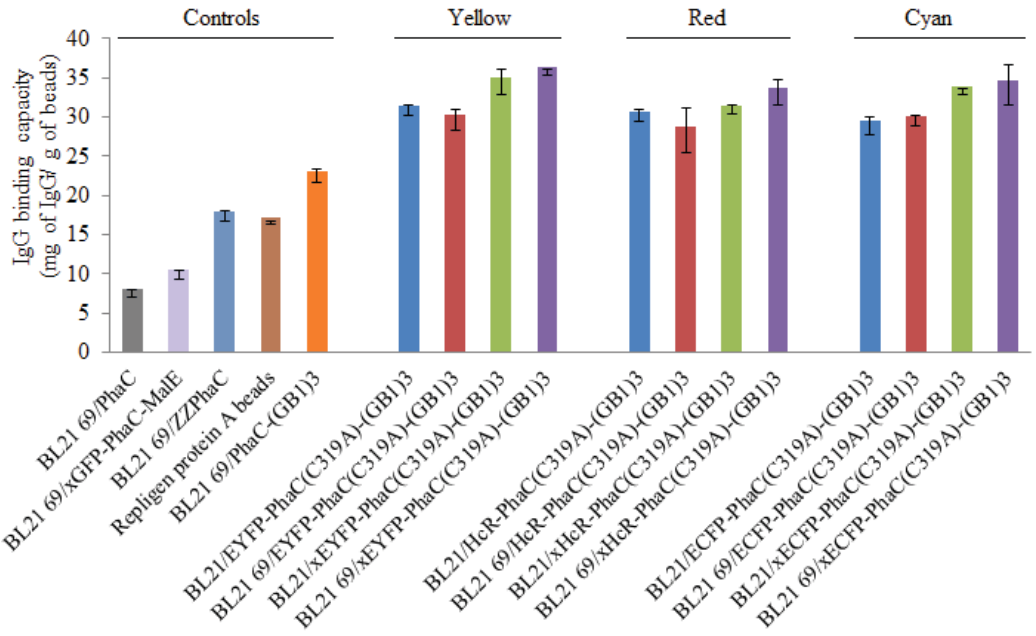

***Figure 18*. Comparative analysis of various FP beads with IgG-binding capacity.** The IgG-binding capacity assay was described in the Materials and Methods chapter (Section 2.13.5.3). Protein concentration was measured by the Bradford assay (Section 2.13.1) using purified goat IgG as the standard. All measurements were performed in triplicate. The mean of IgG binding capacity is reported ±SD (n=3). All beads were produced either in *E. coli* BL21 or BL21(pMCS69) harboring the respective pET-14b plasmid (BL21/; BL21 69/). BL21 69/PhaC, PhaC PHA beads; BL21 69/xGFP-PhaC-MalE, xGFP-PhaC-MalE PHA beads; BL21 69/ZZPhaC, ZZPhaC PHA beads; BL21 69/PhaC-[GB1]3, PhaC-[GB1]3 PHA beads; BL21/EYFP-PhaC(C319A)-[GB1]3, EYFP-PhaC(C319A)-[GB1]3 FP beads; BL21 69/EYFP-PhaC(C319A)-[GB1]3, EYFP-PhaC(C319A)-[GB1]3 FP beads; BL21/xEYFP-PhaC(C319A)-[GB1]3, xEYFP-PhaC(C319A)-[GB1]3 FP beads; BL21 69/xEYFP-PhaC(C319A)-[GB1]3, xEYFP-PhaC(C319A)-[GB1]3 FP beads; BL21/HcR-PhaC(C319A)-[GB1]3, HcR-PhaC(C319A)-[GB1]3 FP beads; BL21 69/HcR-PhaC(C319A)-[GB1]3, HcR-PhaC(C319A)-[GB1]3 FP beads; BL21/xHcR-PhaC(C319A)-[GB1]3, xHcR-PhaC(C319A)-[GB1]3 FP beads; BL21 69/xHcR-PhaC(C319A)-[GB1]3, xHcR-PhaC(C319A)-[GB1]3 FP beads; BL21/ECFP-PhaC(C319A)-[GB1]3, ECFP-PhaC(C319A)-[GB1]3 FP beads; BL21 69/ECFP-PhaC(C319A)-[GB1]3, ECFP-PhaC(C319A)-[GB1]3 FP beads; BL21/xECFP-PhaC(C319A)-[GB1]3, xECFP-PhaC(C319A)-[GB1]3 FP beads; and BL21 69/xECFP-PhaC(C319A)-[GB1]3, xECFP-PhaC(C319A)-[GB1]3 FP beads.

Unbound fractions and elutions from the [GB1]3 domains displaying FP beads incubated with goat IgG were analyzed by SDS-PAGE (Section 2.13.2) in order to check the purity of the eluted IgG fractions. SDS-PAGE results show visible bands corresponding to the molecular weights (~50 kDa and ~25 kDa, respectively) of the heavy and light chains of IgG (Figure 19). However, there were no obvious IgG heavy or light chain bands from the eluted fractions of the negative controls (lanes 3 and 4, Figure 19B). This further confirmed that IgG did not specifically bind to the beads lacking the IgG binding domains ZZ or [GB1]3. Lower molecular weight bands (~49 kDa) were observed in the eluted IgG fractions (Figure 19B), indicating the degradation of the IgG heavy chain.

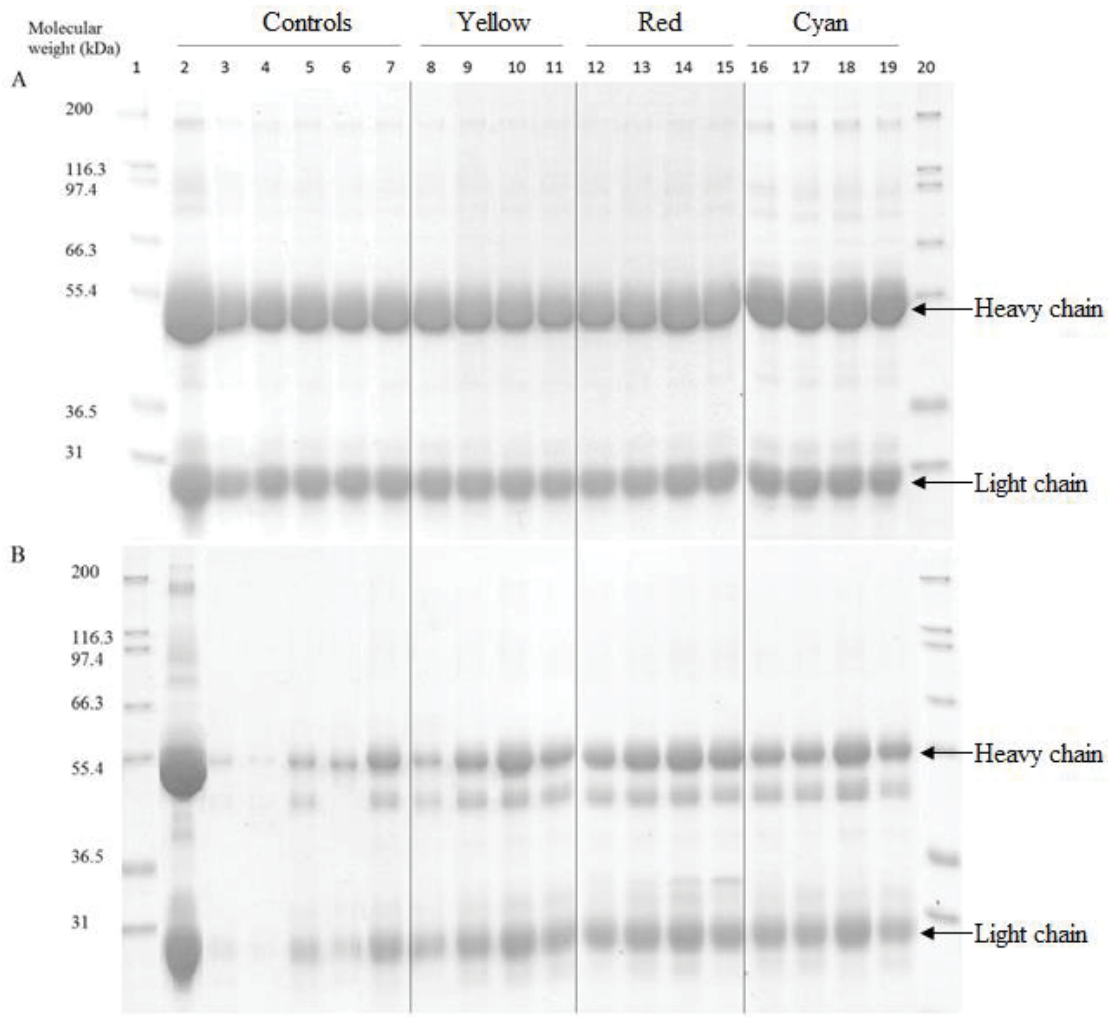

Figure 19. **Protein profiles of unbound fractions (A) and elutions (B) of various FP beads incubated with goat IgG.** The IgG-binding capacity assay was described in the Materials and Methods chapter (Section 2.13.5.3). Protein concentration was determined by the Bradford assay (Section 2.13.1) using purified goat IgG as the standard. All these beads were derived either from *E. coli* BL21 or BL21(pMCS69) harboring the respective pET plasmid (BL21/; BL21 69/). The molecular weights of IgG heavy chain and light chain are approximately 50 and 25 kDa, respectively. Lane 1, molecular weight standard (Mark 12, Invitrogen); lane 2, goat IgG (Innovative Research, USA); lane 3, BL21 69/PhaC; lane 4, BL21 69/xGFP-PhaC-MalE; lane 5, BL21 69/ZZphaC; lane 6, Protein A agarose (Repligen); lane 7, BL21 69/PhaC-[GB1]3; lane 8, BL21/EYFP-PhaC(C319A)-[GB1]3; lane 9, BL21 69/EYFP-PhaC(C319A)-[GB1]3; lane 10, BL21/xEYFP-PhaC(C319A)-[GB1]3; lane 11, BL21 69/xEYFP-PhaC(C319A)-[GB1]3; lane 12, BL21/HcR-PhaC(C319A)-[GB1]3; lane 13, BL21 69/HcR-PhaC(C319A)-[GB1]3; lane 14, BL21/xHcR-PhaC(C319A)-[GB1]3; lane 15, BL21 69/xHcR-PhaC(C319A)-[GB1]3; lane 16, BL21/ECFP-PhaC(C319A)-[GB1]3; lane 17, BL21 69/ECFP-PhaC(C319A)-[GB1]3; lane 18, BL21/xECFP-PhaC(C319A)-[GB1]3; lane 19, BL21 69/xECFP-PhaC(C319A)-[GB1]3; and lane 20, molecular weight standard (Mark 12, Invitrogen).

3.2.5 Application of functionalized FP beads displaying [GB1]3 in bioseparation assay

Various FP beads displaying the [GB1]3 domains were applied for purification of IgG from human blood serum (Section 2.13.5.5). Albumin (65 kDa) is the most abundant protein in human serum. These protein beads were engineered to bind IgG of the human IgG subclass 3. Protein beads comprised of EYFP, HcR, or ECFP showed a clear enrichment of the IgG heavy (~50 kDa) and light (~25 kDa) chain in the eluted IgG fractions when compared to the human serum loading control (Figure 20B). Protein beads made of the extended EYFP or ECFP (Figure 20B, lanes10-11 and18-19) showed a relatively stronger IgG purification power in comparision to the PHA beads displaying the [GB1]3 domains (Figure 20B, lane 7).

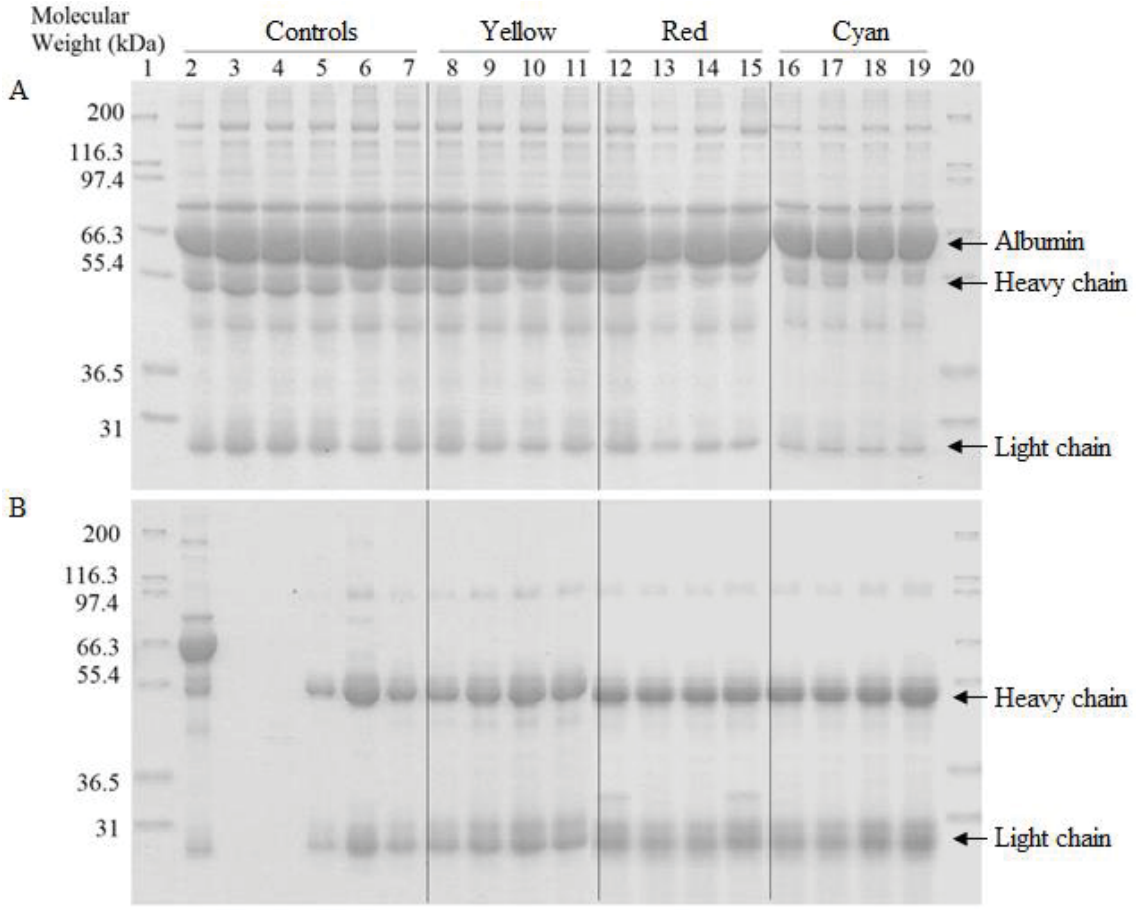

***Figure 20*. Protein profiles of unbound fractions (A) and elutions (B) of various FP beads incubated with human serum.** Purification of IgG from human serum was described in the Materials and Methods chapter (Section 2.13.5.5). The molecular weights of albumin, IgG heavy chain and light chain are 65, 50, and 25 kDa, respectively. All these beads were derived either from *E. coli* BL21 or BL21(pMCS69) harboring the respective pET plasmid (BL21/; BL21 69/). Lane 1, molecular weight standard (Mark 12, Invitrogen); lane 2, human serum (Sigma-Aldrich, USA); lane 3, BL21 69/PhaC; lane 4, BL21 69/xGFP-PhaC-MalE; lane 5, BL21 69/ZZphaC; lane 6, Protein A agarose (Repligen); lane 7, BL21 69/PhaC-[GB1]3; lane 8, BL21/EYFP-PhaC(C319A)-[GB1]3; lane 9, BL21 69/EYFP-PhaC(C319A)-[GB1]3; lane 10, BL21/xEYFP-PhaC(C319A)-[GB1]3; lane 11, BL21 69/xEYFP-PhaC(C319A)-[GB1]3; lane 12, BL21/HcR-PhaC(C319A)-[GB1]3; lane 13, BL21 69/HcR-PhaC(C319A)-[GB1]3; lane 14, BL21/xHcR-PhaC(C319A)-[GB1]3; lane 15, BL21 69/xHcR-PhaC(C319A)-[GB1]3; lane 16, BL21/ECFP-PhaC(C319A)-[GB1]3; lane 17, BL21 69/ECFP-PhaC(C319A)-[GB1]3; lane 18, BL21/xECFP-PhaC(C319A)-[GB1]3; lane 19, BL21 69/xECFP-PhaC(C319A)-[GB1]3; and lane 20, molecular weight standard (Mark 12, Invitrogen).

3.2.6 IgG-binding capacity of FP beads displaying the [GB1]3 domains at different temperatures and pHs

The IgG-binding ability of the [GB1]3 domains immobilized on the surface of various FP beads at different temperature and pH conditions were determined (Section 2.13.5.4). The unbound and eluted IgG fractions were quantified by the Bradford assay (Section 2.13.1). The results of goat IgG binding ability of various FP beads at different temperatures and pHs are shown in Figure 21. The recovery rate of IgG binding at different conditions was between 75% and 90% (data not shown). The negative control was protein beads displaying MalE, a protein which does not bind IgG. As expected, the negative controls bound IgG very inefficiently, regardless of temperature or pH (Figure 21). In contrast, the HcR, ECFP, or EYFP protein beads displaying the IgG-binding domain [GB1]3 showed much greater IgG-binding capacities (Figure 21). Furthermore, the binding capacity of these protein beads was similar to each other across the various temperatures (Figure 21A) and pHs (Figure 21B) tested.

As shown in Figure 21A, a high IgG-binding ability (approximately 38 mg of IgG/ g of beads) was observed at 4^{o}C for all different FP beads. The binding ability also remained at a relatively high level (about 40 mg of IgG/ g of beads), even when the binding temperature was raised to 45^{o}C. However, at higher temperatures, binding capacity began to slowly decrease. The binding capacity was dramatically lowered when the binding temperature was increased to 55^{o}C. These results indicate that the optimal IgG-binding temperature of FP beads displaying [GB1]3 may be at 45^{o}C. Subsequently, IgG binding of all FP beads was tested at 45^{o}C through different pH treatments (Figure 21B). The pH analysis demonstrated that the IgG-binding ability was stable in weak acidic (pH4–7) and weak alkaline (pH8–10) conditions. However, the immobilized [GB1]3 domains showed higher IgG-binding capacities in weak alkaline conditions than those in a weak acidic environment.

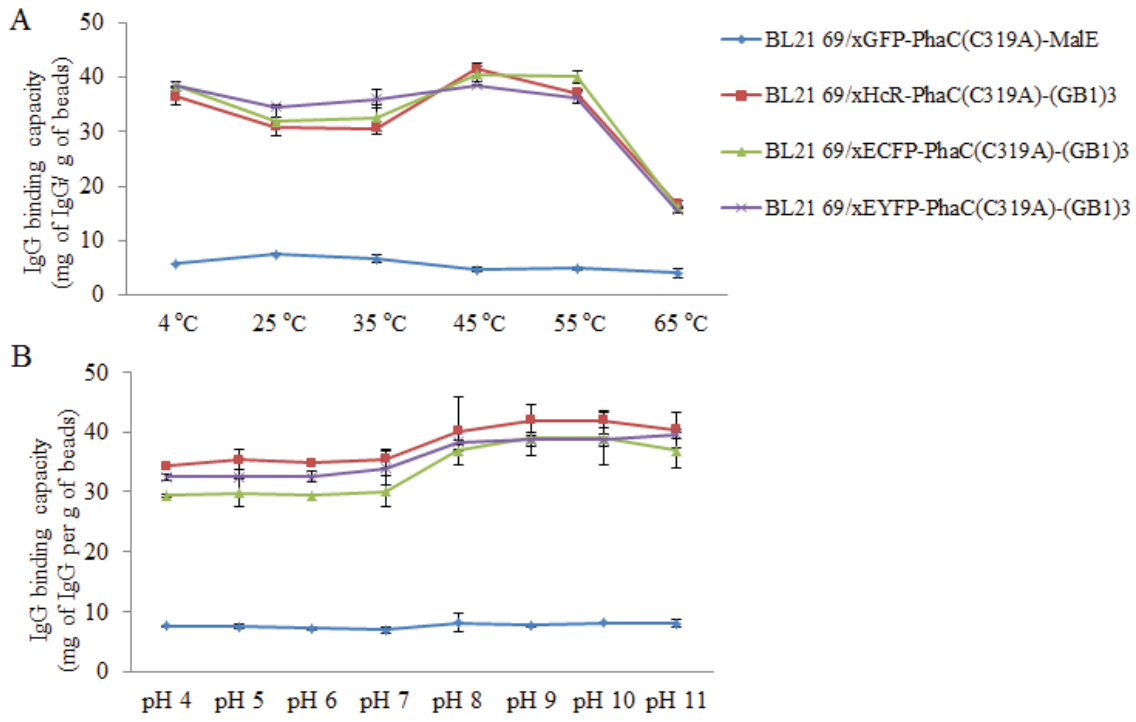

Figure 21. **Goat IgG-binding capacity of various FP beads displaying the [GB1]3 domains at different temperatures (A) and at 45°C through different pH conditions (B).** IgG-binding capacity assay at different temperatures (4, 25, 35, 45, 55, and 65°C) and at different pHs (4, 5, 6, 7, 8, 9, 10, and 11) was described in the Materials and Methods chapter (Section 2.13.5.4). Protein concentration was measured by the Bradford assay (Section 2.13.1) using purified goat IgG as the standard. All measurements were performed in triplicate. The mean of IgG-binding capacity is reported ±SD (n=3). All protein beads were produced in *E. coli* BL21(pMCS69) harboring the respective pET-14b plasmid (BL21 69/). BL21 69/xGFP-PhaC(C319A)-MalE, xGFP-PhaC(C319A)-MalE FP beads; BL21 69/xHcR-PhaC(C319A)-[GB1]3, xHcR-PhaC(C319A)-[GB1]3 FP beads; BL21 69/xECFP-PhaC(C319A)-[GB1]3, xECFP-PhaC(C319A)-[GB1]3 FP beads; and BL21 69/xEYFP-PhaC(C319A)-[GB1]3, xEYFP-PhaC(C319A)-[GB1]3 FP beads.

3.3 Generation of functionalized super-paramagnetic protein beads

To generate functionalized, super-paramagnetic protein beads displaying the ZZ domains, the following plasmids were constructed: pET-14b xgfp-phaC(C319A)-linker-malE; pET-14b xgfp-phaC(C319A)-linker-zz; pET-14b xgfp-3×Fe-phaC(C319A)-linker-zz; and pET-14b xgfp-phaC(C319A)-linker-zz-3×Fe (Table 5, Section 2.1.2). Jahns et al. (2013) cloned the plasmids pET-14b xgfp-phaC(C319A)-linker-malE and pET-14b xgfp-phaC(C319A)-linker-zz. I constructed the plasmids containing genes encoding the triple iron-binding peptides as described below (Sections 3.3.1 and 3.3.2).

As described in Section 1.9, the hypothesis of this section was that GFP beads displaying the triple iron-binding peptides would become magnetized after mixing with ferrofluid. Moreover, the immobilized IgG-binding domains ZZ on the surface of magnetized protein beads would maintain a strong IgG-binding capacity. In order to test these hypotheses, protein beads were firstly magnetized by incubating them with ferrofluid (Section 2.13.5.6). The ferrofluid solution was provided by PolyBatics (Palmerston North, New Zealand). The IgG-binding capacity of magnetized protein beads (Section 2.13.5.6) was then assessed and the results are shown in Section 3.3.5. In addition, due to a limitation of ferrofluid availability, the IgG-binding ability of magnetized protein beads at different temperatures and pHs was not assessed. However, the optimal IgG-binding temperature and pH of non-magnetized protein beads was determined, and the results are shown in Section 3.3.6.

3.3.1 Construction of pET-14b xgfp-3×Fe-phaC(C319A)-linker-zz

Plasmid pET-14b 3×Fe-linker-zz-phaC (Table 5), encoding the triple iron-binding peptides 3×Fe constructed by Anika Jahns, was used as the template for PCR (Section 2.10.3) as shown in Figure 22. The DNA region encoding 3×Fe and *Not*I restriction site was amplified using primers fwd_N-3xFe_*Not*I (forward) and rev_N-3xFe_*Not*I (reverse) designed by Jinping Du (Table 7). These primers were used to introduce the *Not*I restriction site at the N- and C-terminal regions of the 3×Fe DNA fragment to facilitate sub-cloning. An aliquot of the PCR product was subjected to AGE (Section

2.10.4) for DNA size confirmation. Following confirmation, the remaining PCR product was purified using AGE with SYBR-safe DNA gel stain (Section 2.10.4) and recovered from agarose gels (Section 2.10.5). A-tailing reaction (Section 2.10.6.1) was used to add a 3' terminal adenine overhang onto the purified, blunt-ended PCR products using *Taq* DNA polymerase. An aliquot of the A-tailed PCR products were then ligated into the pGEM-T Easy vector (Section 2.10.6.1). pGEM-T Easy is an intermediate cloning vector with a high copy number containing an ampicillin–resistant gene and *lacZα* for blue and white selection (Section 2.10.6.2). The pGEM-T Easy ligation product was transformed into *E. coli* (Section 2.9) cloning strain XL1-Blue (Stratagene, Section 2.1.1) and spread-plated on a X-Gal medium (Section 2.4.1) containing 75μg/ml ampicillin. Single white colonies were selected for plasmid isolation (Section 2.10.1.1) and DNA hydrolysis analysis (Section 2.10.2). The pGEM-T Easy vector containing the DNA fragment of interest was confirmed by DNA sequencing (Section 2.10.8).

After confirmation of the pGEM-T Easy vector by DNA sequencing, the 3×Fe DNA fragment with 93 bp (Figure 23) was excised by RE digestion (Section 2.10.2) using *Not*I. The 3×Fe DNA fragment was separated from the digestion mixture using AGE with SYBR–safe DNA gel stain (Section 2.10.4) and then followed by DNA fragment extraction and purification (Section 2.10.5). In parallel, the plasmid vector, pET-14b xgfp-phaC(C319A)-linker-zz, was linearized by RE digestion (Section 2.10.2) using *Not*I, followed by DNA extraction (Section 2.10.4) and purification (Section 2.10.5). Subsequently, the purified *Not*I-*Not*I fragment gene *3×Fe* was sub-cloned into the *Not*I-*Not*I linearized vector pET-14b *xgfp-phaC(C319A)*-linker-zz, mediated by T4 DNA ligase (Section 2.10.7). This allowed the generation of the final plasmid, pET-14b xgfp-3×Fe-phaC(C319A)-linker-zz, which was transformed into *E. coli* XL-Blue (Section 2.9) and spread-plated on a LB-agar medium containing ampicillin. Single colonies were selected for plasmid isolation (Section 2.10.1) and DNA sequencing (Section 2.10.8) to confirm the gene sequence of the final construct.

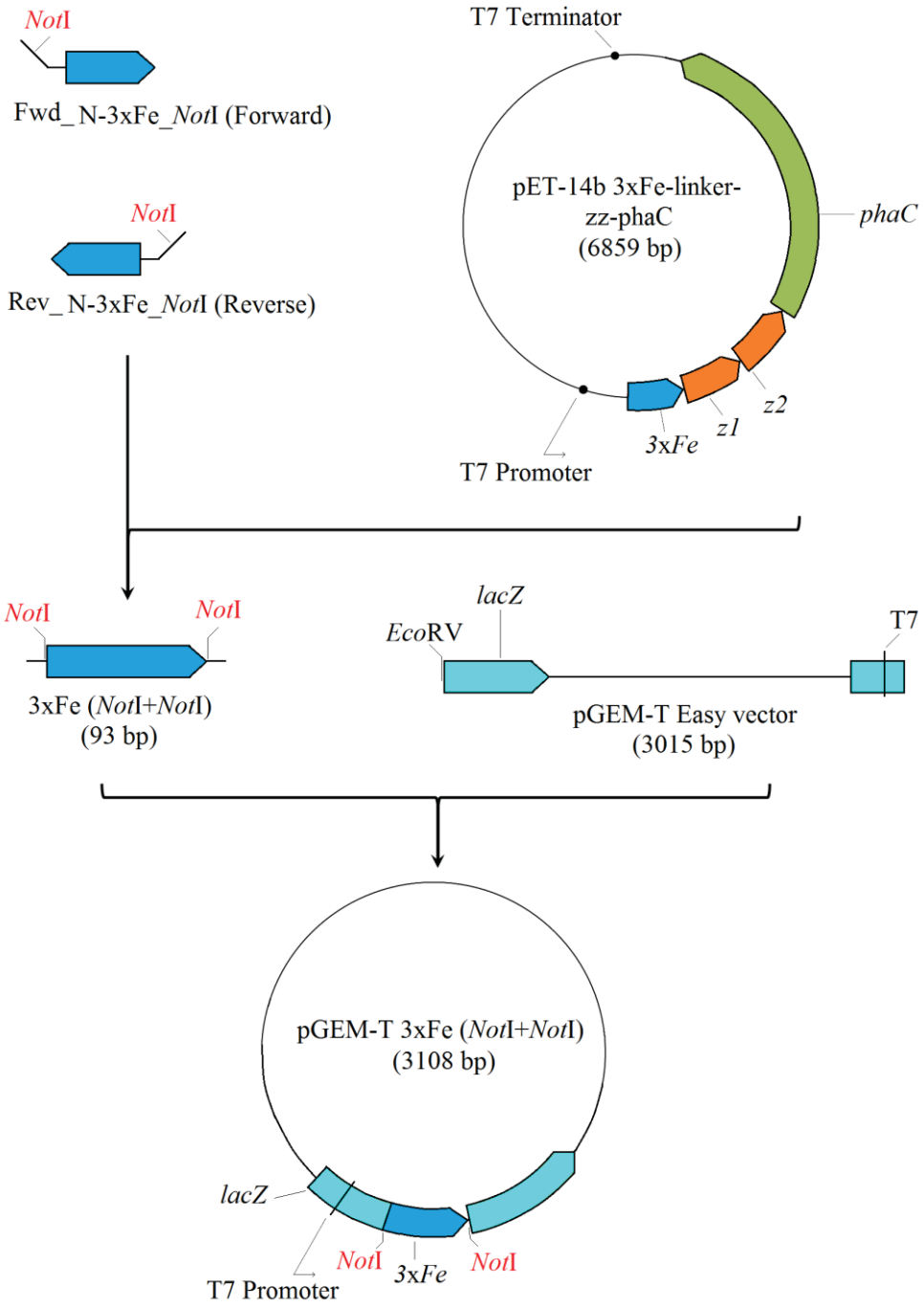

***Figure 22*. Construction of intermediate cloning plasmid pGEM-T 3×Fe (*NotI*+*NotI*) for generation of pET-14b xgfp-3×Fe-phaC(C319A)-linker-zz.** The PCR fragment 3×Fe with flanking *Not*I restriction sites was generated using primers fwd_N-3xFe_*Not*I (forward) and rev_N-3xFe_*Not*I (reverse). The plasmid pET-14b 3×Fe-linker-zz-phaC was used as the PCR template (Section 2.10.3). The resulting 93 bp blunt-ended PCR product was A-tailed (Section 2.10.6.1) and ligated into the intermediate cloning vector, pGEM-T Easy vector (Section 2.10.6.1).

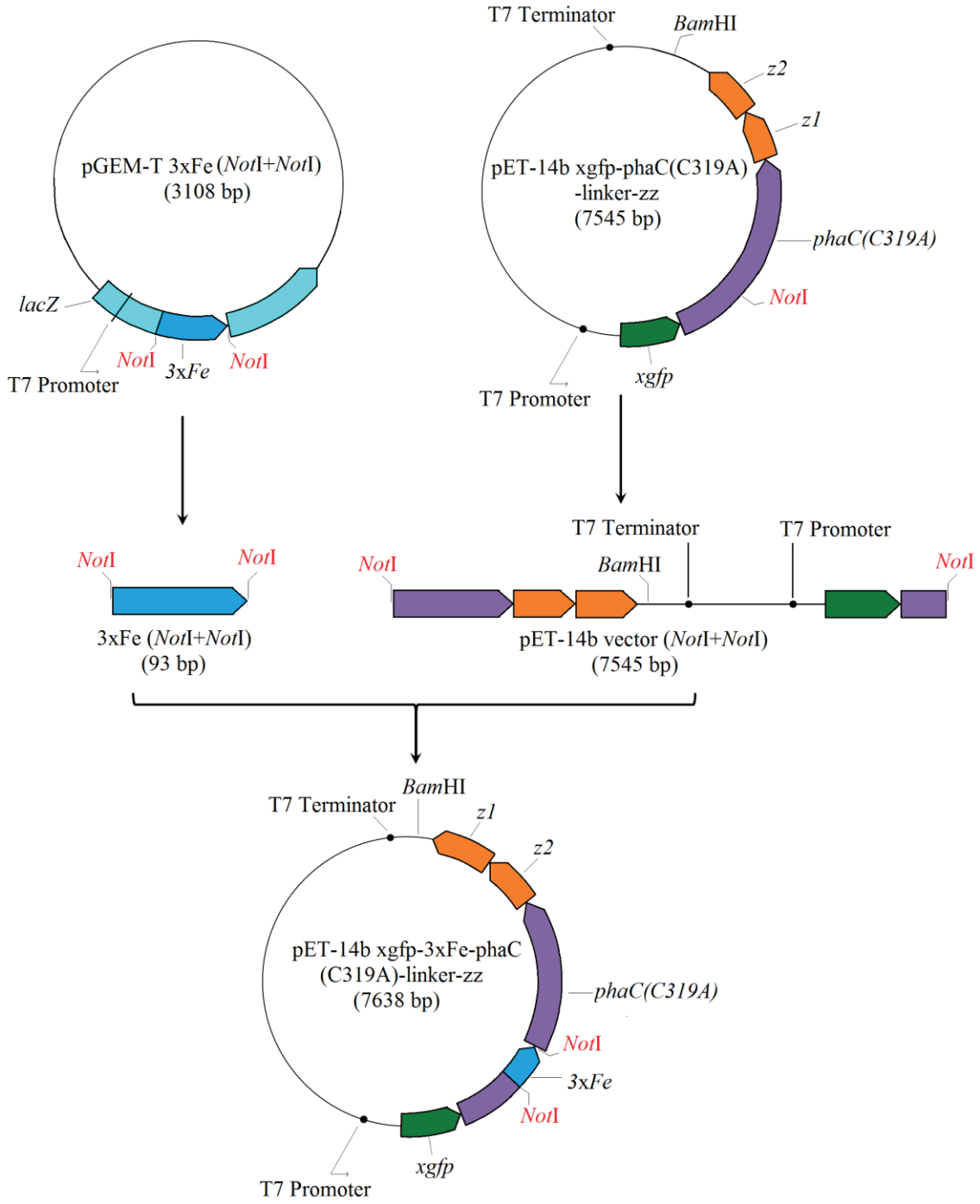

***Figure 23*. Construction of pET-14b xgfp-3×Fe-phaC(C319A)-linker-zz.** The DNA fragment encoding the *3×Fe* gene was isolated from the intermediate cloning plasmid pGEM-T 3×Fe (*Not*I+*Not*I) by restriction digest with *Not*I (Section 2.10.2), followed by separation of DNA fragments using agarose gel electrophoresis (Section 2.10.4) and gel purification (Section 2.10.5). The *3×Fe* gene fragment was ligated into linearized vector pET-14b *xgfp-phaC(C319A)*-linker-zz, hydrolysed with *Not*I, using T4 DNA ligase (Section 2.10.7) to generate the final plasmid, pET-14b xgfp-3×Fe-phaC(C319A)-linker-zz.

3.3.2 Construction of pET-14b xgfp-phaC(C319A)-linker-zz-3×Fe

The construction process of pET-14b xgfp-phaC(C319A)-linker-zz-3×Fe is similar to the generation of the plasmid pET-14b xgfp-3×Fe-phaC(C319A)-linker-zz as described in Section 3.3.1. Briefly, plasmid pET-14b 3×Fe-linker-zz-phaC (Table 5) was used as the PCR template (Section 2.10.3) for the generation of the gene fragment *3×Fe* with flanking *Bam*HI restriction sites (Figure 24). The restriction sites at the N- and C-terminus of 3×Fe DNA fragment were introduced using primers fwd_C-3xFe_*Bam*HI (forward) and rev_C-3xFe_*Bam*HI (reverse) designed by Jinping Du (Table 7). The resulting blunt-ended PCR product was A-tailed (Section 2.10.6.1) and ligated into the pGEM-T Easy vector (Section 2.10.6.1). After confirmation of the pGEM-T Easy vector by DNA sequencing, the 3×Fe DNA fragment with 91 bp (Figure 25) was excised by DNA hydrolysis (Section 2.10.2) using *Bam*HI. T4 DNA ligase was used to ligate the purified *3×Fe* gene fragment into the linearized vector pET-14b *xgfp-phaC(C319A)*-linker-*zz* hydrolyzed with *Bam*HI (Section 2.10.7). This allowed the generation of the final plasmid, pET-14b xgfp-phaC(C319A)-linker-zz-3×Fe.

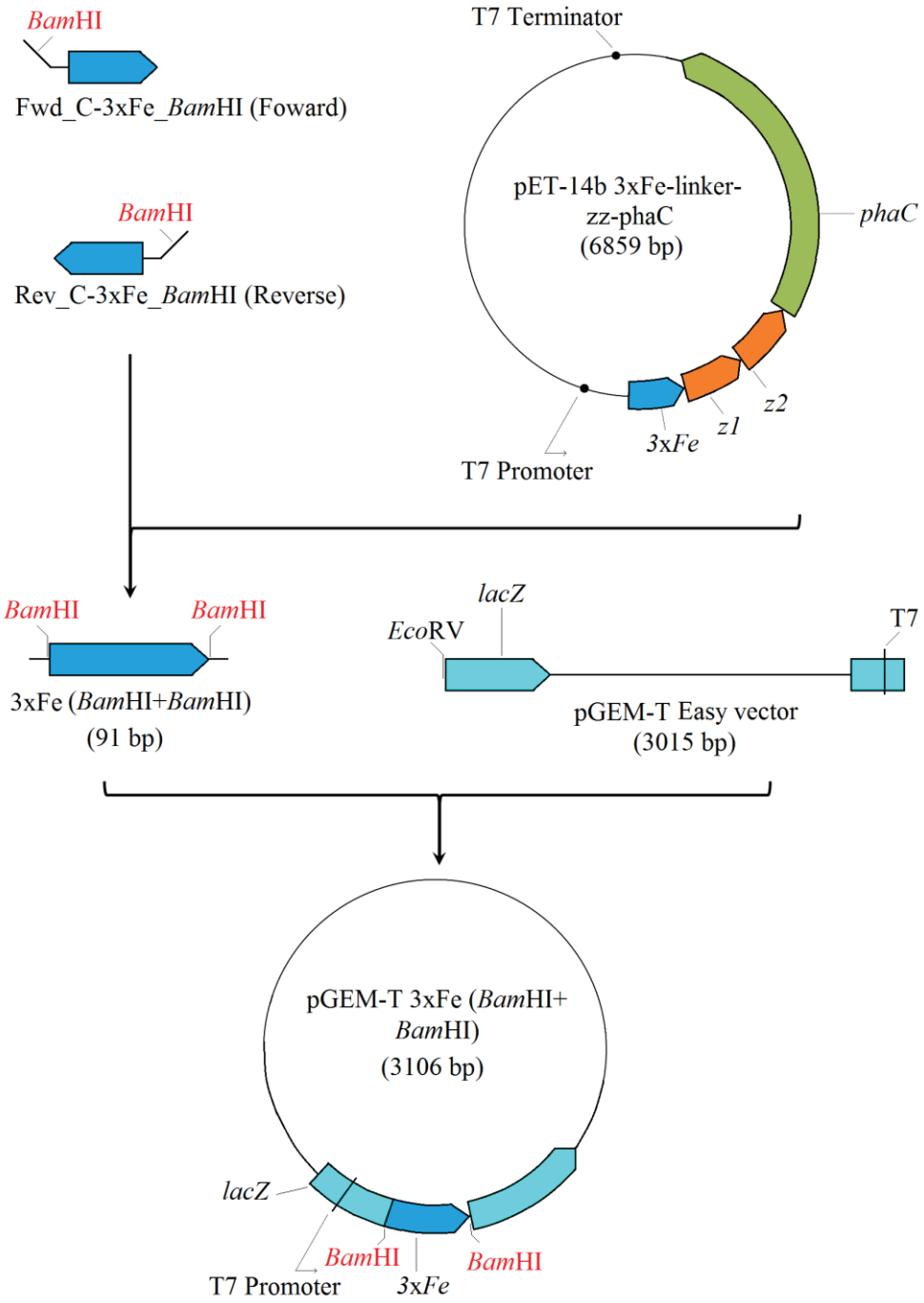

Figure 24. **Construction of the intermediate cloning plasmid pGEM-T 3×Fe (*BamHI*+*BamHI*) for generation of pET-14b xgfp-phaC(C319A)-linker-zz-3×Fe.** The PCR fragment 3×Fe with flanking *Bam*HI restriction sites was generated using primers fwd_C-3xFe_*Bam*HI (forward) and rev_C-3xFe_*Bam*HI (reverse). The plasmid pET-14b 3×Fe-linker-zz-phaC was used as the PCR template (Section 2.10.3). The resulting 91 bp blunt-ended PCR product was A-tailed (Section 2.10.6.1) and ligated into the intermediate cloning vector, pGEM-T Easy vector (Section 2.10.6.1).

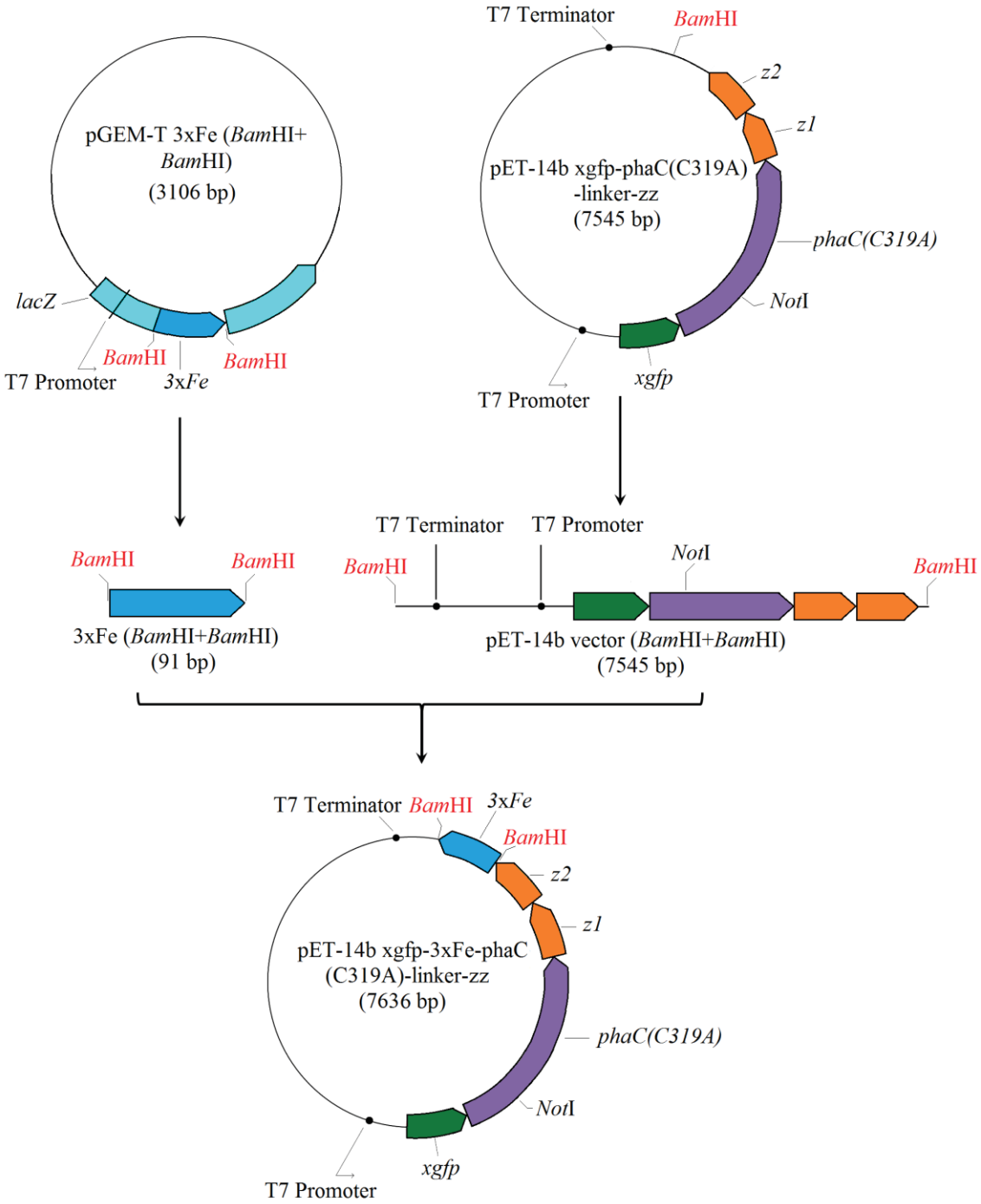

Figure 25. **Construction of pET-14b xgfp-phaC(C319A)-linker-zz-3×Fe.** The DNA fragment encoding the *3×Fe* gene was isolated from the intermediate cloning plasmid pGEM-T 3×Fe (*Bam*HI+*Bam*HI) by restriction digest with *Bam*HI (Section 2.10.2), followed by separation of DNA fragments using agarose gel electrophoresis (Section 2.10.4) and gel purification (Section 2.10.5). The *3×Fe* gene fragment was ligated into linearized vector pET-14b *xgfp-phaC(C319A)*-linker-zz, hydrolyzed with *Bam*HI, using T4 DNA ligase (Section 2.10.7) to generate the final plasmid, pET-14b xgfp-phaC(C319A)-linker-zz-3×Fe.

3.3.3 Plasmid expression and FP bead production

The pET expression vector containing the genes encoding GFP, an inactive synthase PhaC(C319A), 3xFe, and the ZZ domains for *in vivo* protein bead production was transformed (Section 2.9) into *E. coli* BL21 (DE3). *E. coli* cells harboring pMCS69 and target recombinant pET plasmid were cultivated under protein bead accumulating conditions (Section 2.6.1) to produce FP beads displaying the triple iron-binding peptides and ZZ domains. Beads were subsequently isolated (Section 2.11).

Fluorescent microscopy (Section 2.12.1.2) was used to directly visualize GFP beads in recombinant *E. coli* cells. The results of the fluorescent microscopy of GFP bead accumulating cells are shown in Figure 26. The fluorescence suggests that the intracellular FP beads were successfully produced in *E. coli* cells.

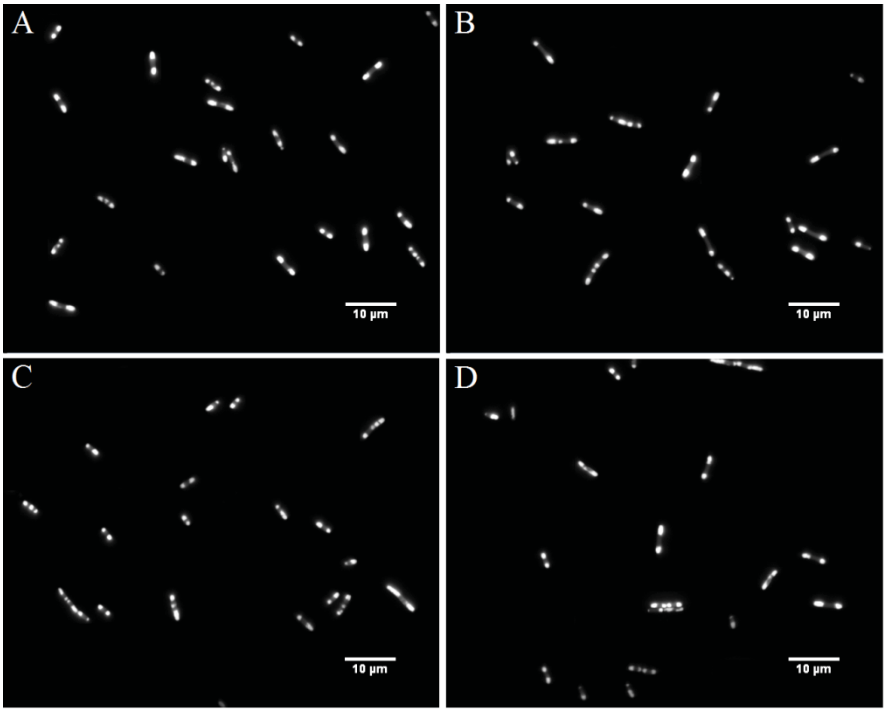

Figure 26. **Fluorescence microscopy images of GFP beads produced in recombinant *E. coli* BL21 (DE3) harboring pMCS69 and the respective pET expression vectors.** (A) pET-14b xGFP-PhaC(C319A)-MalE; (B) pET-14b xGFP-PhaC(C319A)-ZZ; (C) pET-14b xGFP-3xFe-PhaC(C319A)-ZZ; and (D) pET-14b xGFP-PhaC(C319A)-ZZ-3xFe.

3.3.4 Display of 3xFe and the IgG-binding domains ZZ on the surface of protein beads

SDS-PAGE (Section 2.13.2) was used to analyze the GFP bead protein profile (Figure 27). Dominant protein bands were observed corresponding to proteins with theoretical molecular weights of 63 kDa for PhaC, 131.8 kDa for xGFP-PhaC(C319A)-MalE, 104 kDa for xGFP-PhaC(C319A)-ZZ, and 107.4 kDa for xGFP-3xFe-PhaC(C319A)-ZZ and for xGFP-PhaC(C319A)-ZZ-3xFe. Densitometry analysis (Section 2.13.3) of the SDS-PAGE showed that PhaC accounted for about 19% of the total protein in the PhaC bead fraction, while each of the fusion proteins, xGFP-PhaC(C319A)-MalE, xGFP-PhaC(C319A)-ZZ, xGFP-3xFe-PhaC(C319A)-ZZ, and xGFP-PhaC(C319A)-ZZ-3xFe, accounted for approximately 24% of the total protein in their corresponding bead fraction (data not shown).

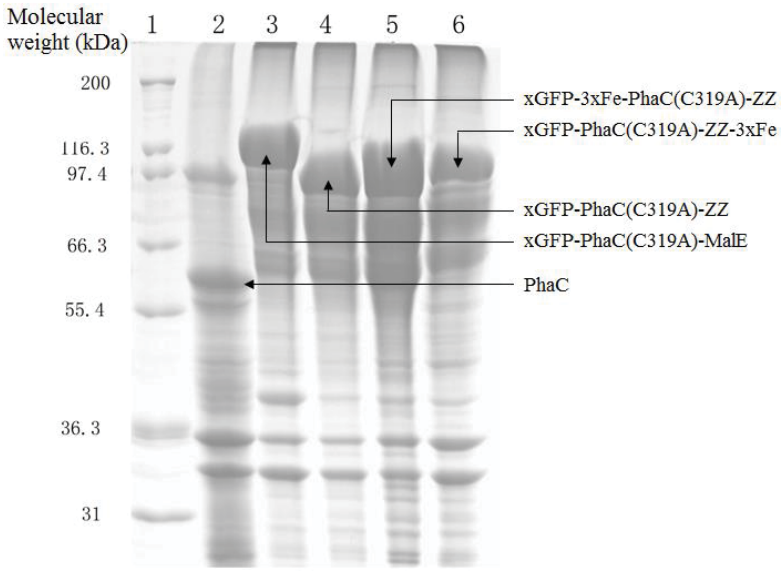

***Figure 27*. Protein profiles of GFP beads isolated from recombinant *E. coli* cells harboring pMCS69 and the respective pET expression vectors.** Lane 1, molecular weight marker (Mark 12, Invitrogen); lane 2, PhaC (WT, 63 kDa); lane 3, xGFP-PhaC(C319A)-MalE (131.8 kDa); lane 4, xGFP-PhaC(C319A)-ZZ (104 kDa); lane 5, xGFP-3xFe-PhaC(C319A)-ZZ (107.4 kDa); and lane 6, xGFP-PhaC(C319A)-ZZ-3xFe (107.4 kDa).

3.3.5 Functional assessment of the IgG-binding domains ZZ on the surface of super-paramagnetic protein beads

Protein beads were magnetized by incubating them with ferrofluid solution (Section 2.13.5.6). Regardless of the presence or absence of 3xFe, after treatment with ferrofluid, all protein beads were attracted to a magnet (data not shown). Therefore, all beads displayed magnetism, suggesting that protein beads lacking 3xFe could bind to iron particles non-specifically. However, protein beads displaying 3xFe retained the magnetism longer than their counterparts lacking this peptide (data not shown). In addition, the size of iron particles in ferrofluid was measured by PolyBatics (Palmerston North, New Zealand) and the results are shown in Figure 28. The size of iron particles varies, ranging between 700 and 1,400 nm in diameter, which is as large as protein beads. It is possibly due to the density and size of iron particles that the unbound and leaching iron particles cannot be obtained in the supernatant fraction using centrifugation at 4,000-6,000 x g (Heraeus Pico 17, Thermo Scientific) for four minutes. Therefore, the iron-binding capacity of protein beads and iron-leaching level of magnetized protein beads cannot be measured.

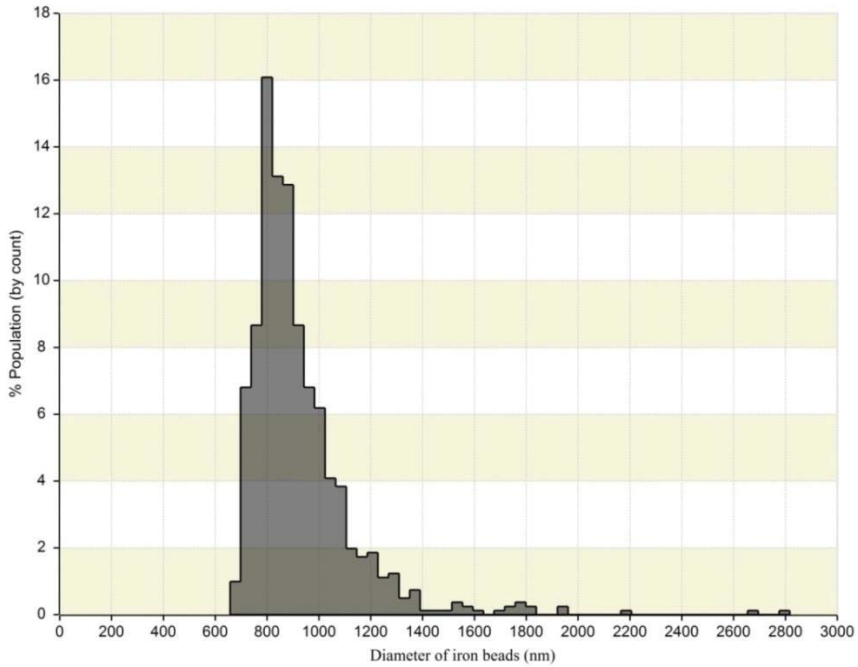

Figure 28. **Diameter of iron particles in ferrofluid.** The measurement of iron particles' size was conducted by PolyBatics (Palmerston North, New Zealand) using qNano as described in the Materials and Methods chapter (Section 2.12.4).

To test the function of the ZZ domains displayed on the surface of magnetized protein beads, the human IgG-binding ability of protein beads before and after magnetization was assessed (Section 2.13.5.6). The unbound and eluted IgG fractions were quantified by the Bradford assay (Section 2.13.1). The IgG-binding results of non-magnetized and magnized protein beads are shown in Figure 29. The recovery rate of IgG-binding capacity for plain beads was between 80% and 90%, while the recovery rate for magnetized protein beads was lower, between 60% and 80% (data not shown).

As shown in Figure 29, there was a very low IgG-binding capacity in negative controls, iron particles, and protein beads displaying MalE, suggesting that human IgG did not specifically bind to iron particles and protein beads lacking the ZZ domains. In contrast, plain beads conaining the ZZ domains showed singinficantly higher IgG-binding abilities. (IgG binding ability before magnetization is based on the wet weight of protein beads = (Feed – unbound IgG)/ Wet weight of protein beads). In particular, the IgG-binding ability of the xGFP-PhaC(C319A)-ZZ and xGFP-PhaC(C319A)-ZZ-3xFe protein beads were 1.5- and 2-fold greater than the xGFP-3xFe-PhaC(C319A)-ZZ beads, respectively. This suggests that the position of 3xFe may affect the IgG-binding ability.

Furthermore, a very low IgG binding of protein beads displaying the ZZ domains was observed after they were magnetized using a ferrofluid with a pH of 14. This indicates that the treatment with a highly alkaline solution could abolish the activity of the immobilized ZZ domains. After magnetization using a ferrofluid with a pH of 7.5, protein beads retained the IgG-binding function. However, the IgG-binding ability of the magnetized protein beads was twice lower than that of plain beads. (IgG binding ability after magnetization is based on the wet weight of magentized protein beads = (Feed – unbound IgG)/ wet weight of protein beads + iron particles). Therefore, the neutral ferrofluid treatment generally decreased their IgG-binding capacity.

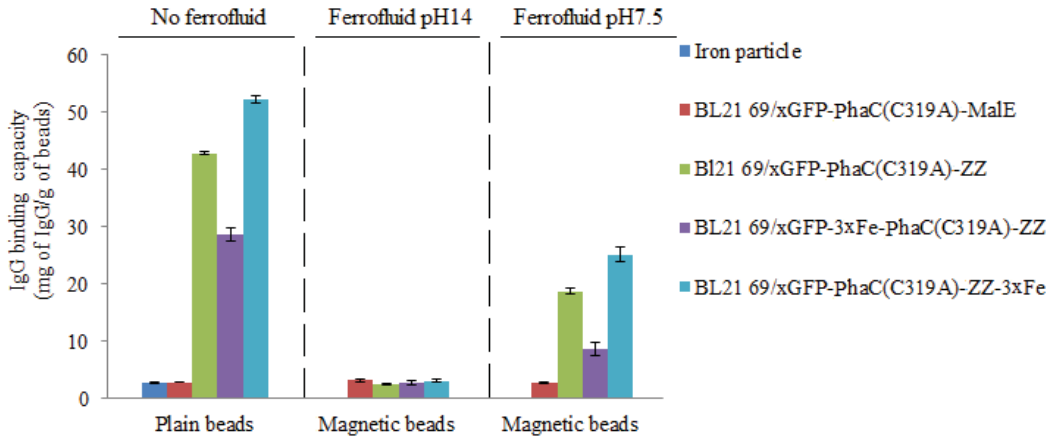

Figure 29. **Human IgG-binding capacity of protein beads displaying the ZZ domains before and after magnetization.** The IgG-binding assay of magnetized protein beads (Section 2.13.5.6) was described in the Material and Methods chapter. Protein concentration was measured by the Bradford assay (Section 2.13.1) using purified human IgG as the standard. All measurements were performed in triplicate. The mean of IgG-binding capacity is shown ±SD (n=3). The functionality of magnetized protein beads was analyzed by human IgG-binding capacity as follows: samples were not treated by ferrofluid; samples were treated by an alkaline ferrofluid (pH14); and samples were treated by a neutral ferrofluid (pH 7.5). All beads were produced in *E. coli* BL21(pMCS69) harboring the respective pET-14b plasmid (BL21 69/). BL21 69/xGFP-PhaC(C319A)-MalE, xGFP-PhaC(C319A)-MalE FP beads; BL21 69/xGFP-PhaC(C319A)-ZZ, xGFP-PhaC(C319A)-ZZ FP beads; BL21 69/xGFP-3xFe-PhaC(C319A)-ZZ, xGFP-3xFe-PhaC(C319A)-ZZ FP beads; and BL21 69/xGFP-PhaC(C319A)-ZZ-3xFe, xGFP-PhaC(C319A)-ZZ-3xFe FP beads.

Unbound fractions and elutions from non-magnetized and magnetized protein beads displaying the ZZ domains that incubated with human IgG were analyzed by SDS-PAGE (Section 2.13.2). The results in Figure 30 show clear protein bands corresponding to the IgG heavy and light chains, approximately 50 and 25 kDa, respectively. As shown in Figure 30B (lanes 3, 4, 8, and 12), no clear IgG heavy or light chain bands were seen in the IgG elution fractions from the negative controls. There are also no heavy and light chain bands in the elution from IgG-binding beads treated by an alkaline ferrofluid (lanes 9, 10, and 11). These results confirm that the negative controls (iron oxide particles and protein beads displaying MalE) with no IgG-binding domains did not specifically bind to human IgG. Moreover, the highly alkaline ferrofluid (pH14) appeared to inactivate the IgG-binding domains ZZ displayed on the surface of protein beads after magnetization. However, IgG-binding capacity was not abolished by ferrofluid treatment at a neutral pH of 7.5 (lanes 13, 14, and 15; Figure 30B).

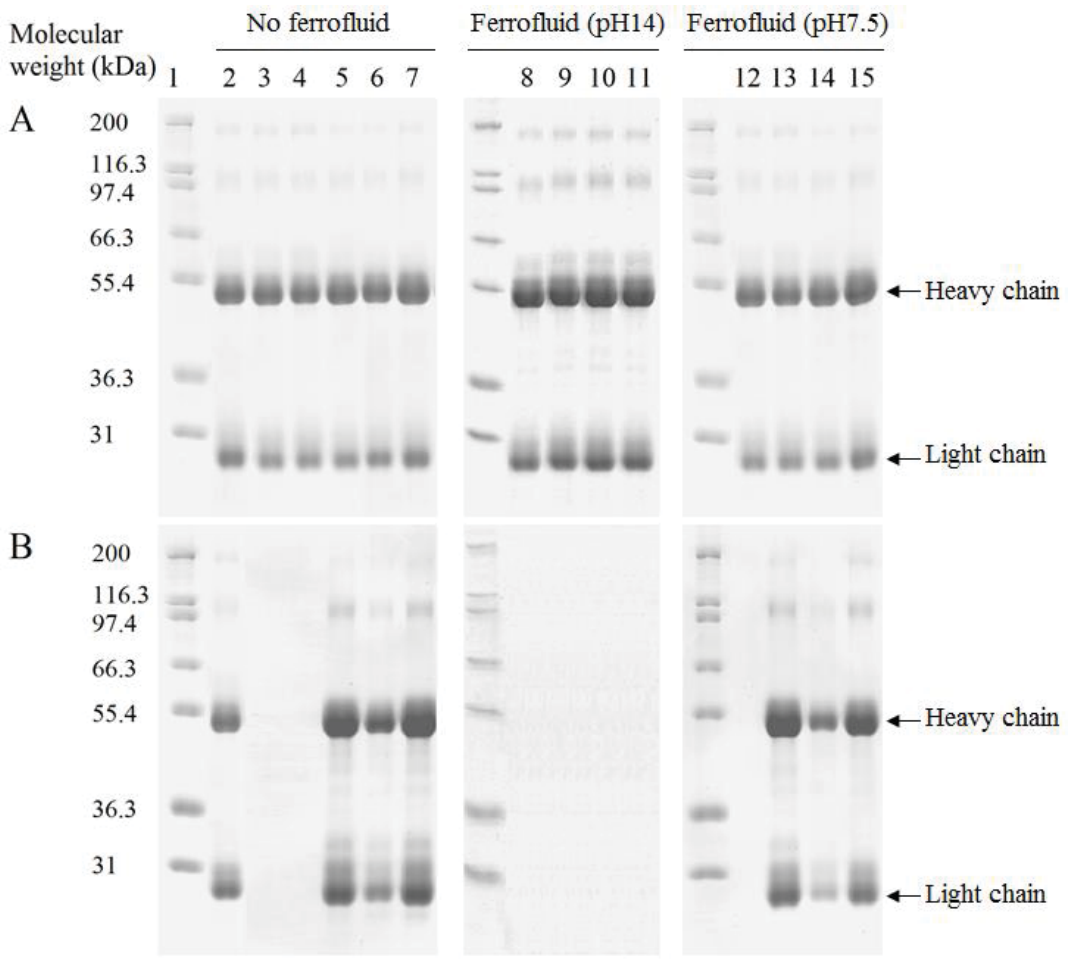

Figure 30. **Protein profile of unbound (A) and eluted (B) fraction of non-magnetized and magnetized protein beads incubated with human IgG.** All these beads were derived from *E. coli* BL21(pMCS69) harboring the respective pET plasmid (BL21 69/). The molecular weights of IgG heavy chain and light chain are approximately 50 and 25 kDa, respectively. Lane 1, molecular weight standard (Mark 12, Invitrogen); lane 2, human IgG (Sigma-Aldrich, USA); lane 3, iron oxide particles; lanes 4, 8, and 12, BL21 69/xGFP-PhaC(C319A)-MalE, xGFP-PhaC(C319A)-MalE FP beads; lanes 5, 9, and 13, BL21 69/xGFP-PhaC(C319A)-ZZ, xGFP-PhaC(C319A)-ZZ FP beads; lanes 6, 10, and 14, BL21 69/xGFP-3xFe-PhaC(C319A)-ZZ, xGFP-3xFe-PhaC(C319A)-ZZ FP beads; and lanes 7, 11, and 15, BL21 69/xGFP-PhaC(C319A)-ZZ-3xFe, xGFP-PhaC(C319A)-ZZ-3xFe FP beads.

3.3.6 IgG-binding capacity of GFP beads displaying the ZZ domains, with or without additional iron-binding peptides at different temperatures and pHs

The IgG-binding capacity of magnetized protein beads at various temperatures and pHs was not measured due to a limitation of ferrofluid availability. Nevertheless, optimal temperatures and pHs for IgG binding of non-magnetized protein beads displaying the ZZ domains with or without additional iron-binding peptides were determined (Section 2.13.5.4). Unbound and eluted IgG fractions were quantified using the Bradford method (Section 2.13.1). The human IgG-binding ability of protein beads displaying the ZZ domains at different temperatures and pHs are shown in Figure 31. Under the various conditions tested, recovery rate of IgG binding was between 75% and 92% (data not shown). For the negative control (xGFP-PhaC(C319A)-MalE), there was a very low IgG-binding ability at different temperatures and pHs (Figure 31), indicating that protein beads lacking the ZZ domains did not specifically bind to IgG. In contrast, only the protein beads displaying the ZZ domains showed much greater IgG-binding capacities (Figure 31). As described in Section 3.3.5, the position of 3xFe could influence the IgG binding. The IgG-binding ability of the xGFP-PhaC(C319A)-ZZ and xGFP-PhaC(C319A)-ZZ-3xFe protein beads was approximately 1.2- and 2-fold stronger than the xGFP-3xFe-PhaC(C319A)-ZZ beads across the various temperatures (Figure 31A) and pHs (Figure 31B).

As shown in Figure 31A, high IgG-binding abilities were observed at 4^{o}C. The binding ability also remained at relatively high levels when the binding temperature was increased to 40^{o}C. However, above this temperature, binding capacity dramatically decreased. These results indicate that the optimal IgG-binding temperature of GFP beads displaying the ZZ domains may be at 40^{o}C. IgG binding of GFP beads was then tested at 40^{o}C through different pH treatments (Figure 31B). The results show that the change of pH from 4 to 11 did not significantly affect the IgG-binding ability of immobilized ZZ domains.

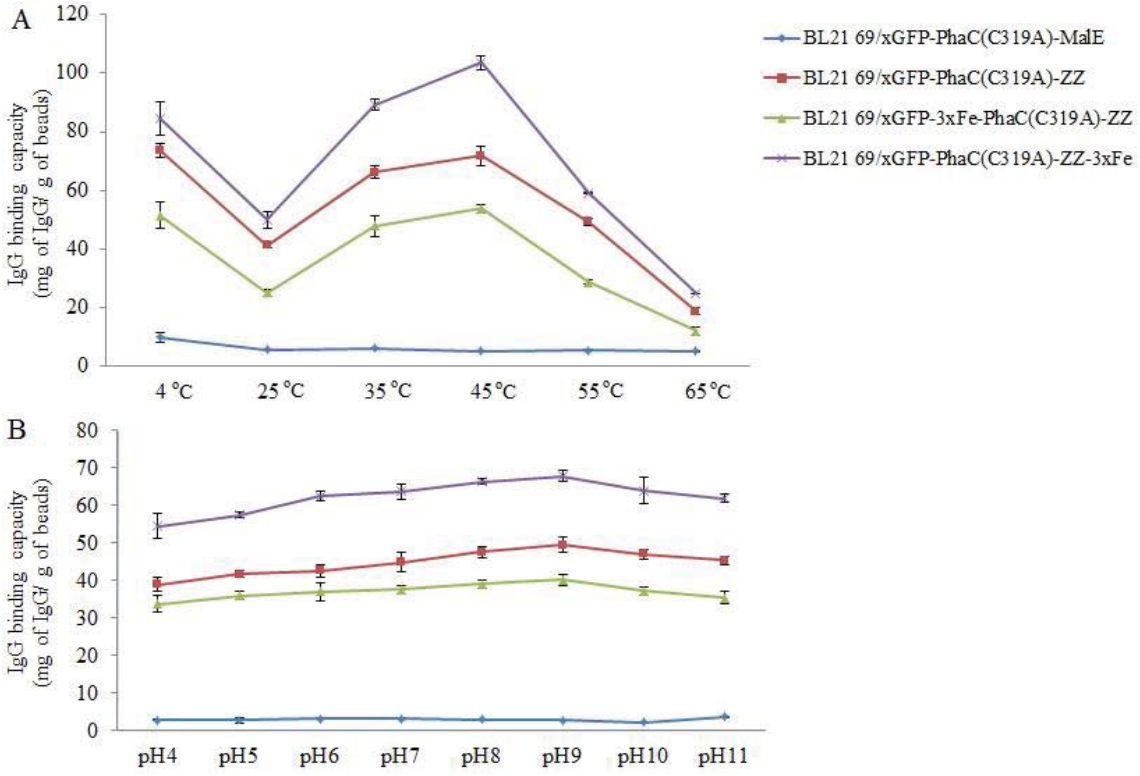

Figure 31. **Human IgG-binding capacity of GFP beads displaying the ZZ domains at different temperatures (A) and at 40°C through different pH conditions (B).** The IgG-binding capacity assay at different temperatures (4, 25, 35, 45, 55, and 65°C) and pHs (4, 5, 6, 7, 8, 9, 10, and 11) was described in the Materials and Methods chapter (Section 2.13.5.4). Protein concentration was measured by the Bradford assay (Section 2.13.1) using purified human IgG as the standard. All measurements were performed in triplicate. The mean of IgG-binding capacity is shown ±SD (n=3). All beads were produced in *E. coli* BL21(pMCS69) harboring the respective pET-14b plasmid (BL21 69/). BL21 69/xGFP-PhaC(C319A)-MalE, xGFP-PhaC(C319A)-MalE FP beads; BL21 69/xGFP-PhaC(C319A)-ZZ, xGFP-PhaC(C319A)-ZZ FP beads; BL21 69/ xGFP-3xFe-PhaC(C319A)-ZZ, xGFP-3xFe-PhaC(C319A)-ZZ FP beads; and BL21 69/ xGFP-PhaC(C319A)-ZZ-3xFe, xGFP-PhaC(C319A)-ZZ-3xFe FP beads.

3.4 Characterization of protein bead morphology and functionality generated via different cell disruption methods

To analyze protein bead morphology and functionality generated via different cell disruption methods, the following two plasmids were utilized: pET-14b xgfp-phaC(C319A)-linker-malE and pET-14b xgfp-phaC(C319A)-linker-zz (Table 5, Section 2.1.2). Jahns et al. (2013) constructed these two plasmids.

The hypotheses in this section were that protein beads extracted by various methods would show different morphologies and affect the activities of the target proteins displayed on the surface of protein beads. In order to test these hypotheses, recombinant *E. coli* cells accumulating FP protein beads were disrupted using three different methods: cell disruptor (Constant Cell Disruption System, UK), microfluidizer (Alphatech Systems), and Bugbuster® Protein Extraction Reagent (Merk, Germany; Section 2.11). The morphology of purified protein beads was subsequently analyzed by TEM and SEM (Section 2.12.3), and the results are presented in Section 3.4.1. The functional activity of protein beads isolated by each disruption method was assessed by IgG-binding assay (Section 2.13.5.3), and the results are shown in Section 3.4.2.

3.4.1 TEM and SEM analysis of protein beads isolated via different cell disruption methods

Protein beads produced in *E.coli* BL21(pMCS69/pET-14b xGFP-PhaC(C319A)-linker-MalE) were isolated by different cell disruption methods (Section 2.11) and analyzed by TEM and SEM (Section 2.12.3). The TEM results show that the protein beads isolated by the cell disruptor (Figure 32B) and Bugbuster® reagent (Figure 32C) were much larger than those isolated by microfluidization (Figure 32D). Furthermore, the SEM results (Figure 33) show that protein beads isolated by the cell disruptor and Bugbuster® reagent methods were aggregates of many small protein beads. In contrast, these protein aggregates were separated when microfluidizer disruption was applied.

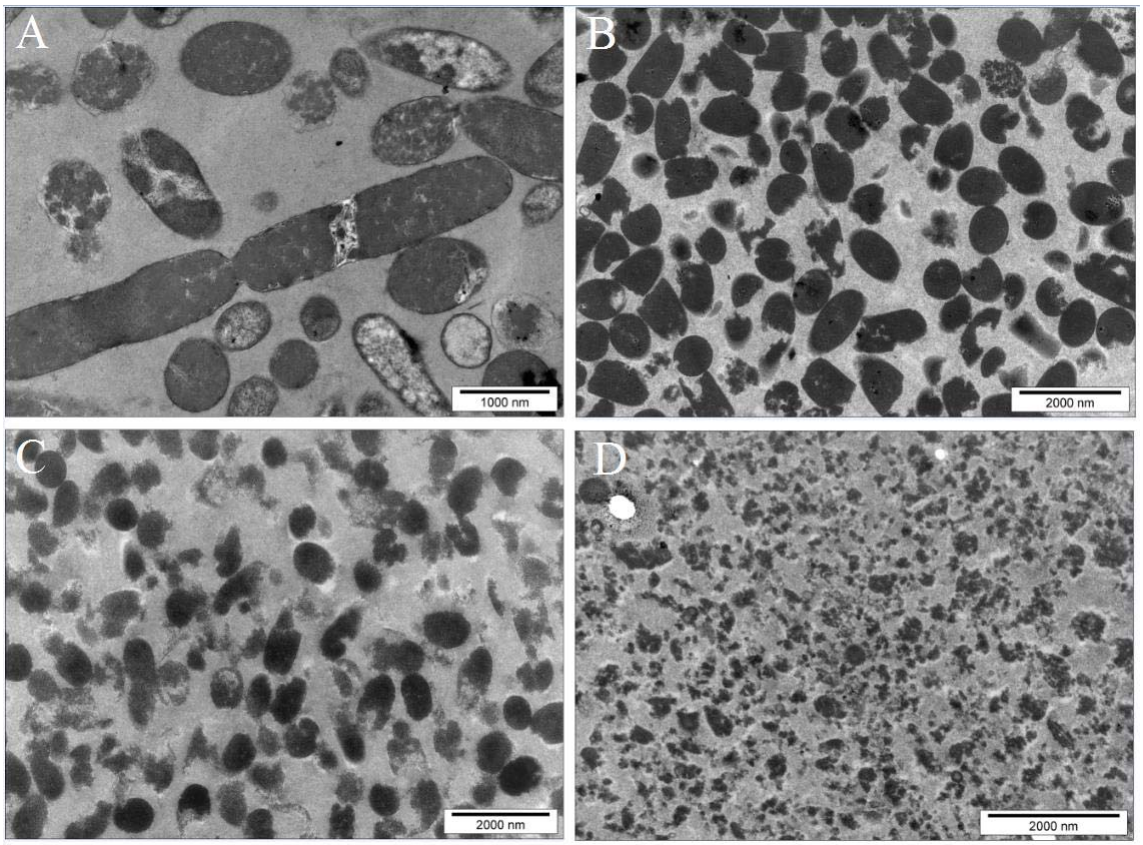

Figure 32. **TEM analysis of protein beads isolated via different cell disruption methods.** The protein beads were produced in *E. coli* BL21(pMCS69) expressing pET-14b xGFP-PhaC(C319A)-linker-MalE. (A) Protein beads accumulating *E. coli* cells; (B) Protein beads isolated by cell disruptor (Section 2.11.1.2); (C) Protein beads isolated by Bugbuster® Protein Extraction Reagent (Section2.11.1.1); and (D) Protein beads isolated by microfluidizer disruption (Section 2.11.1.2).

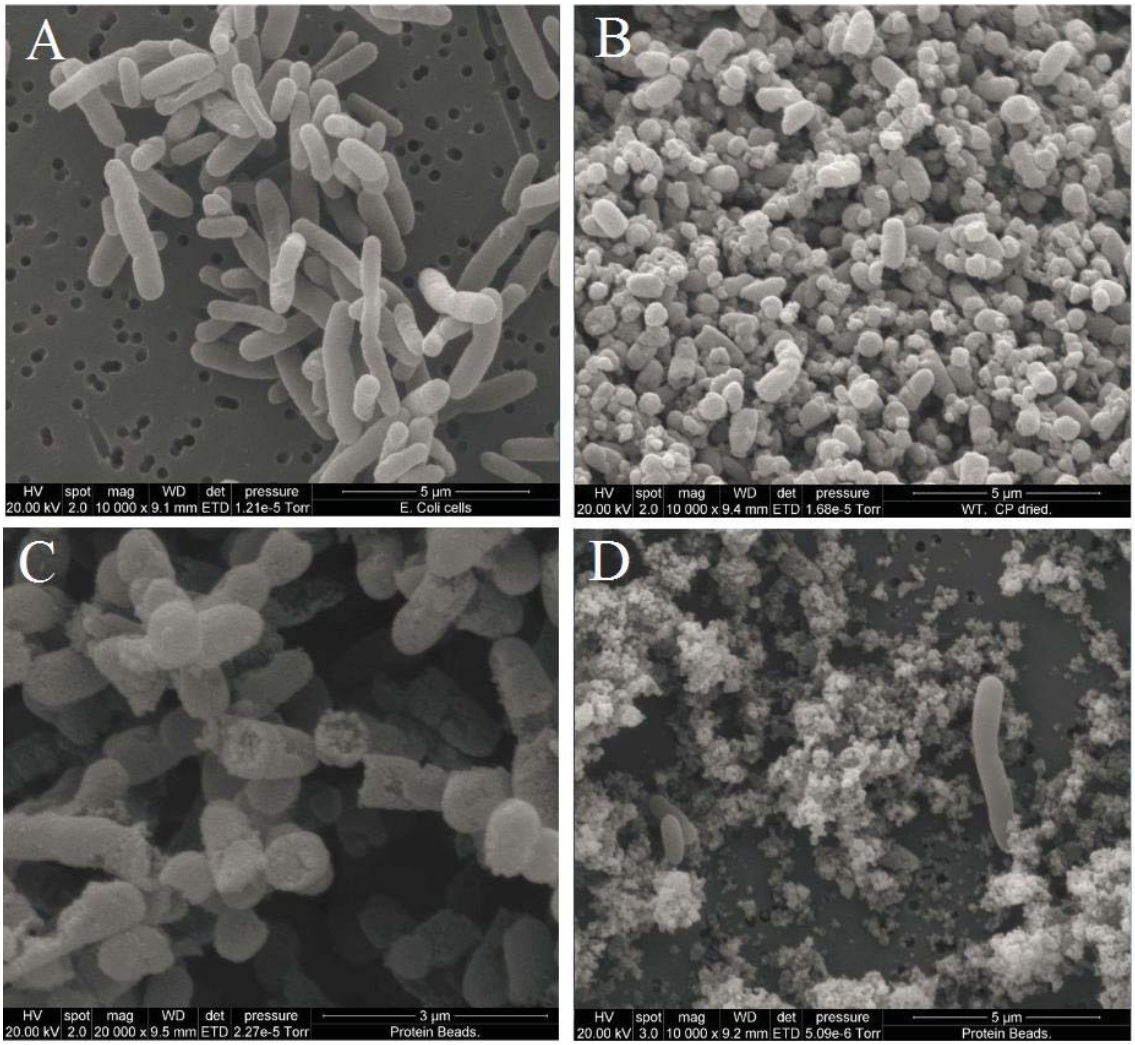

Figure 33. **SEM analysis of protein beads isolated via different cell disruption methods.** The protein beads were produced in BL21(pMCS69) expressing pET-14b xGFP-PhaC(C319A)-linker-MalE. (A) Protein beads accumulating *E. coli* cells; (B) Protein beads isolated by cell disruptor (Section 2.11.1.2); (C) Protein beads isolated by Bugbuster® Protein Extraction Reagent (Section 2.11.1.1); and (D) Protein beads isolated by Microfluidizer disruption (Section 2.11.1.2).

3.4.2 Functional assessment of protein beads displaying the ZZ domains isolated via different cell disruption methods

To test the function of protein beads isolated by different cell disruption methods, the human IgG-binding capacity of the immobilized ZZ domains was assessed (Section 2.13.5.3). The unbound and eluted IgG fractions were measured by the Bradford assay (Section 2.13.1). The IgG-binding assay results are shown in Figure 34. The negative control was protein beads displaying MalE, while the test sample was beads carrying the ZZ domains. Recovery rate of IgG-binding capacity for plain beads was between 78% and 90% (data not shown). As shown in Figure 34, a very low IgG binding of the negative control was observed, suggesting that human IgG did not specifically bind to the protein beads lacking the ZZ domains. Moreover, protein beads displaying the ZZ domains showed a dramatic increase in IgG-binding capacity. The results also show that beads displaying the ZZ domains isolated by chemical cell disruption (Bugbuster®) had a significantly higher IgG-binding capacity compared to beads isolated by mechanical cell disruption (cell disruptor and microfluidizer).

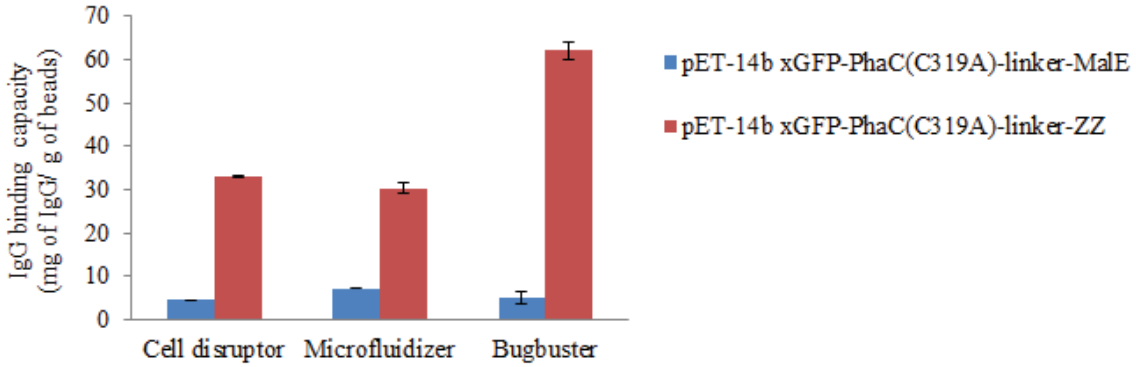

Figure 34. **Human IgG-binding capacity of protein beads displaying the ZZ domains isolated via different cell disruption methods.** The IgG-binding capacity assay (Section 2.13.5.3) was described in the Materials and Methods chapter. Protein concentration was measured by the Bradford assay (Section 2.13.1) using purified human IgG as the standard. All measurements were performed in triplicate. The mean of IgG-binding capacity is reported ±SD (n=3). The functionality of protein beads was analyzed by human IgG-binding capacity after isolation using different cell disruption methods: cell disruptor, microfluidizer and Bugbuster® reagent (Section 2.11). All beads were produced in *E. coli* BL21(pMCS69) harboring the respective pET-14b plasmid (BL21 69/). BL21 69/xGFP-PhaC(C319A)-MalE, xGFP-PhaC(C319A)-MalE FP beads; and BL21 69/xGFP-PhaC(C319A)-ZZ, xGFP-PhaC(C319A)-ZZ FP beads.

Chapter 4: Discussion

4.1 New skin test for detection of bovine TB based on antigen-displaying PHA beads produced by recombinant *E. coli*

A previous study has shown that PHA beads can be genetically engineered to display a range of desired antigens (Jahns & Rehm, 2012). PHA beads displaying antigens showed high immunogenicity *in vivo* and mediated specific Th1 and Th2 immune responses leading to protective immunity against TB (Parlane et al., 2011, 2012; Parlane, Wedlock, Buddle, & Rehm, 2009). The aim in this TB study was to genetically engineer *E. coli* to produce fusion proteins, which mediate formation of PHA beads displaying selected TB antigens (CFP10, ESAT6, Rv3615c) suitable for TB skin test applications. As outlined in Figure 8, various hybrid genes encoding fusion proteins mediated production of PHA beads displaying single or all three TB antigens were constructed. All four hybrid genes mediated PHA bead production in recombinant *E. coli* cells as assessed by fluorescence microscopy (Figure 9), TEM (Figure 10), and GC-MS, suggesting that the PHA synthase PhaC remained active in all of the fusion proteins as they were able to catalyze synthesis of the PHA and mediated bead formation (Rehm, 2006, 2007). Furthermore, SDS-PAGE analysis of proteins attached to the respective PHA beads indicated that full-length fusion proteins were produced as indicated by the detection of a dominant protein with the expected molecular weight (Figure 11). The identity of these TB fusion proteins was further substantiated by tryptic peptide fingerprinting analysis using MALDI-TOF/MS (Figures 11 and 12, Appendix 1; Jahns & Rehm, 2009).

Fusion proteins immobilized on the PHA bead surface which contained the antigen CFP10 were susceptible to protease degradation. However, this was avoided by using protease inhibitors during the bead isolation process (Figure 11). A previous study has shown that CFP10 exists in at least four different forms, likely due to post-translational modifications (MacGurn, Raghavan, Stanley, & Cox, 2005). The degradation of CFP10 observed in this study could reflect the recombinant *E. coli* host's inability to perform such modifications, conceivably causing partial unfolding of this antigen while increasing its susceptibility to protease degradation.

PHA beads displaying TB antigens were analyzed by ELISA using specific anti-TB antigen antibodies (Figure 13A). Analysis of cross-reactivity of the specific anti-TB antigen antibodies, as well as analysis of possible non-specific antibody binding using pre-immune sera, suggests that the anti-TB antigen antibodies were highly specific. It also indicates that PHA beads displaying antigens did not non-specifically bind to antibodies (Figure 13B, C). However, the beads displaying triple TB antigens showed greater reactivity with the specific antibodies when compared to the beads displaying respective single TB antigens. This difference in reactivity was not due to a disparity in protein expression levels because similar amounts of recombinant fusion protein were detected per bead mass (Figure 11). Furthermore, the high reactivity of the immobilized triple TB antigen was not caused by cross-reactivity of antibodies. Each antibody only specifically interacted with its corresponding TB antigen (Figure 13C). Therefore, the different arrangement of the antigens in the triple antigen fusion protein possibly contributed to enhance accessibility by the respective specific antibody.

Due to its high reactivity with specific antibodies, the PHA bead displaying the triple TB antigens was selected to examine its applicability as a TB skin test reagent. In addition, the manufacture of PHA bead-displaying multiple antigens should be more cost-effective than producing several single antigen beads. There is also a demand for a specific diagnostic reagent that could distinguish TB-infected from environmental strain-sensitized or BCG-vaccinated individuals. A comparative cervical skin test has been used in many countries for the diagnosis of bovine TB as both PPD-A and PPD-B contain antigens, which are commonly present in many environmental mycobacteria. Moreover, a stronger response to PPD-B compared to that for PPD-A often indicates an infection with *M. bovis* (Monaghan, Doherty, Collins, Kazda, & Quinn, 1994). Specific TB antigens, CFP10, ESAT6, and Rv3615c, are found in members of the pathogenic *M. tuberculosis* complex, including *M. bovis* (Millington et al., 2011). Therefore, responses to these three TB antigens would indicate a more specific response when compared to that for PPD-B that contains a crude mix of antigens. In the TB skin test study on cattle (Figure 14), all the three reagents (PPD-A, PPD-B, and the triple TB antigen bead) were able to identify *M. bovis*-infected cattle with high sensitivity (Figure 14A). However, only the reagent containing the immobilized triple TB antigens could accurately identify environmental mycobacteria-sensitized cattle, while PPD-A and PPD-B gave false positive results (Figure 14B).

Previous studies have shown that a protein cocktail containing purified soluble CFP10, ESAT6, and Rv3615c could be used as a skin test reagent to distinguish TB-infected from non-infected and BCG-vaccinated cattle (Casal et al., 2012; Whelan et al., 2010). Indeed, the immunodominant antigen Rv3615c has been found to identify ESAT6- and/or CFP10-unresponsive TB-infected cattle (Sidders et al., 2008). The addition of Rv3615c to the reagent containing ESAT6 and CFP10 significantly improves the sensitivity of skin tests in naturally–infected cattle and does not cause responses in vaccinated or healthy cattle (Whelan et al., 2010). This suggests that the use of a protein cocktail comprised of CFP10, ESAT6, and Rv3615c would be beneficial for TB skin testing. Moreover, antigens, such as antigen 85A and ESAT6, from pathogenic mycobacteria have been shown to stimulate relatively strong cellular immune responses when they were displayed on the surface of PHA beads as compared to the free antigens (Parlane et al., 2012). Accordingly, CFP10-Rv3615c-ESAT6 displayed on the surface of PHA beads might act as a more sensitive and cost-effectively producible, diagnostic reagent when compared to the respective free antigens.

However, various factors could potentially confound the interpretation of TB diagnostic results. The genes encoding ESAT6 and CFP10 are absent in most environmental mycobacteria, but are present in *Mycobacterium kansasii,* which can cause infections in both humans and cattle (Arend et al., 2005; Waters et al., 2006). Indeed, humans infected by *M. kansasii* have shown detectable IFN-γ responses to recombinant and peptide mixes of ESAT6 and CFP10 (Arend et al., 2005). In contrast, Waters et al. (2006) observed that no serum antibody responses to ESAT6 or CFP10 were detected in the *M. kansasii*-infected cattle, but these infected cattle could still produce IFN-γ responses in blood cultures after re-induction with recombinant ESAT6-CFP10 antigens. Moreover, the PHA beads reagent may contain lipopolysaccharide and/or heat shock proteins that could potentially affect skin test specificity. One experimentally-infected animal in this TB skin test study produced a positive response to the control beads that may have been a response to heat shock proteins contained in the beads, while none of the control cattle responded to the control beads.

In the bovine TB skin test, no correlation was found between the size of the skin test responses to PPD-B and the triple TB antigen PHA beads in the *M. bovis*-infected cattle. It is possible that the strength of the skin test responses to different specific TB antigens

may vary during the course of the disease, and the disease may progress at different rates in individual animals. Recently, it has been found that the three most immunodominant antigens in PPD for inducing TB skin test responses (GroES, GroEL2, and DnaK) are highly conserved chaperone proteins (Yang et al., 2011). It is recognized that immune responses to proteins such as ESAT6 are first observed at an early stage of *M. bovis* infection in cattle. Thus, responses to the highly conserved chaperone proteins may increase as the disease progresses (Pollock & Andersen, 1997).

The reagent comprised of the triple TB antigen PHA beads might also have a potential use in the diagnosis of human TB, which is mainly caused by *M. tuberculosis*. Indeed, CFP10, ESAT6, and Rv3615c from *M. tuberculosis* strongly cross-react with the orthologous proteins in *M. bovis*, which is a causative agent of bovine TB (Millington et al., 2011; Waters et al., 2004). These three TB antigens are also immunodominant in both active and latent human TB infection (Millington et al., 2011; Sidders et al., 2008).

This novel PHA bead TB diagnostic reagent comprised of the immobilized triple antigens has high specificity and sensitivity, which allows for quick and accurate screening of the TB-infected cattle. In addition, the selected antigens are not produced by BCG strains. Thus the PHA bead-based TB skin test has the potential to differentiate between infected and BCG vaccinated animals. Moreover, the versatility of this PHA bead platform technology would also allow adaptation of this new skin test reagent to a newly developed vaccine by implementing differentiating antigens. Overall, this TB skin test study demonstrated that bacterial PHA beads can be genetically engineered to simultaneously display three TB specific antigens, and that the triple TB antigen PHA beads showed specific and sensitive performance as TB skin test reagents. Furthermore, the novel TB skin test developed in this study showed significantly less false positive results in cattle compared to current commercial skin test reagents, which could, in turn, reduce a significant economic loss for the end-users.

4.2 Characterization of IgG-binding ability of the [GB1]3 domains displayed on the surface of various FP beads

A recent study has shown that the inactivation (C319A) of PhaC inhibited the formation of PHA beads, and that overproduction of engineered GFP-PhaC (C319A) fusion proteins led to the formation of strongly green fluorescent fusion protein beads (Jahns et al., 2013). Jahns et al. (2013) further found that GFP protein beads displaying the triple IgG-binding domains, [GB1]3, showed a significantly elevated IgG-binding capacity compared to the counterpart displayed on PHA beads. In this study, the [GB1]3 domains were employed to investigate whether their enhanced IgG-binding capacity due to GFP beads could be achieved by displaying the domains on other FP beads. As outlined in Figure 15, various hybrid genes encoding N-terminally extended or non-extended FP-PhaC(C319A) fusion mediated production of various fluorescent fusion protein beads displaying the [GB1]3 domains were constructed. All hybrid genes generated in this study mediated different FP bead production in recombinant *E. coli* cells using the strong T7 promoter as indicated by fluorescence microscopy (Figure 16). Further SDS-PAGE analysis of proteins displayed on the respective FP beads suggests that full-length fluorescent fusion proteins were produced. This was indicated by the detection of a dominant protein with the expected molecular weight (Figure 17). Moreover, the influence of pMCS69 (encoding enzymes PhaA and PhaB) on FP production was negligible. In contrast, the recombinant fluorescent fusion proteins containing the N-terminal tetrapeptide extension (AVTS) significantly enhanced FP production when compared to the non-extended versions (Figure 17). It is possible that the four amino acid residues at the N-terminus of FP altered the properties of the FP when fused to C-terminal fusion partners and when produced from the strong T7 promoter, which resulted in a significant enhancement of protein bead production (Jahns et al., 2013).

The functionality of various FP beads displaying the [GB1]3 domains was determined by an IgG-binding assay using purified goat IgG. The results indicate that beads displaying the [GB1]3 domains bound specifically to IgG (Figures 18 and 19). It was found that there was no significant difference in the IgG-binding ability between beads made of extended and non-extended HcR. In contrast, protein beads derived from

extended EYFP or ECFP performed better regarding goat IgG-binding capacities when compared to their non-extended versions (Figure 18). Jahns et al. (2013) demonstrate that the relatively high IgG-binding ability of EYFP or ECFP beads made of extended FP fusion proteins was also observed in GFP beads. This could reflect the high sequence identity between GFP and its derivatives, EYFP and ECFP. In contrast, GFP and HcR share only approximately 21% amino acid similarity; however, despite this, HcR forms a β-barrel structure comparable to GFP and its derivatives (Fradkov et al., 2002; Gurskaya et al., 2001). In general, although the IgG-binding ability of the [GB1]3 domains displayed on various FP beads is similar, it was still much greater than the counterpart immobilized on PHA beads and a control, commercial protein A beads (Figure 18). Furthermore, various FP beads designed to bind to IgG of the human IgG subclass 3 showed specific binding as assessed by goat IgG-binding assay (Figure 18).

The various FP beads displaying the [GB1]3 domains were assessed in their utility in IgG bioseparation from human blood serum (Figure 20). As expected, FP beads lacking the IgG-binding domains [GB1]3 did not specifically bind to IgG or other background proteins, including albumin, the most abundant protein in human serum. However, FP beads displaying the [GB1]3 domains could successfully purify IgG from human serum. Furthermore, the intensity of bands corresponding to the IgG heavy and light chains on SDS-PAGE of eluted factions demonstrated that the IgG-binding domains [GB1]3 displayed on extended EYFP and ECFP beads had a relatively strong IgG purification power. In contrast, the presence and absence of the extension had no significant effect on the IgG purification power of HcR beads displaying [GB1]3. As described in the previous paragraph, this could be due to the amino acid sequence and protein structure difference between GFP-like proteins (EYFP and ECFP) and HcR (Fradkov et al., 2002; Gurskaya et al., 2001).

The effect of temperature and pH on IgG binding of protein beads displaying the [GB1]3 domains were evaluated (Figure 21). IgG was found to only specifically bind to the protein beads displaying the [GB1]3 domains (Figure 21). These beads bound IgG efficiently between 4 and 45^{o}C; however, at 25 and 35^{o}C, the binding capacity was slightly lower and, at higher temperatures (above 55^{o}C), binding efficacy dropped sharply. These results indicate that the binding affinity between IgG and [GB1]3 was strongly temperature dependent (Figure 21A). A previous study has also shown that

IgG-binding proteins, including the GB1 domain of protein G, had weak affinity with IgG at ambient temperature; however, it bound more firmly at 4°C (Tu, Primus, & Goldenberg, 1988). Interestingly, we found for the first time that the [GB1]3 domains displayed on protein beads still bound strongly to IgG at a temperature as high as 45°C, which might be a unique advantage of our protein bead displaying platform. We also assessed the effect of pH on IgG-binding capacity, and the results indicate that the binding capacity was slightly increased at alkaline pH. Thus, the binding affinity of IgG to the immobilized [GB1]3 domains was less dependent on pH (Figure 21B), a finding consistent with previous studies (Akerstrom & Bjorck, 1986; Bjorck & Kronvall, 1984).

Purification of IgG based on the immobilized [GB1]3 domains was previously demonstrated by Jahns et al. (2013) using PHA and protein beads as the solid support. In addition, this study also showed that immobilization of the domains on protein beads derived from GFP could increase their IgG-binding ability (Jahns et al., 2013). In our approach, we displayed the [GB1]3 domains on the surface of other FP protein beads including EYFP, ECFP, and HcR, which also showed enhancement of IgG purification; in addition, the IgG-binding ability was much stronger than the counterpart displayed on PHA beads. That said, using FP beads as a platform for displaying various proteins is a new emerging technology and offers interesting new properties when compared to, for example, the PHA bead technology. Immobilization of functional proteins to FP beads seems to provide a versatile bead platform technology with inherent diagnostic application potential. FP beads which have been engineered to specifically bind antibodies might provide a useful molecular tool for the development of diagnostic assays.

4.3 Development of functionalized super-paramagnetic protein beads

An iron-binding peptide (consisting of the amino acid sequence RRTVKHHVN) isolated from the outer membrane of *E. coli* could facilitate specific binding of iron oxide (Brown, 1992). Beads displaying this peptide could become super-paramagnetic upon binding with iron oxide (Ito, Shinkai, Honda, & Kobayashi, 2005). In a previous study, it was shown that a recombinant fusion, containing haloalkane dehalogenase and three consecutive copies of the aforementioned iron-binding peptide (3xFe), is

successfully purified by uncoated iron oxide nanoparticles (Johnson, Zawadzka, Deobald, Crawford, & Paszczynski, 2008). The aim of present study was to develop GFP beads displaying both the iron binding peptides (3xFe) and the ZZ domains and assess whether these beads would maintain IgG-binding capacity after magnetisation. As shown in Figures 23 and 25, hybrid genes encoding recombinant fusion proteins (xGFP-3xFe-PhaC(C319A)-ZZ and xGFP-PhaC(C319A)-ZZ-3xFe) mediated production of GFP beads displaying the 3xFe and ZZ domains were constructed. As shown by fluorescence microscopy, recombinant *E. coli* cells expressing the hybrid genes produced intracellular GFP beads (Figure 26). In addition, SDS-PAGE analysis of proteins displayed on the GFP beads suggests that full length fluorescent fusion proteins were produced, as indicated by the detection of a dominant protein band corresponding to the expected molecular weight of the fusion protein (Figure 27).

Iron oxide particles existing in ferrofluid (provided by PolyBatics) are 0.7–1.4 μm in diameter (Figure 28). However, in comparison, the protein beads were 0.5–1.5 μm. Although iron particles of the ferrofluid bound to both protein beads lacking or displaying the 3xFe peptides, the results indicate that the latter beads retained magnetism for longer compared to their counterparts lacking this peptide (data not shown). This finding was consistent with a previous study (Liberti & Feeley, 1991). Liberti and Feeley suggest that non-specific binding of iron oxide particles to beads could be attributed to the large surface to volume ratio of the iron particles as well as electrostatic and hydrophobic interactions between the iron particles and beads. Although we attempted to determine the levels of iron-binding capacity and iron-leaching of magnetized beads, the large size of the (unbound and leaching) iron particles led to co-precipitation with protein beads upon centrifugation, making it impractical to separate the two.

The functionality of the ZZ domains displayed on magnetized protein beads was determined by the IgG-binding assay using purified human IgG. The results confirm that human IgG did not specifically bind to iron particles and protein beads lacking the ZZ domains (Figures 29 and 30). This was the case both before and after magnetization. Moreover, before magnetization, the IgG-binding capacity of the xGFP-PhaC(C319A)-ZZ and xGFP-PhaC(C319A)-ZZ-3xFe protein beads was 1.5- and 2-fold greater than the xGFP-3xFe-PhaC(C319A)-ZZ beads, respectively. This indicates

that the position of the iron-binding peptide could affect the IgG-binding ability. The iron-binding peptide at the C-terminus of PhaC(C319A) showed enhanced IgG binding, while the peptide between xGFP and PhaC(C319A) inhibited the IgG binding. Furthermore, their IgG-binding capacity dropped after magnetization with neutral ferrofluid (pH7.5, Figure 29). In contrast, magnetization of the protein beads with highly alkaline ferrofluid (pH14) completely abolished their IgG-binding capacity (Figures 29 and 30). Moreover, protein beads treated by highly alkaline ferrofluid lost fluorescence (data not shown). This could be caused by inactivation of the IgG-binding ZZ domains due to the high pH, which could change the stability of protein structure and cause its denaturation (Stigter, Alonso, & Dill, 1991).

As outlined in Section 3.3.6, due to a limitation of ferrofluid availability, we were not able identify the optimal IgG-binding temperature and pH for the magnetized protein beads. However, the IgG-binding capacity of non-magnetized protein beads at various temperatures and pHs were measured (Figure 31). As expected, across all temperature and pH conditions, IgG only specifically bound to the protein beads displaying the ZZ domains (Figure 31). IgG-binding capacity was the highest at 4 and 40^{o}C (Figure 31A). In contrast, changes of pH did not influence the IgG-binding capacity of the immobilized ZZ domains (Figure 31B). This suggests that the binding affinity between IgG and the ZZ domains was more strongly dependent on temperatures, but less dependent on pH. A previous study has also shown that the ZZ domain of protein A had strong IgG-binding capacity when the binding temperature was lowered to 4^{o}C (Tu, Primus, & Goldenberg). Interestingly, the ZZ domains displayed on protein beads still bound strongly to IgG at a temperature around 40^{o}C. In addition, previous studies have also shown that changes of pH do not strongly correlate to the IgG-binding capacity of the ZZ domain of protein A (Akerstrom & Bjorck, 1986; Bjorck & Kronvall, 1984).

In a previous study, it was shown that functionalized magnetic nanobeads, such as dextran-coated magnetic iron oxides, can be generated by immobilization of functional groups on the surface of iron oxide particles (Laurent et al., 2008). In this study, we provided an alternative preparation approach for making magnetic beads: combination of protein beads displaying the iron-binding peptide and magnetic iron oxide particles. However, iron oxide particles contained in the ferrofluid were in a size range which could have mediated non-specific binding to protein beads. Although we demonstrated

that protein beads displaying 3xFe peptides retained magnetism for longer than the beads lacking the iron-binding peptide (data not shown), it is critical to understand the ferrofluid behaviour and to improve or develop a new one that contains iron particles with a small size which does not provide a surface for non-specific binding. Hence, further experiments are required to generate functional super-paramagnetic beads.

4.4 Characterization of the morphology and functionality of FP beads isolated via different cell disruption techniques

Garcia-Fruitos et al. (2012) have shown that inclusion bodies or protein beads were commonly found in recombinant bacteria. These bacterial protein beads contained improperly folded proteins as well as a significant amount of correctly folded and biologically active proteins (Garcia-Fruitos et al., 2012; Peternel & Komel, 2011). Protein beads, isolated by cell disruptor, were oval-shaped and 0.5–1.5 μm in size (Jahns et al., 2013). The aim of this section was to determine whether using different cell disruption techniques could influence the morphology and functional activity of protein beads. Analysis of TEM and SEM suggests that protein beads disrupted by cell disruptor or Bugbuster® reagent were oval-shaped and comprised of many small protein bead aggregates. However, a microfluidizer could further disrupt these aggregates (Figures 32 and 33). Peternel and Komel (2011) have found that the shape and size of protein beads are diverse and dependent on the host strain and the cultivation time. In particular, protein beads form spheres in the early stage of cultivation. However, beads are not able to retain their spherical shape when they reach the bacterial cell wall. Therefore, after long-term cultivation, beads are normally elongated into large cylinders that almost occupy the entire cytoplasmic space (Peternel & Komel, 2011). Moreover, after the fusion of the proto-aggregates, a cotton-like amorphous matrix fills the spaces between and inside the proto-aggregates and contributes to a porous surface of large protein beads (Peternel & Komel, 2011). They also state that, usually, only one protein bead or rarely two beads are produced in the bacterial cell. During the bacterial cell division, the bead continues to grow and keeps in one cell, while protein synthesis and bead formation will start *de novo* in the other cell.

Functional activity of protein beads isolated by different cell disruption methods was determined by testing the human IgG-binding capacity of the immobilized ZZ domains (Figure 34). Analysis of IgG-binding assay suggests that the IgG-binding ability of protein beads displaying the ZZ domains isolated by the chemical cell disruption (Bugbuster® reagent) was higher than that isolated by the mechanical cell disruptions (cell disruptor and microfluidizer). Bugbuster® Protein Extraction Reagent (Merck, Germany) could gently disrupt the cell membrane of *E. coli*, causing the liberation of soluble protein without denaturing them. Thus, chemical cell disruption did not significantly affect the activity of liberated proteins (Irimia, Tompkins, & Toner, 2004). However, mechanical cell disruption techniques usually generated heat during the disruption process. This may result in denaturation of protein into a non-native state (Di Carlo, Jeong, & Lee, 2003; Jen, Hsiao, & Maslov, 2012).

Proper cell disruption methods may be important for protein extraction and to maintain intracellular protein function. As described above (Section 4.4), different cell disruption techniques could influence the morphology and functional activity of protein beads. Cell disruptor and microfluidizer are mechanical cell disruption techniques that are commonly used in the laboratory and can be applied for large-scale bead isolation. Chemical-based cell lysis, such as Bubuster® Protein Extraction Reagent, is an alternative to mechanical cell disruption. However, the Bugbuster® reagent is relatively expensive and only applied for specific use. Therefore, this method is not suitable for large-scale industrial protein isolation.

4.5 Directions for future research

TB is a worldwide health problem for both humans and cattle. It is critical to accurately diagnose TB-infected individuals and restrict TB transmission within and among populations. The reagent comprised of the triple TB antigen PHA beads developed in this study could distinguish TB-infected from non-infected cattle with high specificity and sensitivity. This reagent might also have a potential use in the diagnosis of human TB, which is mainly caused by *M. tuberculosis*. Indeed, CFP10, ESAT6, and Rv3615c from *M. tuberculosis* strongly cross-react with the orthologous proteins in *M. bovis*, which is a causative agent of bovine TB. The PHA beads reagent for cattle may contain

lipopolysaccharide and/or heat shock proteins that could potentially affect skin test specificity. Thus, the purity of the reagent should be increased to make the assay more specific and suitable for testing human TB in the future. In addition, the sensitivity of the assay should be further improved by involving other specific TB antigens, which are present in pathogenic mycobacteria, but absent from the majority of non-pathogenic environmental mycobacteria.

Recombinant fluorescent fusion proteins containing the N-terminal tetrapeptide extension (AVTS) significantly enhanced FP bead production when compared to the non-extended versions. In this study, protein beads were produced from the strong T7 promoter in recombinant *E. coli* cells. Thus, in the future, we could assess the enhancement of protein bead production by producing them from other strong promoters into *E. coli* or different hosts.

In addition, this study demonstrated that iron oxide particles contained in the ferrofluid Polybatics (Palmerston North, New Zealand) generated were too large, which could lead to non-specific binding to protein beads. Moreover, a highly alkaline ferrofluid completely abolished the functionalities displayed on protein beads, while a neutral ferrofluid could retain their functions. Future studies could improve or develop a new ferrofluid (pH 7.5), which contains small iron particles and does not cause non-specific binding to protein beads.

Moreover, the results also demonstrated that the morphology and function of FP protein beads are highly dependent on the cell disruption technique used to isolate the beads. In the future, we could generate an optimal cell disruption technique that does not have a significant impact on bead morphology and functionality. Subsequently, we could find the size distribution of protein beads.

4.6 Summary

In the TB skin test study on cattle, three immunodominant TB antigens, CFP10, ESAT6, and Rv3615c, are observed in pathogenic mycobacteria, but absent from the majority of non-pathogenic environmental mycobacteria. To increase their immunogenicity, these TB antigens were displayed on PHA beads' surfaces by fusing them to PhaC, which mediated formation of antigen–displaying PHA beads. It has been demonstrated that the PHA beads displaying triple TB antigens have greater reactivity with the specific antibodies when compared to the beads displaying respective single TB antigens. The results also show that all the three reagents (PPD-A, PPD-B, and the triple TB antigen bead) are able to identify *M. bovis*-infected cattle with high sensitivity. However, only the reagent containing the immobilized triple TB antigens could accurately identify environmental mycobacteria-sensitized cattle, while PPD-A and PPD-B give false positive results. Therefore, the PHA bead TB diagnostic reagent comprised of the immobilized triple antigens has high specificity and sensitivity, which allows for quick and accurate screening of TB-infected cattle. Moreover, the selected antigens are not produced by BCG strains. Thus, the PHA bead-based TB skin test has the potential to differentiate between infected and BCG-vaccinated animals. In addition, the manufacture of PHA beads displaying multiple antigens should be more cost-effective than producing several single antigen beads. These findings support the hypotheses that the triple TB antigens displayed on the surface of PHA beads have a better performance than single antigens displayed on the beads, and the triple TB antigens on beads are able to differentiate TB-infected from non-infected cattle to act as a cost-effective diagnostic test.

It has been shown that the [GB1]3 domains of protein G displayed on various FP (including EYFP, ECFP, and HcRed) protein beads show approximately 1.5-2 fold greater IgG-binding ability when compared to the counterpart displayed on PHA beads. This binding ability suggests that it may be advantageous for displaying foreign proteins on the surface of protein beads as the proteins may obtain a relatively high activity when compared to the display on PHA beads. In addition, the results showed that protein beads containing 3xFe could be magnetized by a neutral ferrofluid (pH 7.5) and the resulting magnetized protein beads displaying the ZZ domains of protein A retain a

high IgG binding ability. However, the position of 3xFe could affect the IgG-binding ability of protein beads, and the iron oxide particles contained in ferrofluid can cause non-specific binding to protein beads with no 3xFe displayed. The IgG-binding ability of protein beads displaying the [GB1]3 or ZZ domains is strongly dependent on temperatures but less dependent on pH. Moreover, protein beads isolated by various methods may influence protein bead morphologies and functional activities.

Overall, these results demonstrate that genetic engineering of the active and inactive PHA synthase provides a novel molecular tool for a covalent display of desired proteins (antigens and binding domains) on the surface of PHA and protein beads, respectively. Moreover, one-step generation and isolation of foreign proteins displaying PHA or protein beads are cost-effective and time-saving, and could enhance the stability and activity of immobilized proteins. This facilitates the generation of various diagnostic reagents and strongly enhances the applied potential of these bio-beads in biotechnology and medicine.

Appendix I:

MALDI-TOF/MS analysis of PhaC-TB fuion proteins

Protein/Protein sequence	Peptide fragments assigned to the various protein regions
CFP10-PhaC (MW: 75.2 kDa)	
MAEMKTDAATLAQEAGNFERISGDLKTQIDQVESTA GSLQGQWRGAAGTAAQAAVVRFQEAANKQKQELD EISTNIRQAGVQYSRADEEQQQALSSQMGFHMATGK GAAASTQEGKSQPFKVTPGPFDPATWLEWSRQWQG TEGNGHAAASGIPGLDALAGVKIAPAQLGDIQQRYM KDFSALWQAMAEGKAEATGPLHDRRFAGDAWRTNL PYRFAAAFYLLNARALTELADAVEADAKTRQRIRFAI SQWVDAMSPANFLATNPEAQRLLIESGGESLRAGVR NMMEDLTRGKISQTDESAFEVGRNVAVTEGAVVFEN EYFQLLQYKPLTDKVHARPLLMVPPCINKYYILDLQP ESSLVRHVVEQGHTVFLVSWRNPDASMAGSTWDDYI EHAAIRAIEVARDISGQDKINVLGFCVGGTIVSTALAV LAARGEHPAASVTLLTTLLDFADTGILDVFVDEGHVQ LREATLGGGAGAPCALLRGLELANTFSFLRPNDLVW NYVVDNYLKGNTPVPFDLLFWNGDATNLPGPWYCW YLRHTYLQNELKVPGKLTVCGVPVDLASIDVPTYIYG SREDHIVPWTAAYASTALLANKLRFVLGASGHIAGVI NPPAKNKRSHWTNDALPESPQQWLAGAIEHHGSWW PDWTAWLAGQAGAKRAAPANYGNARYRAIEPAPGR YVKAKA	CFP10: A2-R20, T27-R57, Q78-R85 PhaC: V122-R137, I164-R175, D179-R209, F216-R226, F247-R281, I296-R308, Y351-R400, I414-K514, L557-K599, F602-K619, S623-K663, A665-R674
Rv3615c-PhaC (MW: 75.2 kDa)	
MTENLTVQPERLGVLASHHDNAAVDASSGVEAAAG LGESVAITHGPYCSQFNDTLNVYLTAHNALGSSLHTA GVDLAKSLRIAAKIYSEADEAWRKAIDGLFTHMATG KGAAASTQEGKSQPFKVTPGPFDPATWLEWSRQWQ GTEGNGHAAASGIPGLDALAGVKIAPAQLGDIQQRY MKDFSALWQAMAEGKAEATGPLHDRRFAGDAWRT NLPYRFAAAFYLLNARALTELADAVEADAKTRQRIR FAISQWVDAMSPANFLATNPEAQRLLIESGGESLRAG VRNMMEDLTRGKISQTDESAFEVGRNVAVTEGAVVF ENEYFQLLQYKPLTDKVHARPLLMVPPCINKYYILDL QPESSLVRHVVEQGHTVFLVSWRNPDASMAGSTWD DYIEHAAIRAIEVARDISGQDKINVLGFCVGGTIVSTA LAVLAARGEHPAASVTLLTTLLDFADTGILDVFVDEG HVQLREATLGGGAGAPCALLRGLELANTFSFLRPND LVWNYVVDNYLKGNTPVPFDLLFWNGDATNLPGPW YCWYLRHTYLQNELKVPGKLTVCGVPVDLASIDVPT YIYGSREDHIVPWTAAYASTALLANKLRFVLGASGHI AGVINPPAKNKRSHWTNDALPESPQQWLAGAIEHHG SWWPDWTAWLAGQAGAKRAAPANYGNARYRAIEP APGRYVKAKA	Rv3615c: T2-R11, I86-K96 PhaC: V125-R140, I167-R178, D182-R212, F219-R229, F250-R284, I299-R311, Y354-R403, I417-K517, L560-K602, F605-K622, S626-K666, A668-R677

ESAT6-PhaC (MW: 74.3 kDa)	
MTEQQWNFAGIEAAASAIQGNVTSIHSLLDEGKQSLT KLAAAWGGSGSEAYQGVQQKWDATATELNNALQN LARTISEAGQAMASTEGNVTGMFAHMATGKGAAAS TQEGKSQPFKVTPGPFDPATWLEWSRQWQGTEGNG HAAASGIPGLDALAGVKIAPAQLGDIQQRYMKDFSA LWQAMAEGKAEATGPLHDRRFAGDAWRTNLPYRFA AAFYLLNARALTELADAVEADAKTRQRIRFAISQWV DAMSPANFLATNPEAQRLLIESGGESLRAGVRNMME DLTRGKISQTDESAFEVGRNVAVTEGAVVFENEYFQL LQYKPLTDKVHARPLLMVPPCINKYYILDLQPESSLV RHVVEQGHTVFLVSWRNPDASMAGSTWDDYIEHAA IRAIEVARDISGQDKINVLGFCVGGTIVSTALAVLAAR GEHPAASVTLLTTLLDFADTGILDVFVDEGHVQLREA TLGGGAGAPCALLRGLELANTFSFLRPNDLVWNYVV DNYLKGNTPVPFDLLFWNGDATNLPGPWYCWYLRH TYLQNELKVPGKLTVCGVPVDLASIDVPTYIYGSRED HIVPWTAAYASTALLANKLRFVLGASGHIAGVINPPA KNKRSHWTNDALPESPQQWLAGAIEHHGSWWPDWT AWLAGQAGAKRAAPANYGNARYRAIEPAPGRYVKA KA	ESAT6: M1-K33, W58-R74 PhaC: V117-R132, I159-R170, D174-R204, F211-K235, F242-R276, I291-R303, Y346-R395, I409-K509, L552-K594, F597-K614, S618-K658, A660-R669
CFP10-RV3615C-PhaC-ESAT6 (MW: 98.1 kDa)	
MAEMKTDAATLAQEAGNFERISGDLKTQIDQVESTA GSLQGQWRGAAGTAAQAAVVRFQEAANKQKQELD EISTNIRQAGVQYSRADEEQQQALSSQMGFGPGGGG GPMTENLTVQPERLGVLASHHDNAAVDASSGVEAA AGLGESVAITHGPYCSQFNDTLNVYLTAHNALGSSLH TAGVDLAKSLRIAAKIYSEADEAWRKAIDGLFTTSAT GKGAAASTQEGKSQPFKVTPGPFDPATWLEWSRQW QGTEGNGHAAASGIPGLDALAGVKIAPAQLGDIQQR YMKDFSALWQAMAEGKAEATGPLHDRRFAGDAWR TNLPYRFAAAFYLLNARALTELADAVEADAKTRQRI RFAISQWVDAMSPANFLATNPEAQRLLIESGGESLRA GVRNMMEDLTRGKISQTDESAFEVGRNVAVTEGAV VFENEYFQLLQYKPLTDKVHARPLLMVPPCINKYYIL DLQPESSLVRHVVEQGHTVFLVSWRNPDASMAGST WDDYIEHAAIRAIEVARDISGQDKINVLGFCVGGTIVS TALAVLAARGEHPAASVTLLTTLLDFADTGILDVFVD EGHVQLREATLGGGAGAPCALLRGLELANTFSFLRP NDLVWNYVVDNYLKGNTPVPFDLLFWNGDATNLPG PWYCWYLRHTYLQNELKVPGKLTVCGVPVDLASID VPTYIYGSREDHIVPWTAAYASTALLANKLRFVLGAS GHIAGVINPPAKNKRSHWTNDALPESPQQWLAGAIE HHGSWWPDWTAWLAGQAGAKRAAPANYGNARYR AIEPAPGRYVKAKAHMVLAVAIDKRGGGGGLEMTE QQWNFAGIEAAASAIQGNVTSIHSLLDEGKQSLTKLA AAWGGSGSEAYQGVQQKWDATATELNNALQNLAR TISEAGQAMASTEGNVTGMFA	CFP10: A2-R20, T27-R57, Q78-R85 Rv3615c: T108-R117, I192-K202 PhaC: V233-R248, I275-R286, D290-R320, F327-R337, F358-R392, I407-R419, Y462-R511, I525-K625, L668-K710, F713-K730, S734-K774, A776-R785 ESAT6: W877-R893

Appendix II:
Publications

The current study has contributed to the following publications:

Chen, S., Parlane, N. A., Lee, J., Wedlock, D. N., Buddle, B. M., & Rehm, B. (2013). *New skin test for detection of bovine tuberculosis based on antigen-displaying polyester inclusions produced by recombinant Escherichia coli* [Unpublished manuscript]. Palmerston North, New Zealand: Institute of Fundamental Science, Massey University.*

Jahns, A. C., Maspolim, Y., **Chen, S.**, Guthrie, J., Blackwell, L., & Rehm, B. (2013). *In vivo* self-assembly of fluorescent protein microparticles displaying specific binding domains. *Bioconjugate Chemistry, 24*(8), 1314-1323.

* The TB manuscript will be submitted for publication after approval of a patent application.

References

Akerstrom, B., & Bjorck, L. (1986). A physicochemical study of protein G, a molecule with unique immunoglobulin G-binding properties. *Journal of Biological Chemistry, 261*(22), 240-247.

Amara, A. A., & Rehm, B. H. A. (2003). Replacement of the catalytic nucleophile cysteine-296 by serine in class II polyhydroxyalkanoate synthase from *Pseudomonas aeruginosa*-mediated synthesis of a new polyester: Identification of catalytic residues. *Biochemical Journal, 374*, 413-421.

Andersen, P., Doherty, T. M., Pai, M., & Weldingh, K. (2007). The prognosis of latent tuberculosis: Can disease be predicted? *Trends in Molecular Medicine, 13*(5), 175-182.

Arend, S. M., de Haas, P., Leyten, E., Rosenkrands, I., Rigouts, L., Andersen, P., . . . van Soolingen, D. (2005). ESAT-6 and CFP-10 in clinical versus environmental isolates of *Mycobacterium kansasii*. *Journal of Infectious Diseases, 191*(8), 1301-1310.

Arnau, J., Lauritzen, C., Petersen, G. E., & Pedersen, J. (2006). Current strategies for the use of affinity tags and tag removal for the purification of recombinant proteins. *Protein Expression and Purification, 48*(1), 1-13.

Atwood, J. A., & Rehm, B. H. A. (2009). Protein engineering towards biotechnological production of bifunctional polyester beads. *Biotechnology Letters, 31*(1), 131-137.

Backstrom, B. T., Brockelbank, J. A., & Rehm, B. H. A. (2007). Recombinant *Escherichia coli* produces tailor-made biopolyester granules for applications in fluorescence activated cell sorting: Functional display of the mouse interleukin-2 and myelin oligodendrocyte glycoprotein. *BMC Biotechnology, 7*(3), 1-12.

Banki, M. R., Gerngross, T. U., & Wood, D. W. (2005). Novel and economical purification of recombinant proteins: Intein-mediated protein purification using *in vivo* polyhydroxybutyrate (PHB) matrix association. *Protein Science, 14*(6), 1387-1395.

Berger, P., Adelman, N. B., Beckman, K. J., Campbell, D. J., Ellis, A. B., & Lisensky, G. C. (1999). Preparation and properties of an aqueous ferrofluid. *Journal of Chemical Education, 76*(7), 943-948.

Bjorck, L., & Kronvall, G. (1984). Purification and some properties of Streptococcal protein G, a novel IgG-binding reagent. *Journal of Immunology, 133*(2), 969-974.

Blanco, F. J., & Serrano, L. (1995). Folding of protein G B1 domain studied by the conformational characterization of fragments comprising its secondary structure elements. *European Journal of Biochemistry, 230*(2), 634-649.

Blatchford, P. A., Scott, C., French, N., & Rehm, B. H. A. (2012). Immobilization of organophosphohydrolase OpdA from *Agrobacterium radiobacter* by overproduction at the surface of polyester inclusions inside engineered *Escherichia coli*. *Biotechnology and Bioengineering, 109*(5), 1101-1108.

Bradford, M. M. (1976). A rapid and sensitive method for the quantitation of microgram quantities of protein utilizing the principle of protein-dye binding. *Analytical Biochemistry, 72*(1/2), 248-254.

Brady, D., & Jordaan, J. (2009). Advances in enzyme immobilisation. *Biotechnology Letters, 31*(11), 1639-1650.

Brandl, H., Gross, R. A., Lenz, R. W., & Fuller, R. C. (1988). *Pseudomonas oleovorans* as a source of poly(beta-hydroxyalkanoates) for potential applications as biodegradable polyesters. *Applied and Environmental Microbiology, 54*(8), 1977-1982.

Brock, I., Weldingh, K., Lillebaek, T., Follmann, F., & Andersen, P. (2004). Comparison of tuberculin skin test and new specific blood test in tuberculosis contacts. *American Journal of Respiratory and Critical Care Medicine, 170*(1), 65-69.

Brockelbank, J. A., Peters, V., & Rehm, B. H. A. (2006). Recombinant *Escherichia coli* strain produces a ZZ domain displaying biopolyester granules suitable for immunoglobulin G purification. *Applied and Environmental Microbiology, 72*(11), 7394-7397.

Brown, S. (1992). Engineered iron oxide-adhesion mutants of the *Escherichia coli* phage lambda receptor. *Proceedings of the National Academy of Sciences of the United States of America, 89*(18), 8651-8655.

Buddle, B. M., Keen, D., Thomson, A., Jowett, G., McCarthy, A. R., Heslop, J., . . . Aldwell, F. E. (1995). Protection of cattle from bovine tuberculosis by vaccination with BCG by the respiratory or subcutaneous route, but not by

vaccination with killed *Mycobacterium vaccae*. *Research in Veterinary Science, 59*(1), 10-16.

Buddle, B. M., Livingstone, P. G., & Lisle, G. W. D. (2009). Advances in ante-mortem diagnosis of tuberculosis in cattle. *New Zealand Veterinary Journal, 57*(4), 173-180.

Buddle, B. M., Parlane, N. A., Keen, D. L., Aldwell, F. E., Pollock, J. M., Lightbody, K., & Andersen, P. (1999). Differentiation between *Mycobacterium bovis* BCG-vaccinated and *M.bovis*-infected cattle by using recombinant mycobacterial antigens. *Clinical and Diagnostic Laboratory Immunology, 6*(1), 1-5.

Campisano, A., Overhage, J., & Rehm, B. H. A. (2008). The polyhydroxyalkanoate biosynthesis genes are differentially regulated in planktonic- and biofilm-grown *Pseudomonas aeruginosa*. *Journal of Biotechnology, 133*(4), 442-452.

Carr, P. D., & Ollis, D. L. (2009). Alpha/beta hydrolase fold: An update. *Protein and Peptide Letters, 16*(10), 1137-1148.

Casal, C., Bezos, J., Diez-Guerrier, A., Alvarez, J., Romero, B., de Juan, L., . . . Aranaz, A. (2012). Evaluation of two cocktails containing ESAT-6, CFP-10 and Rv-3615c in the intradermal test and the interferon-gamma assay for diagnosis of bovine tuberculosis. *Preventive Veterinary Medicine, 105*(1-2), 149-154.

Chung, C. W., Kim, H. W., Kim, Y. B., & Rhee, Y. H. (2003). Poly(ethylene glycol)-grafted poly(3-hydroxyundecenoate) networks for enhanced blood compatibility. *International Journal of Biological Macromolecules, 32*(1-2), 17-22.

Cody, C. W., Prasher, D. C., Westler, W. M., Prendergast, F. G., & Ward, W. W. (1993). Chemical structure of the hexapeptide chromophore of the Aequorea green-fluorescent protein. *Biochemistry, 32*(5), 1212-1218.

Cornejo, B. J., Sahagun-Ruiz, A., Suarez-Guemes, F., Thornton, C. G., Ficht, T. A., & Adams, L. G. (1998). Comparison of C-18-carboxypropylbetaine and glass bead DNA extraction methods for detection of *Mycobacterium bovis* in bovine milk samples and analysis of samples by PCR. *Applied and Environmental Microbiology, 64*(8), 3099-3101.

Costello, E., Doherty, M. L., Monaghan, M. L., Quigley, F. C., & O'Reilly, P. F. (1998). A study of cattle-to-cattle transmission of *Mycobacterium bovis* infection. *Veterinary Journal, 155*(3), 245-250.

de Groot, N. S., Espargaro, A., Morell, M., & Ventura, S. (2008). Studies on bacterial inclusion bodies. *Future Microbiology, 3*(4), 423-435.

de Groot, N. S., & Ventura, S. (2006). Protein activity in bacterial inclusion bodies correlates with predicted aggregation rates. *Journal of Biotechnology, 125*(1), 110-113.

Di Carlo, D., Jeong, K. H., & Lee, L. P. (2003). Reagentless mechanical cell lysis by nanoscale barbs in microchannels for sample preparation. *Lab on a Chip, 3*(4), 287-291.

Dunlop, W. F., & Robards, A. W. (1973). Ultrastructural study of poly-beta-hydroxybutyrate granules from *Bacillus cereus*. *Journal of Bacteriology, 114*(3), 1271-1280.

Ehrmann, M. A., Scheyhing, C. H., & Vogel, R. F. (2001). *In vitro* stability and expression of green fluorescent protein under high pressure conditions. *Letters in Applied Microbiology, 32*(4), 230-234.

Esposito, D., & Chatterjee, D. K. (2006). Enhancement of soluble protein expression through the use of fusion tags. *Current Opinion in Biotechnology, 17*(4), 353-358.

Forsgren, A. (1970). Significance of protein A production by Staphylococci. *Infection and Immunity, 2*(5), 672-673.

Fradkov, A. F., Verkhusha, V. V., Staroverov, D. B., Bulina, M. E., Yanushevich, Y. G., Martynov, V. I., . . . Lukyanov, K. A. (2002). Far-red fluorescent tag for protein labelling. *Biochemical Journal, 368*, 17-21.

Garcia-Fruitos, E., Gonzalez-Montalban, N., Morell, M., Vera, A., Ferraz, R. M., Aris, A., . . . Villaverde, A. (2005). Aggregation as bacterial inclusion bodies does not imply inactivation of enzymes and fluorescent proteins. *Microbial Cell Factories, 4*(27), 1-6.

Garcia-Fruitos, E., Rodriguez-Carmona, E., Diez-Gil, C., Ferraz, R. M., Vazquez, E., Luis Corchero, J., . . . Villaverde, A. (2009). Surface cell growth engineering assisted by a novel bacterial nanomaterial. *Advanced Materials, 21*(42), 4249-4253.

Garcia-Fruitos, E., Vazquez, E., Diez-Gil, C., Luis Corchero, J., Seras-Franzoso, J., Ratera, I., . . . Villaverde, A. (2012). Bacterial inclusion bodies: Making gold from waste. *Trends in Biotechnology, 30*(2), 65-70.

Gerngross, T. U., & Martin, D. P. (1995). Enzyme-catalyzed synthesis of poly (R)-(-)-3-hydroxybutyrate: Formation of macroscopic granules *in vitro*. *Proceedings of the National Academy of Sciences of the United States of America, 92*(14), 6279-6283.

Gerngross, T. U., Reilly, P., Stubbe, J., Sinskey, A. J., & Peoples, O. P. (1993). Immunocytochemical analysis of poly-beta-hydroxybutyrate (PHB) synthase in *Alcaligenes eutrophus* H16: Localization of the synthase enzyme at the surface of PHB granules. *Journal of Bacteriology, 175*(16), 5289-5293.

Gerngross, T. U., Snell, K. D., Peoples, O. P., Sinskey, A. J., Csuhai, E., Masamune, S., & Stubbe, J. (1994). Overexpression and purification of the soluble polyhydroxyalkanoate synthase from *Alcaligenes eutrophus*: Evidence for a required posttranslational modification for catalytic activity. *Biochemistry, 33*(31), 9311-9320.

Grage, K., Jahns, A. C., Parlane, N., Palanisamy, R., Rasiah, I. A., Atwood, J. A., & Rehm, B. H. A. (2009). Bacterial polyhydroxyalkanoate granules: Biogenesis, structure, and potential use as nano-/micro-beads in biotechnological and biomedical applications. *Biomacromolecules, 10*(4), 660-669.

Grage, K., Peters, V., & Rehm, B. H. A. (2011). Recombinant protein production by *in vivo* polymer inclusion display. *Applied and Environmental Microbiology, 77*(18), 6706-6709.

Gurskaya, N. G., Fradkov, A. F., Terskikh, A., Matz, M. V., Labas, Y. A., Martynov, V. I., . . . Lukyanov, S. A. (2001). GFP-like chromoproteins as a source of far-red fluorescent proteins. *Febs Letters, 507*(1), 16-20.

Hanahan, D. (1983). Studies on transformation of *Escherichia coli* with plasmids. *Journal of Molecular Biology, 166*(4), 557-580.

Hanefeld, U., Gardossi, L., & Magner, E. (2009). Understanding enzyme immobilisation. *Chemical Society Reviews, 38*(2), 453-468.

Hazer, B., & Steinbuechel, A. (2007). Increased diversification of polyhydroxyalkanoates by modification reactions for industrial and medical applications. *Applied Microbiology and Biotechnology, 74*(1), 1-12.

Heim, R., Prasher, D. C., & Tsien, R. Y. (1994). Wavelength mutations and posttranslational autoxidation of green fluorescent protein. *Proceedings of the National Academy of Sciences of the United States of America, 91*(26), 12501-12504.

Hengen, P. N. (1995). Cloning PCR products using T-vectors. *Trends in Biochemical Sciences, 20*(2), 85-86.

Hezayen, F. F., Steinbuchel, A., & Rehm, B. H. A. (2002). Biochemical and enzymological properties of the polyhydroxybutyrate synthase from the extremely halophilic archaeon strain 56. *Archives of Biochemistry and Biophysics, 403*(2), 284-291.

Hooks, D. O., Blatchford, P. A., & Rehm, B. H. A. (2013). Bioengineering of bacterial polymer inclusions catalyzing the synthesis of *N*-acetyl Neuraminic acid. *Applied and Environmental Microbiology* [In press].

Huse, K., Bohme, H. J., & Scholz, G. H. (2002). Purification of antibodies by affinity chromatography. *Journal of Biochemical and Biophysical Methods, 51*(3), 217-231.

Irimia, D., Tompkins, R. G., & Toner, M. (2004). Single-cell chemical lysis in picoliter-scale closed volumes using a microfabricated device. *Analytical Chemistry, 76*(20), 6137-6143.

Ito, A., Shinkai, M., Honda, H., & Kobayashi, T. (2005). Medical application of functionalized magnetic nanoparticles. *Journal of Bioscience and Bioengineering, 100*(1), 1-11.

Jahns, A. C., Haverkamp, R. G., & Rehm, B. H. A. (2008). Multifunctional inorganic-binding beads self-assembled inside engineered bacteria. *Bioconjugate Chemistry, 19*(10), 2072-2080.

Jahns, A. C., Maspolim, Y., Chen, S., Guthrie, J., Blackwell, L., & Rehm, B. (2013). *In vivo* self-assembly of fluorescent protein microparticles displaying specific binding domains. *Bioconjugate Chemistry, 24*(8), 1314-1323.

Jahns, A. C., & Rehm, B. H. A. (2009). Tolerance of the *Ralstonia eutropha* Class I polyhydroxyalkanoate synthase for translational fusions to its C terminus reveals a new mode of functional display. *Applied and Environmental Microbiology, 75*(17), 5461-5466.

Jahns, A. C., & Rehm, B. H. A. (2012). Relevant uses of surface proteins**:** Display on self-organized biological structures. *Microbial Biotechnology, 5*(2), 188-202.

Jen, C. P., Hsiao, J. H., & Maslov, N. A. (2012). Single-cell chemical lysis on microfluidic chips with arrays of microwells. *Sensors, 12*(1), 347-358.

Jendrossek, D. (2005). Fluorescence microscopical investigation of poly(3-hydroxybutyrate) granule formation in bacteria. *Biomacromolecules, 6*(2), 598-603.

Jensen, T. E., & Sicko, L. M. (1971). Fine structure of poly-beta-hydroxybutyric acid granules in a blue-green alga, Chlorogloea-fritschII. *Journal of Bacteriology, 106*(2), 683-686.

Jeyaratnam, J. (1990). Acute pesticide poisoning: A major global health problem. *World Health Statistics Quarterly, 43*(3), 139-144.

Jia, Y., Yuan, W., Wodzinska, J., Park, C., Sinskey, A. J., & Stubbe, J. (2001). Mechanistic studies on class I polyhydroxybutyrate (PHB) synthase from *Ralstonia eutropha*: Class I and III synthases share a similar catalytic mechanism. *Biochemistry, 40*(4), 1011-1019.

Johnson, A. K., Zawadzka, A. M., Deobald, L. A., Crawford, R. L., & Paszczynski, A. J. (2008). Novel method for immobilization of enzymes to magnetic nanoparticles. *Journal of Nanoparticle Research, 10*(6), 1009-1025.

Kamath, A. B., Woodworth, J., Xiong, X. W., Taylor, C., Yu, W., & Behar, S. M. (2004). Cytolytic CD8(+) T cells recognizing CFP10 are recruited to the lung after *Mycobacterium tuberculosis* infection. *Journal of Experimental Medicine, 200*(11), 1479-1489.

Keshavarz, T., & Roy, I. (2010). Polyhydroxyalkanoates: Bioplastics with a green agenda. *Current Opinion in Microbiology, 13*(3), 321-326.

Kikkawa, Y., Narike, M., Hiraishi, T., Kanesato, M., Sudesh, K., Doi, Y., & Tsuge, T. (2005). Organization of polyhydroxyalkanoate synthase for *in vitro* polymerization as revealed by atomic force microscopy. *Macromolecular Bioscience, 5*(10), 929-935.

Koller, M., Salerno, A., Dias, M., Reiterer, A., & Braunegg, G. (2010). Modern biotechnological polymer synthesis: A review. *Food Technology and Biotechnology, 48*(3), 255-269.

Laurent, S., Forge, D., Port, M., Roch, A., Robic, C., Elst, L. V., & Muller, R. N. (2008). Magnetic iron oxide nanoparticles: Synthesis, stabilization, vectorization, physicochemical characterizations, and biological applications. *Chemical Reviews, 108*(6), 2064-2110.

Lee, S. Y. (1996). High cell-density culture of *Escherichia coli*. *Trends in Biotechnology, 14*(3), 98-105.

Legat, A., Gruber, C., Zangger, K., Wanner, G., & Stan-Lotter, H. (2010). Identification of polyhydroxyalkanoates in Halococcus and other haloarchaeal species. *Applied Microbiology and Biotechnology, 87*(3), 1119-1127.

Lemoigne, M. (1926). Produits de déshydration et de polymérisation de l'acide β-oxybutyrique. *Bull. Soc. Chim. Biol, 8*, 770-782.

Liberti, P. A., & Feeley, B. P. (1991). Analytical- and process-scale cell separation with bioreceptor ferrofluids and high-gradient magnetic separation. *Acs Symposium Series, 464*, 268-288.

Lundgren, D. G., Merrick, J. M., & Pfister, R. M. (1964). Structure of poly-beta-hydroxybutyric acid granules. *Journal of General Microbiology, 34*(3), 441-446.

MacGurn, J. A., Raghavan, S., Stanley, S. A., & Cox, J. S. (2005). A non-RD1 gene cluster is required for Snm secretion in *Mycobacterium tuberculosis*. *Molecular Microbiology, 57*(6), 1653-1663.

Madison, L. L., & Huisman, G. W. (1999). Metabolic engineering of poly(3-hydroxyalkanoates): From DNA to plastic. *Microbiology and Molecular Biology Reviews, 63*(1), 21-53.

Marchuk, D., Drumm, M., Saulino, A., & Collins, F. S. (1991). Construction of T-vectors, a rapid and general system for direct cloning of unmodified PCR products. *Nucleic Acids Research, 19*(5), 1154-1154.

Mayer, F., & Hoppert, M. (1997). Determination of the thickness of the boundary layer surrounding bacterial PHA inclusion bodies, and implications for models describing the molecular architecture of this layer. *Journal of Basic Microbiology, 37*(1), 45-52.

Millington, K. A., Fortune, S. M., Low, J., Garces, A., Hingley-Wilson, S. M., Wickremasinghe, M., . . . Lalvani, A. (2011). Rv3615c is a highly immunodominant RD1 (Region of Difference 1)-dependent secreted antigen specific for *Mycobacterium tuberculosis* infection. *Proceedings of the National Academy of Sciences of the United States of America, 108*(14), 5730-5735.

Monaghan, M. L., Doherty, M. L., Collins, J. D., Kazda, J. F., & Quinn, P. J. (1994). The tuberculin test. *Veterinary Microbiology, 40*(1-2), 111-124.

Mori, T., Sakatani, M., Yamagishi, F., Takashima, T., Kawabe, Y., Nagao, K., . . . Tsuyuguchi, I. (2004). Specific detection of tuberculosis infection: An

interferon-gamma-based assay using new antigens. *American Journal of Respiratory and Critical Care Medicine, 170*(1), 59-64.

Mullaney, J. A., & Rehm, B. H. A. (2010). Design of a single-chain multi-enzyme fusion protein establishing the polyhydroxybutyrate biosynthesis pathway. *Journal of Biotechnology, 147*(1), 31-36.

Naylor, L. H. (1999). Reporter gene technology: The future looks bright. *Biochemical Pharmacology, 58*(5), 749-757.

Nomine, Y., Ristriani, T., Laurent, C., Lefevre, J. F., Weiss, E., & Trave, G. (2001). Formation of soluble inclusion bodies by HPV E6 oncoprotein fused to maltose-binding protein. *Protein Expression and Purification, 23*(1), 22-32.

Ollis, D. L., Cheah, E., Cygler, M., Dijkstra, B., Frolow, F., Franken, S. M., . . . Goldman, A. (1992). The alpha/beta-hydrolase fold. *Protein Engineering, 5*(3), 197-211.

Ormo, M., Cubitt, A. B., Kallio, K., Gross, L. A., Tsien, R. Y., & Remington, S. J. (1996). Crystal structure of the Aequorea victoria green fluorescent protein. *Science, 273*(5280), 1392-1395.

Parlane, N. A., Grage, K., Lee, J. W., Buddle, B. M., Denis, M., & Rehm, B. H. A. (2011). Production of a particulate hepatitis C vaccine candidate by an engineered *Lactococcus lactis* strain. *Applied and Environmental Microbiology, 77*(24), 8516-8522.

Parlane, N. A., Grage, K., Mifune, J., Basaraba, R. J., Wedlock, D. N., Rehm, B. H. A., & Buddle, B. M. (2012). Vaccines displaying mycobacterial proteins on biopolyester beads stimulate cellular immunity and induce protection against tuberculosis. *Clinical and Vaccine Immunology, 19*(1), 37-44.

Parlane, N. A., Wedlock, D. N., Buddle, B. M., & Rehm, B. H. A. (2009). Bacterial polyester inclusions engineered to display vaccine candidate antigens for use as a novel class of safe and efficient vaccine delivery agents. *Applied and Environmental Microbiology, 75*(24), 7739-7744.

Peoples, O. P., & Sinskey, A. J. (1989a). Poly-β-hydroxybutyrate biosynthesis in *Alcaligenes eutrophus* H16: Characterization of the genes encoding β-ketothiolase and acetoacetyl-CoA reductase. *Journal of Biological Chemistry, 264*, 15,293-15,297.

Peoples, O. P., & Sinskey, A. J. (1989b). Poly-β-hydroxybutyrate(PHB) biosynthesis in *Alcaligenes eutrophus* H16: Identification and characterization of the PHB polmerase gene (*phbC*). *Journal of Biological Chemistry, 264*, 15,298-15,303.

Peternel, S., Jevsevar, S., Bele, M., Gaberc-Porekar, V., & Menart, V. (2008). New properties of inclusion bodies with implications for biotechnology. *Biotechnology and Applied Biochemistry, 49*, 239-246.

Peternel, S., & Komel, R. (2011). Active protein aggregates produced in *Escherichia coli*. *International Journal of Molecular Sciences, 12*(11), 8275-8287.

Peters, V., Becher, D., & Rehm, B. H. A. (2007). The inherent property of polyhydroxyalkanoate synthase to form spherical PHA granules at the cell poles: The core region is required for polar localization. *Journal of Biotechnology, 132*(3), 238-245.

Peters, V., & Rehm, B. H. A. (2005). *In vivo* monitoring of PHA granule formation using GFP-labeled PHA synthases. *Fems Microbiology Letters, 248*(1), 93-100.

Philip, S., Keshavarz, T., & Roy, I. (2007). Polyhydroxyalkanoates: Biodegradable polymers with a range of applications. *Journal of Chemical Technology and Biotechnology, 82*(3), 233-247.

Pollock, J. M., & Andersen, P. (1997). Predominant recognition of the ESAT-6 protein in the first phase of infection with *Mycobacterium bovis* in cattle. *Infection and Immunity, 65*(7), 2587-2592.

Pym, A. S., Brodin, P., Brosch, R., Huerre, M., & Cole, S. T. (2002). Loss of RD1 contributed to the attenuation of the live tuberculosis vaccines *Mycobacterium bovis* BCG and *Mycobacterium microti*. *Molecular Microbiology, 46*(3), 709-717.

Qi, Q. S., & Rehm, B. H. A. (2001). Polyhydroxybutyrate biosynthesis in *Caulobacter crescentus*: Molecular characterization of the polyhydroxybutyrate synthase. *Microbiology, 147*, 3353-3358.

Rasiah, I. A., & Rehm, B. H. A. (2009). One-step production of immobilized alpha-amylase in recombinant *Escherichia coli*. *Applied and Environmental Microbiology, 75*(7), 2012-2016.

Ravn, P., Munk, M. E., Andersen, A. B., Lundgren, B., Lundgren, J. D., Nielsen, L. N., . . . Weldingh, K. (2005). Prospective evaluation of a whole-blood test using *Mycobacterium tuberculosis*-specific antigens ESAT-6 and CFP-10 for

diagnosis of active tuberculosis. *Clinical and Diagnostic Laboratory Immunology, 12*(4), 491-496.

Rehm, B. H. A. (2003). Polyester synthases: Natural catalysts for plastics. *Biochemical Journal, 376*, 15-33.

Rehm, B. H. A. (2006). Genetics and biochemistry of polyhydroxyalkanoate granule self-assembly: The key role of polyester synthases. *Biotechnology Letters, 28*(4), 207-213.

Rehm, B. H. A. (2007). Biogenesis of microbial polyhydroxyalkanoate granules: A platform technology for the production of tailor-made bioparticles. *Current Issues in Molecular Biology, 9*, 41-62.

Rehm, B. H. A., Antonio, R. V., Spiekermann, P., Amara, A. A., & Steinbuchel, A. (2002). Molecular characterization of the poly(3-hydroxybutyrate) (PHB) synthase from *Ralstonia eutropha*: *in vitro* evolution, site-specific mutagenesis and development of a PHB synthase protein model. *Biochimica Et Biophysica Acta-Protein Structure and Molecular Enzymology, 1594*(1), 178-190.

Rehm, B. H. A., Qi, Q. S., Beermann, B. B., Hinz, H. J., & Steinbuchel, A. (2001). Matrix-assisted *in vitro* refolding of *Pseudomonas aeruginosa* class II polyhydroxyalkanoate synthase from inclusion bodies produced in recombinant *Escherichia coli*. *Biochemical Journal, 358*, 263-268.

Ren, Q., de Roo, G., Kessler, B., & Witholt, B. (2000). Recovery of active medium-chain-length-poly-3-hydroxyalkanoate polymerase from inactive inclusion bodies using ion-exchange resin. *Biochemical Journal, 349*, 599-604.

Renshaw, P. S., Lightbody, K. L., Veverka, V., Muskett, F. W., Kelly, G., Frenkiel, T. A., . . . Carr, M. D. (2005). Structure and function of the complex formed by the tuberculosis virulence factors CFP-10 and ESAT-6. *Embo Journal, 24*(14), 2491-2498.

Sambrook, J., Fritsch, E. F., & Maniatis, T. (1989). *Molecular cloning: A laboratory manual*. New York, NY: Cold Spring Harbor Laboratory Press.

Schubert, P., Kruger, N., & Steinbuchel, A. (1991). Molecular analysis of the *Alcaligenes eutrophus* poly(3-hydroxybutyrate) biosynthetic operon: Identification of the N-terminus of poly(3-hydroxybutyrate) synthase and identification of the promoter. *Journal of Bacteriology, 173*(1), 168-175.

Shewale, S. D., & Pandit, A. B. (2007). Hydrolysis of soluble starch using *Bacillus licheniformis* alpha-amylase immobilized on superporous CELBEADS. *Carbohydrate Research, 342*(8), 997-1008.

Shimomura, O., Johnson, F. H., & Saiga, Y. (1962). Extraction, purification and properties of aequorin, a bioluminescent protein from the luminous hydromedusan, Aequorea. *Journal of Cellular and Comparative Physiology, 59*(3), 223-239.

Sidders, B., Pirson, C., Hogarth, P. J., Hewinson, R. G., Stoker, N. G., Vordermeier, H. M., & Ewer, K. (2008). Screening of highly expressed mycobacterial genes identifies Rv3615c as a useful differential diagnostic antigen for the *Mycobacterium tuberculosis* complex. *Infection and Immunity, 76*(9), 3,932-3,939.

Spiekermann, P., Rehm, B. H. A., Kalscheuer, R., Baumeister, D., & Steinbuchel, A. (1999). A sensitive, viable-colony staining method using Nile red for direct screening of bacteria that accumulate polyhydroxyalkanoic acids and other lipid storage compounds. *Archives of Microbiology, 171*(2), 73-80.

Steinmann, B., Christmann, A., Heiseler, T., Fritz, J., & Kolmar, H. (2010). *In vivo* enzyme immobilization by inclusion body display. *Applied and Environmental Microbiology, 76*(16), 5,563-5,569.

Stigter, D., Alonso, D. O. V., & Dill, K. A. (1991). Protein stability: Electrostatics and compact denatured states. *Proceedings of the National Academy of Sciences of the United States of America, 88*(10), 4176-4180.

Stuurman, N., Bras, C. P., Schlaman, H. R. M., Wijfjes, A. H. M., Bloemberg, G., & Spaink, H. P. (2000). Use of green fluorescent protein color variants expressed on stable broad-host-range vectors to visualize rhizobia interacting with plants. *Molecular Plant-Microbe Interactions, 13*(11), 1163-1169.

Taguchi, S., & Doi, Y. (2004). Evolution of polyhydroxyalkanoate (PHA) production system by "enzyme evolution": Successful case studies of directed evolution. *Macromolecular Bioscience, 4*(3), 145-156.

Tashiro, M., Tejero, R., Zimmerman, D. E., Celda, B., Nilsson, B., & Montelione, G. T. (1997). High-resolution solution NMR structure of the Z domain of staphylococcal protein A. *Journal of Molecular Biology, 272*(4), 573-590.

Thomson, N., Summers, D., & Sivaniah, E. (2010). Synthesis, properties and uses of bacterial storage lipid granules as naturally occurring nanoparticles. *Soft Matter, 6*(17), 4,045-4,057.

Tian, J. M., Sinskey, A. J., & Stubbe, J. (2005). Kinetic studies of polyhydroxybutyrate granule formation in *Wautersia eutropha* H16 by transmission electron microscopy. *Journal of Bacteriology, 187*(11), 3814-3824.

Tsien, R. Y. (1998). The green fluorescent protein. *Annual Review of Biochemistry, 67*, 509-544.

Tu, Y. Y., Primus, F. J., & Goldenberg, D. M. (1988). Temperature affects binding of murine monoclonal IgG antibodies to protein A. *Journal of Immunological Methods, 109*(1), 43-47.

Valappil, S. P., Boccaccini, A. R., Bucke, C., & Roy, I. (2007). Polyhydroxyalkanoates in Gram-positive bacteria: Insights from the genera Bacillus and Streptomyces. *Antonie Van Leeuwenhoek International Journal of General and Molecular Microbiology, 91*(1), 1-17.

Vinton, P., Mihrshahi, S., Johnson, P., Jenkin, G. A., Jolley, D., & Biggs, B. A. (2009). Comparison of QuantiFERON-TB gold in-tube test and tuberculin skin test for identification of latent *Mycobacterium tuberculosis* infection in healthcare staff and association between positive test results and known risk factors for infection. *Infection Control and Hospital Epidemiology, 30*(3), 215-221.

Vordermeier, H. M., Whelan, A., Cockle, P. J., Farrant, L., Palmer, N., & Hewinson, R. G. (2001). Use of synthetic peptides derived from the antigens ESAT-6 and CFP-10 for differential diagnosis of bovine tuberculosis in cattle. *Clinical and Diagnostic Laboratory Immunology, 8*(3), 571-578.

Waters, W. R., Nonnecke, B. J., Palmer, M. V., Robbe-Austermann, S., Bannantine, J. P., Stabel, J. R., . . . Minion, F. C. (2004). Use of recombinant ESAT-6: CFP-10 fusion protein for differentiation of infections of cattle by *Mycobacterium bovis* and by *M. avium subsp avium* and *M. avium subsp paratuberculosis*. *Clinical and Diagnostic Laboratory Immunology, 11*(4), 729-735.

Waters, W. R., Palmer, M. V., Buddle, B. M., & Vordermeier, H. M. (2012). Bovine tuberculosis vaccine research: Historical perspectives and recent advances. *Vaccine, 30*(16), 2611-2622.

Waters, W. R., Palmer, M. V., Thacker, T. C., Payeur, J. B., Harris, N. B., Minion, F. C., . . . Lyashchenko, K. P. (2006). Immune responses to defined antigens of

Mycobacterium bovis in cattle experimentally infected with *Mycobacterium kansasii*. *Clinical and Vaccine Immunology, 13*(6), 611-619.

Waugh, D. S. (2005). Making the most of affinity tags. *Trends in Biotechnology, 23*(6), 316-320.

Whelan, A. O., Clifford, D., Upadhyay, B., Breadon, E. L., McNair, J., Hewinson, G. R., & Vordermeier, M. H. (2010). Development of a skin test for bovine tuberculosis for differentiating infected from vaccinated animals. *Journal of Clinical Microbiology, 48*(9), 3176-3181.

Yang, H., Troudt, J., Grover, A., Arnett, K., Lucas, M., Cho, Y. S., . . . Dobos, K. M. (2011). Three protein cocktails mediate delayed-type hypersensitivity responses indistinguishable from that elicited by purified protein derivative in the guinea pig model of *Mycobacterium tuberculosis* infection. *Infection and Immunity, 79*(2), 716-723.

Yuan, W., Jia, Y., Tian, J. M., Snell, K. D., Muh, U., Sinskey, A. J., . . . Stubbe, J. (2001). Class I and III polyhydroxyalkanoate synthases from *Ralstonia eutropha* and *Allochromatium vinosum*: characterization and substrate specificity studies. *Archives of Biochemistry and Biophysics, 394*(1), 87-98.

Zhang, S. M., Kolvek, S., Lenz, R. W., & Goodwin, S. (2003). Mechanism of the polymerization reaction initiated and catalyzed by the polyhydroxybutyrate synthase of *Ralstonia eutropha*. *Biomacromolecules, 4*(3), 504-509.

Zheng, D. Y., Aramini, J. M., & Montelione, G. T. (2004). Validation of helical tilt angles in the solution NMR structure of the Z domain of Staphylococcal protein A by combined analysis of residual dipolar coupling and NOE data. *Protein Science, 13*(2), 549-554.

Zheng, Z., Li, M., Xue, X. J., Tian, H. L., Li, Z., & Chen, G. Q. (2006). Mutation on N-terminus of polyhydroxybutyrate synthase of *Ralstonia eutropha* enhanced PHB accumulation. *Applied Microbiology and Biotechnology, 72*(5), 896-905.

Zimmer, M. (2002). Green fluorescent protein (GFP): Aapplications, structure, and related photophysical behavior. *Chemical Reviews, 102*(3), 759-781.